

Politecnico di Torino



Master Degree Thesis

Experimental and analytical characterization of an automotive electromechanical device

Supervisors

Prof. Elvio Bonisoli
Domenico Lisitano, PhD

Candidate

Tony Di Buono

Academic Year 2018 - 2019

Index

Politecnico di Torino.....	1
Experimental and analytical characterization of an automotive electromechanical device.....	1
Index.....	3
Abstract.....	5
1. Model description	6
1.1 Discrete model	6
1.2 Equations of motion	8
1.3 Material characterisation.....	8
1.4 Material properties	9
1.5 Inertial properties	11
1.5.1 Omega pad	11
1.5.2 Core assembly	15
1.5.2.1 Coil equivalent model and windings assembly.....	15
1.5.2.2. Metallic Body.....	18
1.5.2.3 Equivalent core assembly.....	20
1.5.3 Rubber elements and screw.....	21
1.5.4 Assembly.....	22
1.6 Conclusions.....	23
2. Mass balancing.....	24
2.1 Preliminary results	24
2.2 Corrective factor	24
2.3 Results.....	25
2.4 Conclusions.....	25
3. Experimental static analysis for stiffness characterization	26
3.1 Test and results.....	26
3.1.1 Rotational stiffness.....	27
3.1.1.1 Rotational stiffness: pitch motion	27
3.1.1.2 Rotational stiffness: roll motion.....	34
3.2 Experimental analysis: axial stiffness	41
3.3 Conclusions.....	48
4. Finite elements static analysis.....	49
4.1 Results from experimental analyses.....	49
4.2 Procedure	49
4.2.1 Mathematical model.....	50
4.2.1.1 Clean up	50
4.2.2 Material properties and boundary conditions.....	51
4.3 Axial motion analysis.....	52
4.3.1 Mathematical model refinements	53
4.3.2 Results.....	53
4.3.2.1 Static analysis 1 - axial.....	54
4.3.2.2 Static analysis 2 - axial.....	56
4.3.2.3 Static analysis 3 - axial.....	58
4.3.2.4 Static analysis 4 - axial.....	60
4.3.2.5 Static analysis 5 - axial.....	62
4.3.2.6 Static analysis 5 rev1 - axial	64
4.3.2.7 Static analysis 6 - axial.....	66
4.3.2.8 Static analysis 7 - axial.....	68
4.3.2.9 Static analysis 8 - axial.....	70
4.3.2.10 Results for axial static analysis	72

4.4 Pitch and roll motion analyses	73
4.4.1 Mathematical model for pitch motion.....	73
4.4.1.1 Static analysis 1 - pitch	75
4.4.1.2 Static analysis 2 - pitch	77
4.4.1.3 Static analysis 3 - pitch	79
4.4.1.4 Static analysis 4 - pitch	81
4.4.1.5 Static analysis 5 - pitch	83
4.4.1.6 Static analysis 6 - pitch	85
4.4.1.7 Static analysis 7 - pitch	87
4.4.1.8 Static analysis 8 - pitch	89
4.4.1.9 Static analysis 9 - pitch	91
4.4.1.10 Static analysis 10 - pitch	93
4.4.1.11 Static analysis for pitch motion: results	95
4.4.2 Mathematical model for roll motion	96
4.4.2.1 Static analysis 1 - roll.....	97
4.5 Conclusions.....	100
5. Modal experimental analysis	101
5.1 Test definition	101
5.2 System setup	103
5.2.1 System setup: accelerometers and structure.....	103
5.2.2 System setup: accelerometers and structure.....	104
5.2.3 Test setup: input parameters and configurations.....	107
5.3 Results.....	108
5.3.1 Input vibration amplitude: 0.01 mm	108
5.3.2 Input vibration amplitude: 0.005 mm	112
5.4 Conclusions.....	117
6. Finite elements modal analysis	118
6.1 Mathematical model and boundary conditions	118
6.2 Analyses and results.....	119
6.3 Conclusions.....	123
7. Conclusions.....	124
Reference	125

Abstract

The purpose of this thesis is to present the activity carried out on an electromechanical actuator, in order to define its behaviour in a non-operating mode.

The activity is primarily based on the method behind the steps required to achieve a simplified model which is representative of the physical body under analysis.

The first section of the thesis will examine the overall description of the model. In particular due to the complexity of the system under analysis, a simplified discretization is proposed. In this sense, the principal characteristic motions and the elements of the system are described.

Materials and technical drawings are collected with the supervision of Valeo technical office, and a first version of the model is built.

Then, the inertial and elastic properties of the physical body are computed at Valeo laboratory.

The acquired data are subsequently processed in order to characterize the mass of each component of the model and the elastic stiffness of the elastic elements.

In the final section of the thesis the experimental modal analysis, performed at DIMEAS laboratory, are illustrated.

The experimental data are then compared with the one obtained by the finite elements modal analysis.

1. Model description

In the following chapter the definition of the discrete model of the component under analysis is presented.

The discrete model identification is essential in order to proceed with the system parameters identification.

The steps that lead to its definition are:

1. visual identification and preliminary measurements of the device under test;
2. component disassembly;
3. measurement comparison between device parts and technical drawings;
4. material assignment to each part from technical drawings requirements;
5. CAD models creation from technical drawings;
6. inertial properties extraction from CAD models;
7. material properties tuning to reach equivalence between device and CAD model.

A final error estimation is performed to guarantee the goodness of the results of tuning procedure.

1.1 Discrete model

The discrete model for the actuator is presented.

The complexity of the component under analysis make it necessary to simplify the system using a discrete parameter model approach.

Both masses, springs and damper are defined and the relative equation of motion for the free behaviour are derived.

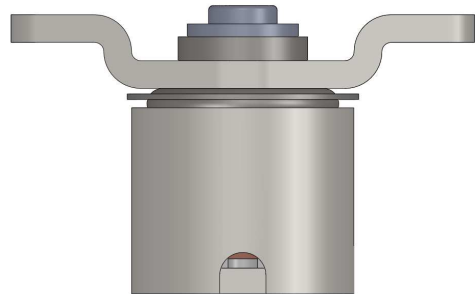


Figure 1.1 – Actuator, model isometric view.

Figure 1.2 – Actuator, model frontal view

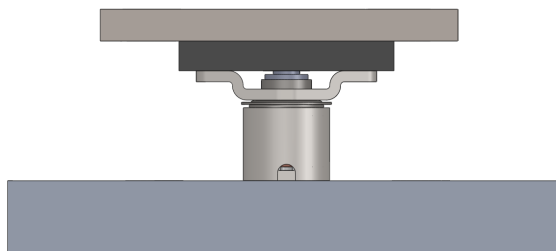


Figure 1.3 – Actuator, model working configuration with external loads

As depicted in Figures°1.4 and 1,5, the model is made up by:

1. lower support;
2. metallic body;
3. inner core: coil and plastic body;
4. omega pad;
5. tightening screw;
6. applied loads.

The symmetry of the model make it easier to describe it with respect to the two planes $\langle X,Z \rangle$ and $\langle Y,Z \rangle$.

In Figure°1.4 and 1.5 the discrete model is represented.

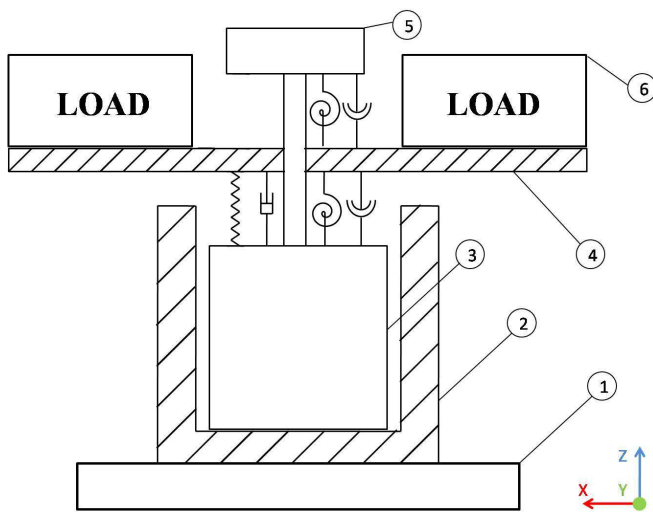


Figure 1.4 – Discrete model. $\langle X,Z \rangle$ plane.

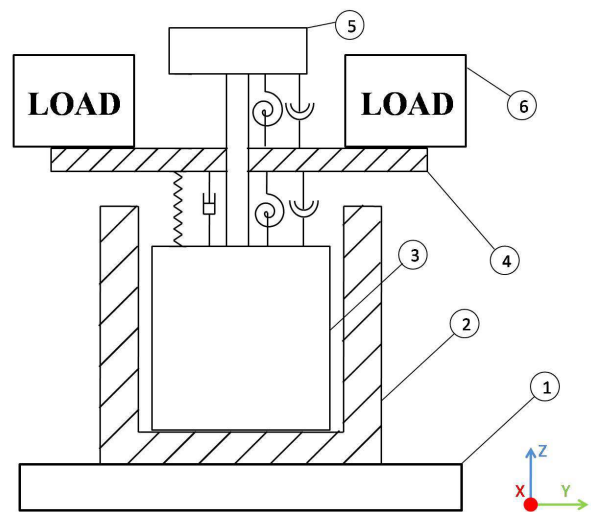


Figure 1.5 – Discrete model, $\langle Y,Z \rangle$ plane.

The following hypothesis are considered in order to simplify the model analysis::

- omega pad characterized by infinite stiffness with respect to elastic elements (o-ring and spacer);
- inner core and the external metallic case characterized by infinite stiffness with respect to elastic elements (o-ring and spacer).

Considering the hypothesis, given the symmetry of the model, it is decided to describe the motion of the omega pad according to 3 principal motions:

- axial displacement along z axis;
- rotation about y axis (pitch);
- rotation about x axis (roll);

In this sense, the discretisation of the elastic and dissipative components into lumped parameter elements is presented:

- elastic elements:
 - O-ring axial spring: $K_{Or,z}$;
 - O-ring torsional spring in $\langle Y,Z \rangle$: $K_{T,Or,x}$;
 - O-ring torsional spring in $\langle X,Z \rangle$: $K_{T,Or,y}$;
 - Spacer torsional spring in $\langle Y,Z \rangle$: $K_{T,S,x}$;
 - Spacer torsional spring in $\langle X,Z \rangle$: $K_{T,S,y}$.

- Damping elements:
 - O-ring axial damper: $C_{Or,z}$;
 - O-ring torsional damper in $\langle Y,Z \rangle$: $C_{T,Or,x}$;
 - O-ring torsional damper in $\langle X,Z \rangle$: $C_{T,Or,y}$;
 - Spacer torsional damper in $\langle Y,Z \rangle$: $C_{T,S,x}$;
 - Spacer torsional damper in $\langle X,Z \rangle$: $C_{T,S,y}$.

1.2 Equations of motion

Being the model defined, the equations of motion for free behaviour can be derived.
For axial displacement it results:

$$(M_{\Omega} + M_L) \ddot{z} + (C_{Or,z}) \dot{z} + (K_{Or,z}) z = 0 \quad (1.1)$$

For rotation about y axis it results:

$$(I_{\Omega,y} + I_{L,y}) \ddot{\vartheta}_y + (C_{T,Or,y} + C_{T,S,y}) \dot{\vartheta}_y + (K_{T,Or,y} + K_{T,S,y}) \vartheta_y = 0 \quad (1.2)$$

For rotation about x axis it results:

$$(I_{\Omega,x} + I_{L,x}) \ddot{\vartheta}_x + (C_{T,Or,x} + C_{T,S,x}) \dot{\vartheta}_x + (K_{T,Or,x} + K_{T,S,x}) \vartheta_x = 0 \quad (1.3)$$

By rewriting the dynamic equations in matrix formulation it results:

$$\begin{aligned} & \begin{bmatrix} (M_{\Omega} + M_L) & 0 & 0 \\ 0 & (I_{\Omega,y} + I_{L,y}) & 0 \\ 0 & 0 & (I_{\Omega,x} + I_{L,x}) \end{bmatrix} \begin{Bmatrix} \ddot{z} \\ \ddot{\vartheta}_y \\ \ddot{\vartheta}_x \end{Bmatrix} + \begin{bmatrix} (C_{Or,z}) & 0 & 0 \\ 0 & (C_{T,Or,y} + C_{T,S,y}) & 0 \\ 0 & 0 & (C_{T,Or,x} + C_{T,S,x}) \end{bmatrix} \begin{Bmatrix} \dot{z} \\ \dot{\vartheta}_y \\ \dot{\vartheta}_x \end{Bmatrix} + \\ & + \begin{bmatrix} (K_{Or,z}) & 0 & 0 \\ 0 & (K_{T,Or,y} + K_{T,S,y}) & 0 \\ 0 & 0 & (K_{T,Or,x} + K_{T,S,x}) \end{bmatrix} \begin{Bmatrix} z \\ \vartheta_y \\ \vartheta_x \end{Bmatrix} = \begin{Bmatrix} 0 \\ 0 \\ 0 \end{Bmatrix} \end{aligned} \quad (1.4)$$

1.3 Material characterisation

The device under analysis is made of materials that can be considered:

- isotropic;
- homogeneous.

In Table 1.1 is presented the material description of each the sub components.
The data are referred to Valeo technical drawings

Table 1.1 – Materials and components

Material	Sub component
11SMn30 (1.0715, AISI 1213)	Metallic ELM body
	Omega Pad
Copper	Coil
PA6 GF30	Plastic body
Silicone 20 ShA	O-Ring
Silicone 80 ShA	Spacer
Alloy Steel	Flanged screw

1.4 Material properties

Being the material of each component known, it's possible to proceed defining the principal characteristics of each of them.

The following datasheets are referred to Valeo technical drawings.

In Table 1.2 are shown the properties for AISI 1213 (11SMn30).

Table 1.2 – Material properties for AISI 1213.

Physical property	Unit of measurement	Value
Density (ρ)	[kg/m ³]	7800
Young modulus (E)	MPa	2.1E+5
Poisson ratio (ν)	-	0.28
Ultimate tensile strength (σ_R)	MPa	460
Yield strength (σ_Y)	MPa	375

In Table 1.3 are shown the properties for Copper.

Table 1.3 – Material properties for Copper.

Physical property	Unit of measurement	Value
Density (ρ)	[kg/m ³]	8930
Young modulus (E)	MPa	1.1E+5
Poisson ratio (ν)	-	0.34
Ultimate tensile strength (σ_R)	MPa	210
Yield strength (σ_Y)	MPa	33

In Table 1.4 are shown the properties for Silicone 20ShA.

Table 1.4 – Material properties for Silicone 20 ShA.

Physical property	Unit of measurement	Value
Density (ρ)	[kg/m ³]	1080 ± 20
Modulus at 100% elongation	MPa	*0.35
Poisson ratio (ν)	-	0.45
Ultimate tensile strength (σ_R)	MPa	*5.4
Yield strength (σ_Y)	MPa	Not def
Young Modulus	MPa	50
Allungamento a rottura	%	*750
Hardness	Sh	*A 23 ± 5

* Values are derived from datasheet (Valeo);

Poisson ratio is set 0.5 as an average value for a silicon rubber

Young modulus is set at 0.05 GPa as a starting qualitative value, based on average values from silicon rubber and natural rubber values.

In Table 1.5 are shown the properties for Silicone 80ShA.

Table 1.5 – Material properties for Silicone 80 ShA.

Physical property	Unit of measurement	Value
Density (ρ)	[kg/m ³]	1210 ± 20
Modulus at 100% elongation	MPa	*3.6
Poisson ratio (ν)	-	0.45
Ultimate tensile strength (σ_R)	MPa	*9.2
Yield strength (σ_Y)	MPa	Not def
Young Modulus	MPa	50
Allungamento a rottura	%	*400
Hardness	Sh	*A 80 ± 5

* Values are derived from datasheet (Valeo);

Poisson ratio is set 0.5 as an average value for a silicon rubber

Young modulus is set at 0.05 GPa as a starting qualitative value, based on average values from silicon rubber and natural rubber values.

In Table 1.6 are shown the properties for PA6 GF30.

Table 1.6 – Material properties for PA6 GF30.

Physical property	Unit of measurement	Value
Density (ρ)	[kg/m ³]	1360
Young modulus (E)	MPa	9.61E+3
Poisson ratio (ν)	-	0.38
Ultimate tensile strength (σ_R)	MPa	184.9
Yield strength (σ_Y)	MPa	184.9

In Table 1.7 are shown the properties for Steel.

Table 1.7 – Material properties for Alloy Steel.

Physical property	Unit of measurement	Value
Density (ρ)	[kg/m ³]	7700
Young modulus (E)	MPa	2.1E+5
Poisson ratio (ν)	-	0.28
Ultimate tensile strength (σ_R)	MPa	723.8
Yield strength (σ_Y)	MPa	620.4

1.5 Inertial properties

The inertial properties of each subcomponent and of the assembly are derived from CAD models. A comparison between results obtained from direct measurements and results from CAD models is required to check the goodness of results.

1.5.1 Omega pad

The following model is considered:

- Omega pad

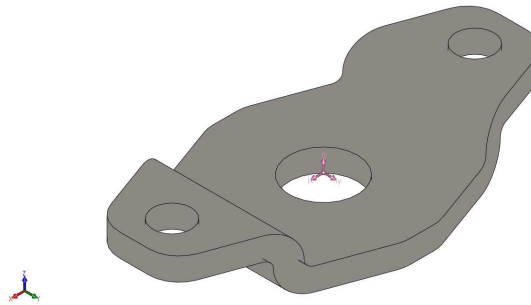


Figure 1.6 – Omega pad, model isometric view.

In Table 1.8 are shown the inertial properties, computed in SW 2015.

Table 1.8 – Omega pad inertial properties.

Physical property	Unit of measurement	Value
Mass (M)	[g]	2.68
Volume (V)	[mm ³]	344.16
Moment of Inertia. (I)	I _{XX} [g·mm ²]	29,08
	I _{YY} [g·mm ²]-	109,87
	I _{ZZ} [g·mm ²]	131.44

In Table 1.9 are presented the main geometric properties of the omega pad.
 A comparison between CAD model, Real component and Technical drawing is presented.

Table 1.9 – Data comparison.

Property	Unit of measurement	NVO Padded tablet 230118	Real component	Tech drw
Length (l)	[mm]	25	25.03	25 +/- 0.1
Width (w)	[mm]	13	12.89	13 +/- 0.15
Thickness (s)	[mm]	1.5	1.49	1.5 +/- 0.05
Mass (M)	[g]	2.68	2.76	-

In the following Figures are shown the results from measurements of the omega pad disassembled from the actuator

Measurements were taken at Valeo, Laboratory, using laboratory equipments.



Figure 1.7 – Omega pad, width.



Figure 1.8 – Omega pad, length



Figure 1.9 – Omega pad, thickness



Figure 1.10 – Omega pad, main hole diameter



Figure 1.11 – Omega pad, lateral hole diameter



Figure 1.12 – Omega pad, lateral holes distance

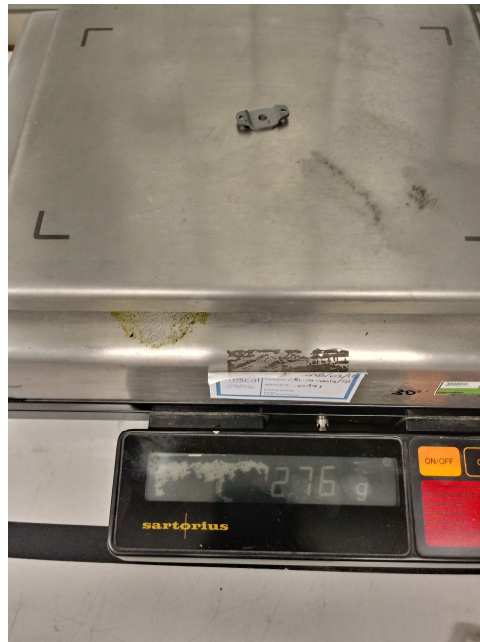


Figure 1.13 – Omega pad, mass measurement.

Comparison between measurements performed on real component and technical drawings, from which the CAD model is derived, show some differences, in particular for what concerns the shape of the "side wings" along Y - axis.

This leads to an error both on the overall mass of the object, plus 0.08 g of real device with respect to the model, and on the moment of inertia with respect X - and Y - axes.

These errors are considered to be negligible.

1.5.2 Core assembly

Due to component complexity and dimensions, and considering the dynamics of the device, that can be reduced to the motion of the omega pad with respect to the body, it was decided to study the metallic body, plastic body and coil as an assembly, the Core assembly

In the following Figures is shown the core assembly model and real device.



Figure 1.14 – Core assembly, model isometric view

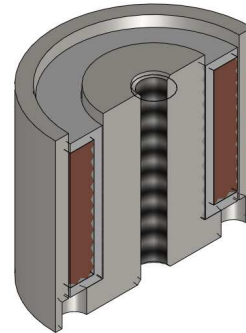


Figure 1.15 – Core assembly, model section view.

1.5.2.1 Coil equivalent model and windings assembly

Speaking about the coil, a minor simplifications is considered. In particular, starting from real data ,wire dimensions and coil properties, an equivalent model is computed and substituted in the assembly to simulate the coil windings.

The equivalent coil model takes into account the coil geometric constructive properties.

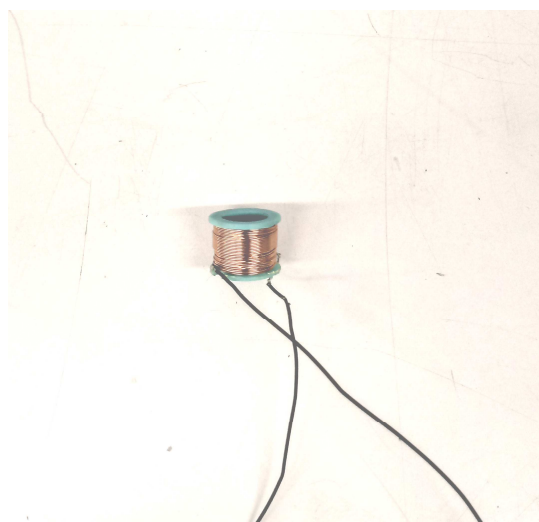


Figure 1.16 – Windings assembly.

In Table 1.10 are shown the parameters used to build the equivalent model.

Table 1.10 – Coil geometric characteristics, from Valeo technical drawings

Property	Unit of measurement	Value
Number of turns (n)	-	155 (or 190)
Wire diameter	[mm]	0,18
Inner radius (Ri)	[mm]	3.65
External radius(Re)	[mm]	5.1
Height (h)	[mm]	7.1
Packing factor (δ)	-	0.38

By taking into account the Copper density (Table 2.3), and the packing factor (Table 3.3), the equivalent copper density was computed according to the following equation.

$$\delta = \frac{A_{wire} N_{turns}}{A_{housing}} = \frac{(\pi r_{wire}^2) N_{turns}}{(r_e - r_i) h} \quad (3.1)$$

$$\rho_{equivalent} = \rho_{Cu} \delta \quad (3.2)$$

From computation it results:

$$\rho_{equivalent} = \rho_{Cu} \delta = 8930 \cdot 0.38 = 3393.4 \frac{kg}{m^3} \quad (3.3)$$

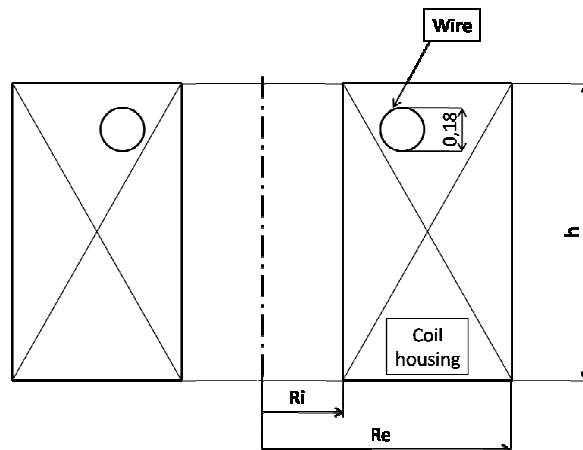


Figure 1.17 – Equivalent coil scheme.

The equivalent mass of the windings assembly, made by coil - plastic body, computed through the model, and the relative comparison with the measurement performed on the real windings assembly can be defined.

Table 1.11 – Data comparison. windings assembly (coil and its housing).

Property	Unit of measurement	Real assembly	Model assembly
Mass	M [g]	0.85	1.13
Height (h)	[mm]	7.74	8.10
Diameter (d)	[mm]	9.95	10.20

In the following Figures are shown the results from measurements.



Figure 1.18 – Windings assembly, height.



Figure 1.19 – Windings assembly, diameter.



Figure 1.20 – Windings assembly, mass measurement.



Figure 1.21 – Windings assembly with protective foil, mass measurement.

Results from comparison show strong differences between real device and models.

1.5.2.2. Metallic Body

The metallic body is the housing for the windings assembly. Together they constitute the Core assembly.

It acts like a constraint upon which the rubber elements and the omega pad are constraint through the screw.

In the following Figures are shown both the CAD model and the real disassembled component.

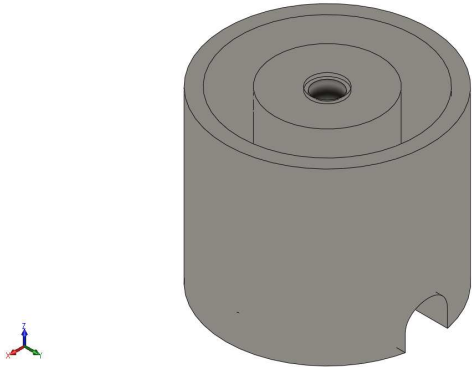


Figure 1.22 – Metallic body, model isometric view.

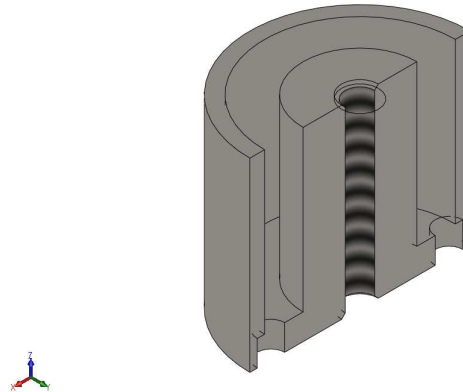


Figure 1.23 – Metallic body, model section view

The comparison between the measurement performed on the real body and the data collected from the model is shown in the following Table:

Table 1.12 – Data comparison, metallic body.

Property	Unit of measurement	Real body	Model
Mass	M [g]	4.80	4.92
Height (h)	[mm]	10.07	10.10
Diameter (d)	[mm]	11.97	12

In the following Figures are shown the results from measurements.

Measurements results are shown in the following Figures.



Figure 1.24 – Metallic body, diameter.



Figure 1.25 – Metallic body, height.



Figure 1.26 – Metallic body, mass measurement

Results shows some differences (0.12 g) between real body and its model.

1.5.2.3 Equivalent core assembly

The equivalent core assembly is produced from the following parts:

- Metallic Body;
- Plastic Body;
- Equivalent Coil model, (Coil δ 0.38).

In Table 1.13 are shown the inertial properties relative to the sub assembly, computed in SW 2015.

Table 1.13 – Equivalent core properties.

Property	Unit of measurement	Value
Mass	M [g]	6,06
Volume	V [mm ³]	1039.18

Comparison between measurements performed on real components and data collected from model is shown in Table 1.14.

Table 1.14 – Data comparison, core assembly.

Property	Unit of measurement	Real body	Model
Mass	M [g]	5.65	6,06

Results show a strong difference between the collected data.

By analysing each contribute, it is clear that the source of the error is strongly linked to the windings assembly, where the error accounts for 70% of the overall.

1.5.3 Rubber elements and screw

In the following figures the results from measurements.

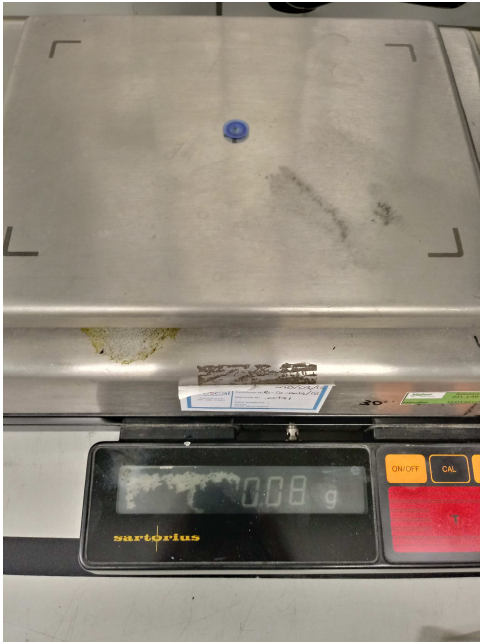


Figure 1.27 – O-ring, mass measurement.



Figure 1.28 – Spacer, mass measurement.



Figure 1.29 – Screw, mass measurement.

In Table 1.15 are shown the results

Table 1.15 – Data from measurements on physical bodies.

Property	Unit of measurement	O-ring	Spacer	Screw
Mass	M [g]	0.08	0.07	0.50

1.5.4 Assembly

The assembly is finally produced. The following models are considered:

- metallic body;
- plastic body;
- equivalent Coil model, Coil (δ 0.38);
- omega pad;
- o-ring;
- spacer;
- screw M2x7.

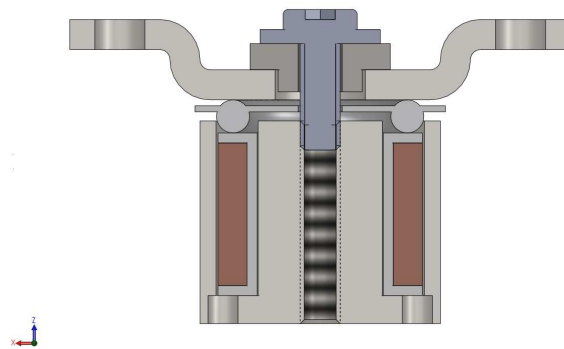


Figure 1.30 – Electromechanical actuator, section view.

Comparison between measurements performed on real assembly and model properties is shown in Table 1.16.

Table 1.16 – Properties comparison.

Part	Real body [g]	Model [g]
Omega pad	2.76	2.68
Metallic body	4.80	4.92
Windings assembly*	0.85	1.13
Screw	0.50	0.35
O-ring	0.08	0.09
Spacer	0.07	0.07
Total	9.06	9.26

*Not considering the protective foil

NB: data related to spacer and oring are not robust because of the difficulty to collect information about materials. Further updates are oncoming

1.6 Conclusions

Considering the level of uncertainty on collected data (material properties on oring and spacer) and on the measurements error, results show a little difference between the total mass of the model and that of the real device.

A balancing procedure is required to fix this issue in order to get the equivalence of the results.

2. Mass balancing

The comparison between inertial properties of the physical body and the model shows differences concerning the mass values.

In order to reproduce a model that has to be as much as possible similar to the physical body, a procedure to adjust the mass properties of the model parts is required.

In particular, being the geometry fully defined by the technical drawings, the only parameter that can actually be tuned to achieve the equivalence is the density.

A reverse process is then followed, starting from the actual mass and volume values of each component of physical body, the density corrective factor for each part of the model is computed.

In the following report are presented both the procedure and the final corrective factors.

2.1 Preliminary results

From mass measurements of physical body and mass computation of models the following results, listed in Table 2.1, are obtained.

Table 2.1 – Mass properties comparison.

Part	Real body [g]	Model [g]
Omega pad	2.76	2.68
Metallic body	4.80	4.92
Windings assembly	0.85	1.13
Screw	0.50	0.35
O-ring	0.09	0.09
Spacer	0.07	0.07
Total	9.06	9.26

The tuning procedure is applied to each part whose mass value, defined through SW material database, is discordant with respect to measurements on physical body.

2.2 Corrective factor

Considering Equation 2.1:

$$M = V \cdot \rho \quad (2.1)$$

where:

- M = mass [kg];
- V = volume [m³];
- ρ = density [kg/m³].

Considering the volume as an "exact" parameter, being computed directly from the Valeo technical drawings, the objective is to compute a corrective factor, α:

$$\alpha = \frac{M'}{M} \quad (2.2)$$

where:

- M = mass of physical body [kg];
- M' = mass of model [kg].

This factor allows to compute the density equivalent value, starting from its reference value defined through SW materials database, ρ_{ref} .

$$\rho' = \frac{\rho_{ref}}{\alpha} \quad (2.3)$$

As a check, it has to be:

$$M_{model} = V \cdot \rho' = M_{physical} \quad (2.4)$$

2.3 Results

Results for each component are listed in Table 2.1.

Table 2.1 – Results from mass balancing.

Part	Ref. density [kg/m ³]	Corrective factor [α]	Updated density [kg/m ³]
Omega pad	7800	0.97	8032.8
Metallic body	7800	1.03	7609.7
Plastic body*	1360	1	1360
Coil*	3393.4	1.41	2403.7
Screw	7700	0.70	11000
O-ring	1080	1	1080
Spacer	1210	1	1210

Considering the windings assembly, coil and its housing that accounts for 0.85g, it has been considered the mass contribute from plastic body as exact, 0.17g. The corrective factor is then computed on coil only and, in turn, the correction is applied of coil density.

2.4 Conclusions

Taking into account the corrected quantities for density, it is now possible to update the model achieving the inertial equivalence with the physical one.

3. Experimental static analysis for stiffness characterization

In the following chapter are presented the experimental analyzes carried out at Valeo laboratory, where the device is tested in order to collect data for the computation of the axial and rotational stiffness.

The analyzes aims to compute the characteristic curves of the device, a load-stroke curve, under different levels of applied loads, in the 3 principal configurations represented in Figure 3.1:

- pitch motion;
- roll motion;
- axial motion.

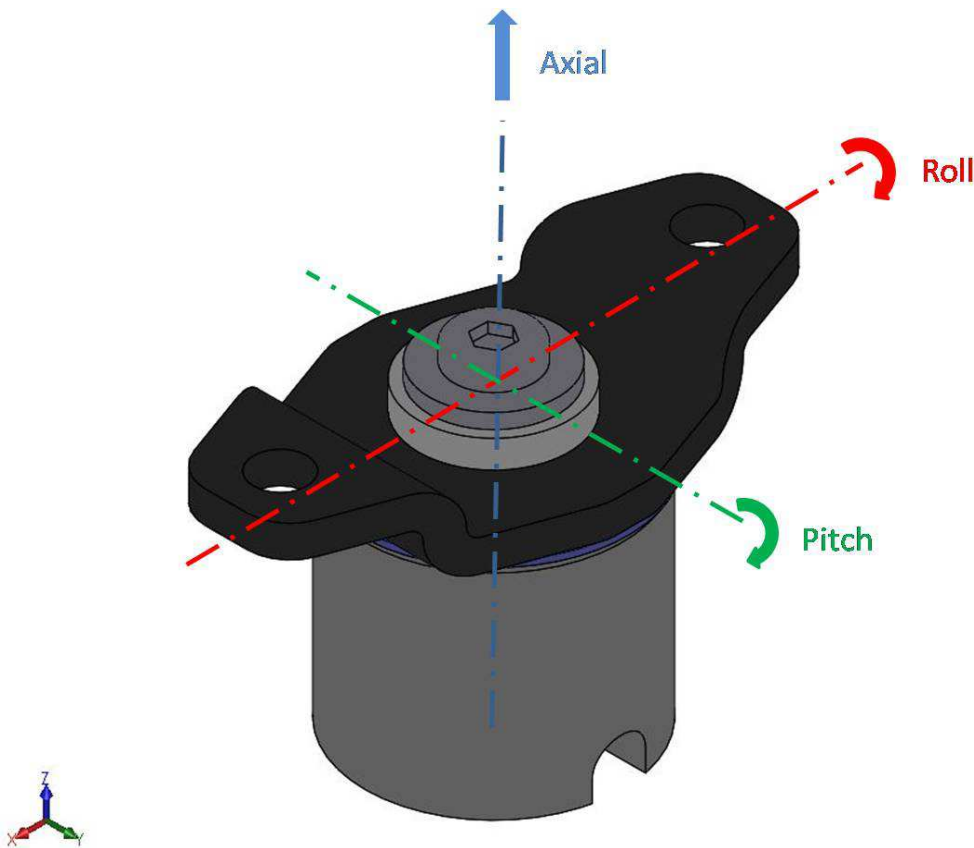


Figure 3.1 – Omega pad principal motions.

Data are collected using Microsoft Excel and then elaborated on MATLAB in order to get plots and numerical calculations.

3.1 Test and results

The machine performs a load cycle applying an increasing-decreasing force along Z axis in a specific point of the device through a probe.

Simultaneously, it measures the probe displacement along Z axis, which corresponds to the displacement of the point upon which the load is applied.

These data, applied load and corresponding displacement, plotted together represent the characteristic curve of the device in that specific configuration under that specific load cycle.

Multiple tests for each configuration are performed in order to have a significant set of data for the computation of the stiffness.

3.1.1 Rotational stiffness

The measuring machine is set up according the parameters in Table 3.1:

Table 3.1 – Measuring machine set up parameters.

Characteristic	Property	Value
Force sensor	Gain	0.5
	Maximum Force [N]	5
	Offset [N]	- 0.03
Position sensor	Gain	0.005
	Maximum distance [mm]	5
	Offset [mm]	0
Supply voltage	Voltage [V]	24
Feeding speed	Speed [$\mu\text{m/s}$]	25

The rotational stiffness is computed considering two different motion of the device:

- pitch motion, about Y axis,
- roll motion, about X axis.

3.1.1.1 Rotational stiffness: pitch motion

In order to ascertain the symmetrical behaviour of the component two different configurations are tested, corresponding to the two wings of the omega pad.

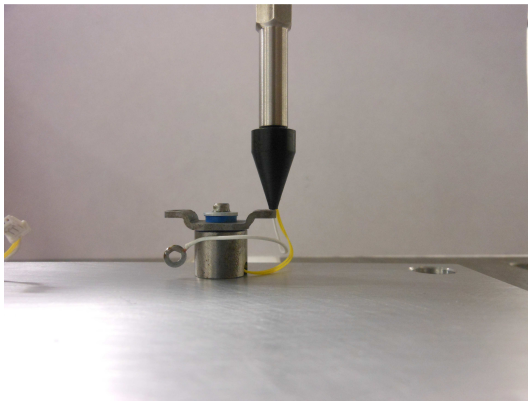


Figure 3.2 – Test setup, configuration A.

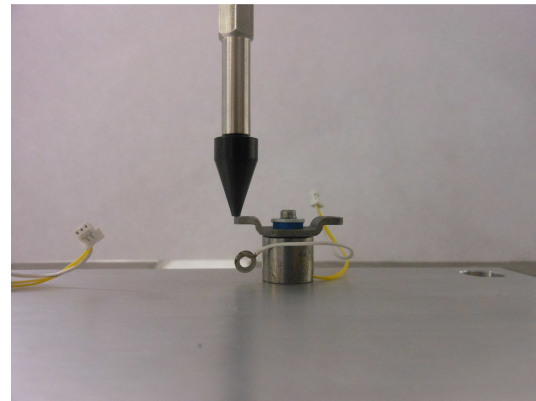


Figure 3.3 – Test setup, configuration B.

As depicted in Figure 3.2 and Figure 3.3, a conical probe is adopted.

The load is applied on two point symmetric with respect to the component transversal centerline plane.

For each configuration are collected 4 sets of data which are manipulated in MATLAB in order to produce the characteristic curves of the device, showing the displacement [mm] on X-axis and the applied load [N] on Y-axis.

In Figure 3.4 and Figure 3.5 are presented the characteristic curves of the acquisition related to configuration A and B.

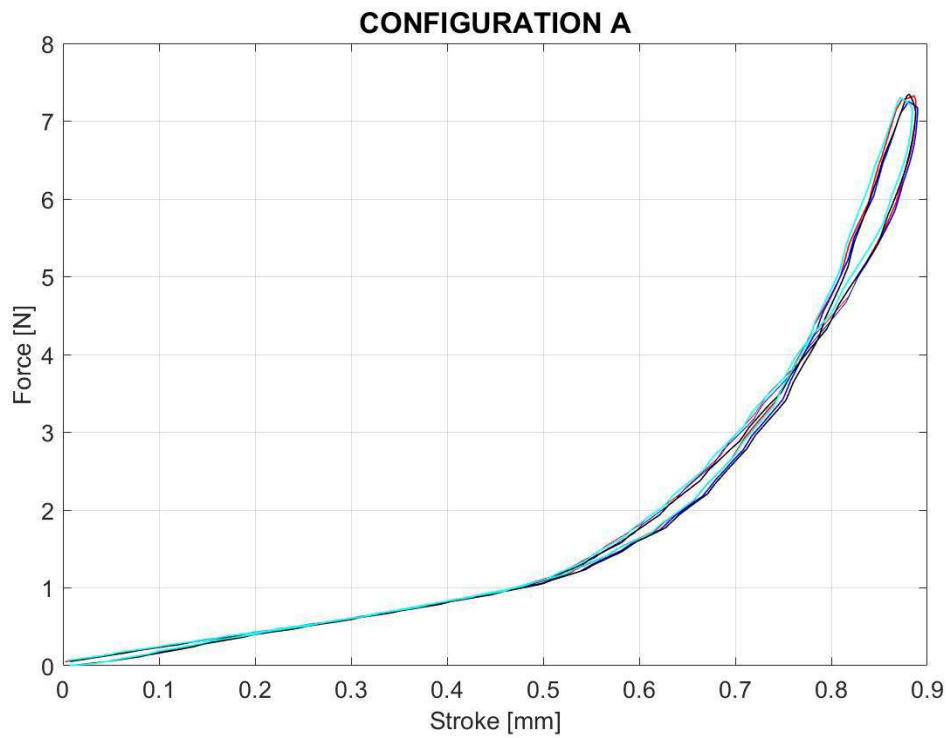


Figure 3.4 – Characteristic curve, configuration. A.

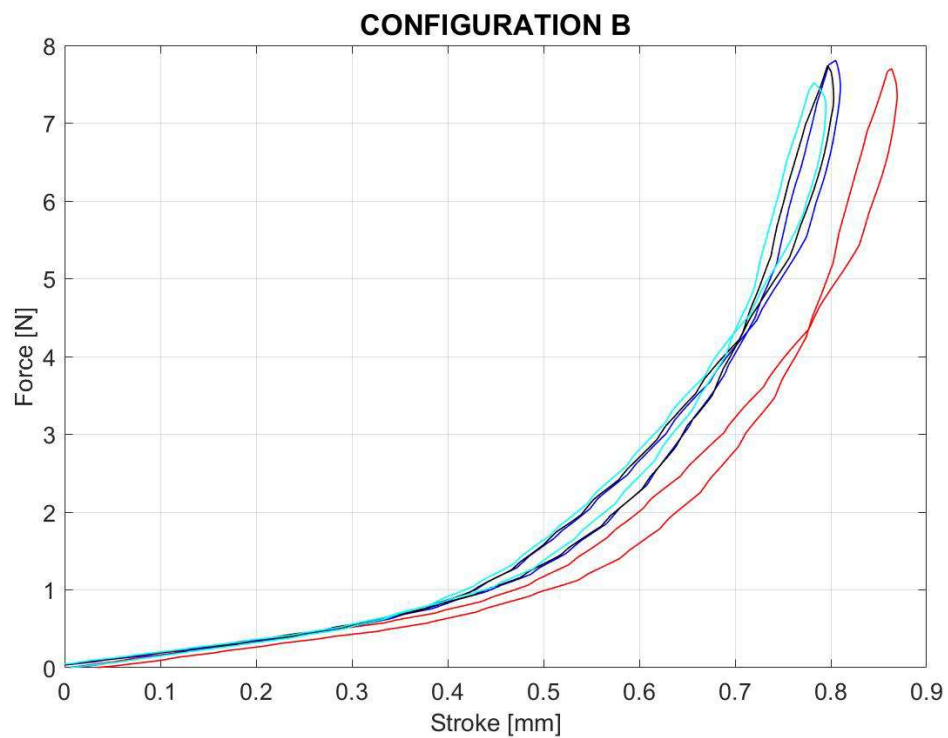


Figure 3.5 – Characteristic curve, configuration. B.

For analysis are considered only the charge strokes.

Being the analysis focused on the acquisition of the rotational stiffness, a transformation of the coordinates is required.

The transformation is computed considering the following equation for the resulting torque:

$$C = F \cdot b \quad (3.1)$$

$$b = 11.875 \text{ mm} \quad (3.2)$$

$$\vartheta = \arcsin\left(\frac{z}{b}\right) \sim \frac{z}{b} \quad (\text{for small oscillations approximation}) \quad (3.3)$$

where:

- C is the resulting torque [Nmm];
- F is the applied axial load [N];
- b is the arm of the applied torque [mm];
- z is the displacement along Z axis of the point where the force is applied [mm];
- ϑ is the angle corresponding to the axial displacement [rad].

The following characteristic curves are obtained.

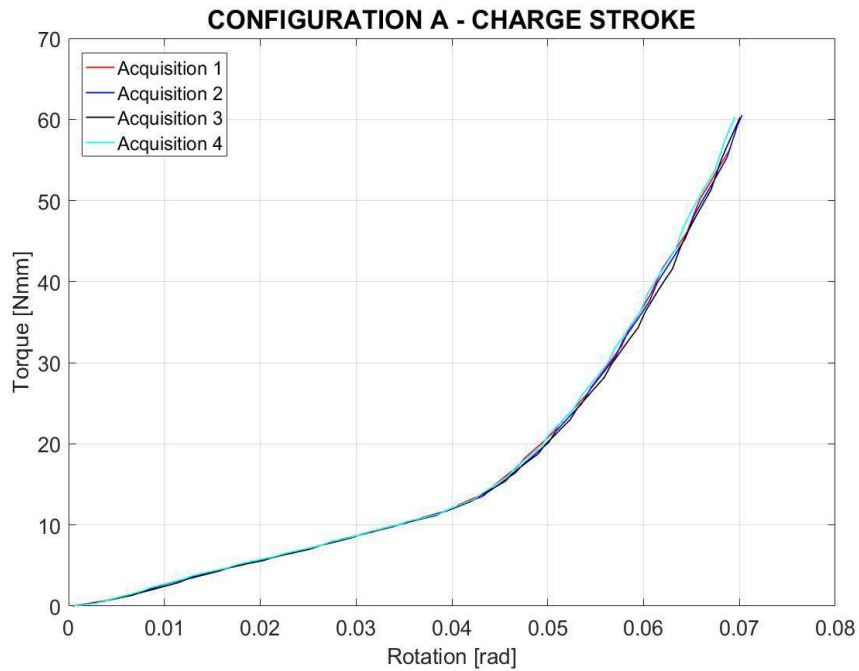


Figure 3.6 – Characteristic curve, configuration A, coordinates transformation.

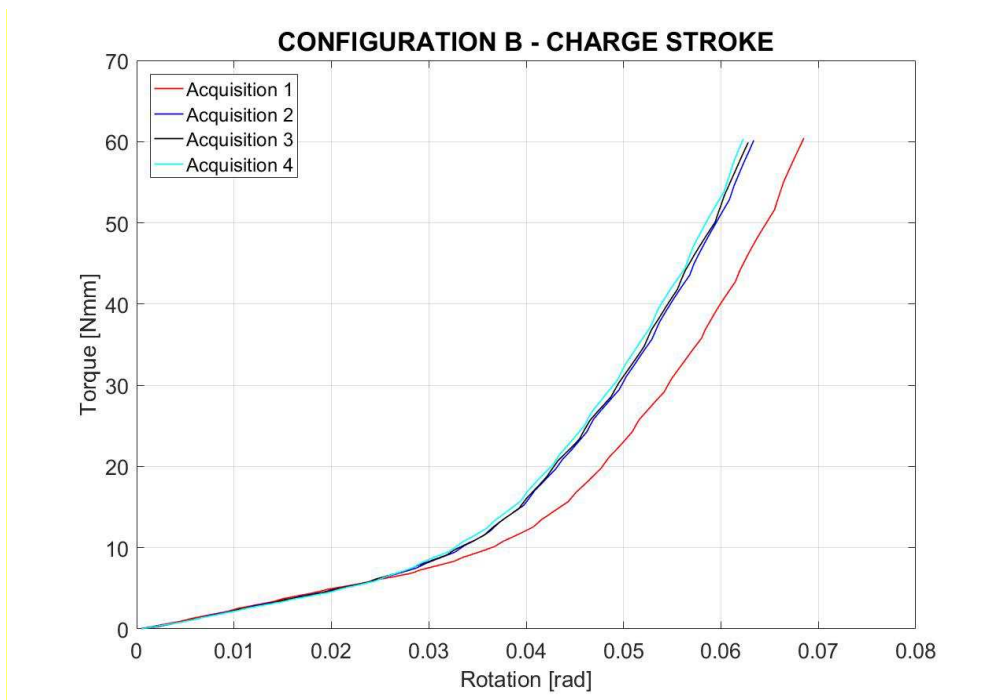


Figure 3.7 – Characteristic curve, configuration B, coordinates transformation.

The stiffness is computed as the punctual derivative of the torque/rotation data according to Eq.3.4:

$$k = \frac{C}{g} \left[\frac{Nmm}{rad} \right] \quad (3.4)$$

The curves showing the stiffness trend for configuration A is presented in Figure 3.8.

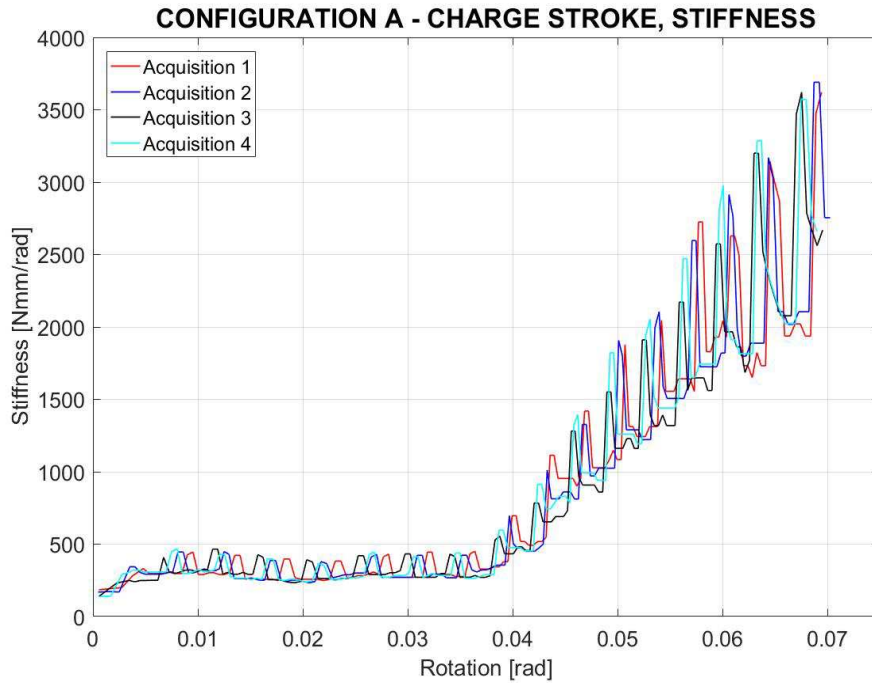


Figure 3.8 – Characteristic curve, configuration A, stiffness trend.

The significant displacement, useful for the stiffness computation, ranges between 0 rad and 0.04 rad. For rotations higher than 0.04 rad, the sudden increase of the stiffness value suggests contacts/seizure within the device. The significant range is presented in Figure 3.9.

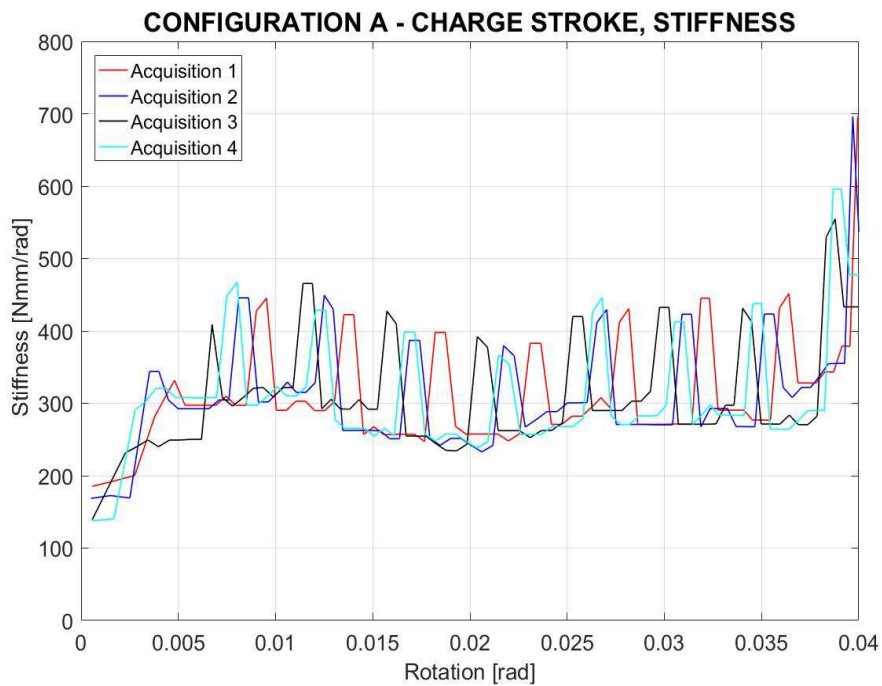


Figure 3.9 – Characteristic curve, configuration A, stiffness trend within significant range.

The curves showing the stiffness trend for configuration B is presented in Figure 3.10.

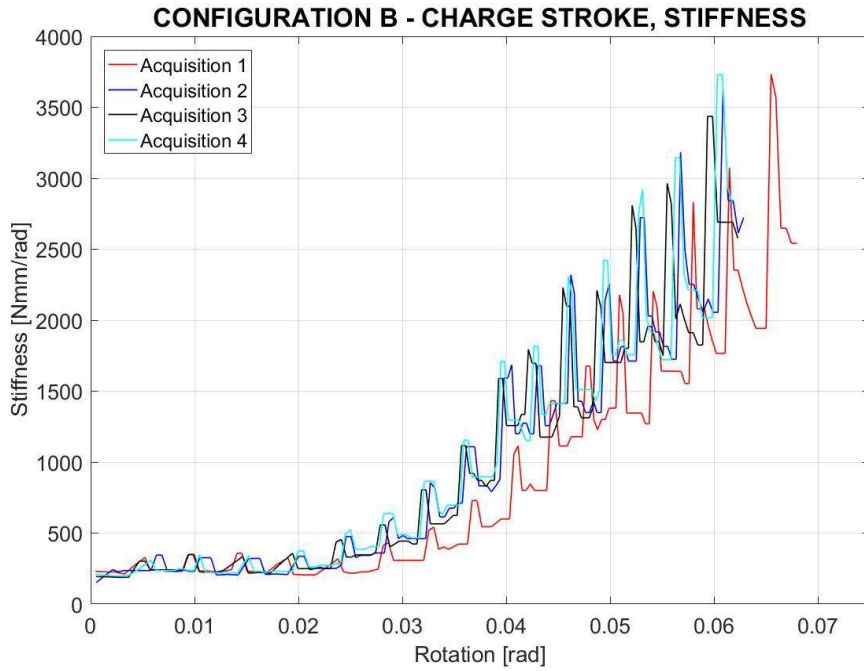


Figure 3.10 – Characteristic curve, configuration. B, stiffness trend.

The same significant displacement range 0 - 0.04 rad is considered for configuration B and presented in Figure 3.11.

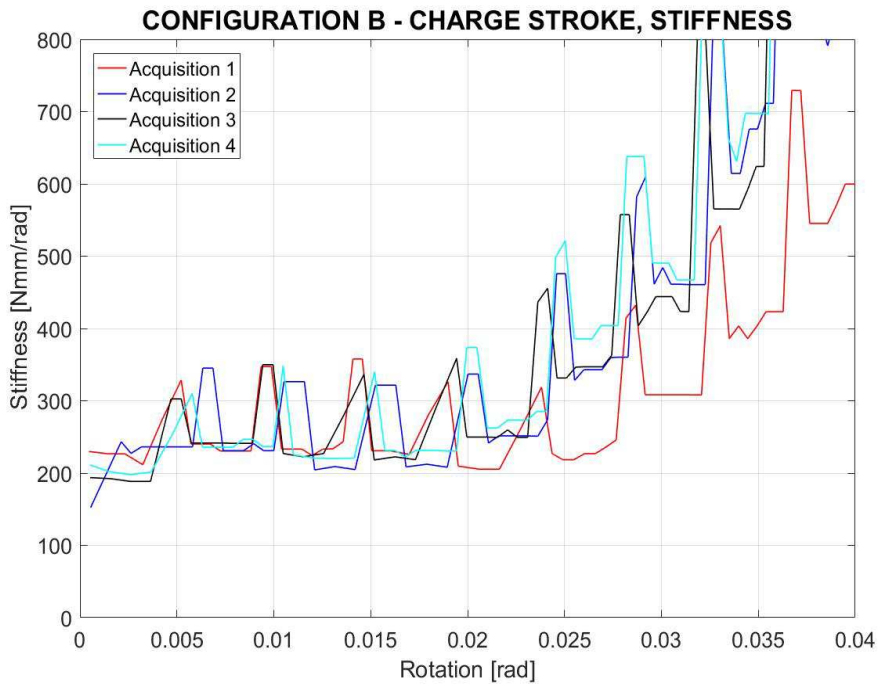


Figure 3.11 – Characteristic curve, configuration B, stiffness trend within significant range.

It is important to note the asymmetry between the two configurations over the same significant range. This suggests that the system, at steady condition, is not perfectly aligned with respect the ideal pitch line at 0°.

In this sense, a further curve-cleaning step is performed.

Furthermore, both characteristics show spikes, sharp and cyclical increase in stiffness, probably caused by the measuring machine.

This spikes have to be removed in order to obtain a better approximation of the stiffness.

The numerical values for the rotational stiffness for both configuration are presented in table 3.2

Table 3.2 – Results for rotational stiffness for pitch motion.

Property	Unit of measurement	Value
Rotational stiffness, config. A	[Nmm/rad]	283.99
Rotational stiffness, config. B	[Nmm/rad]	233,67

3.1.1.2 Rotational stiffness: roll motion

In order to ascertain the symmetrical behaviour of the component two different configurations were tested, corresponding to the two sides of the Omega pad.

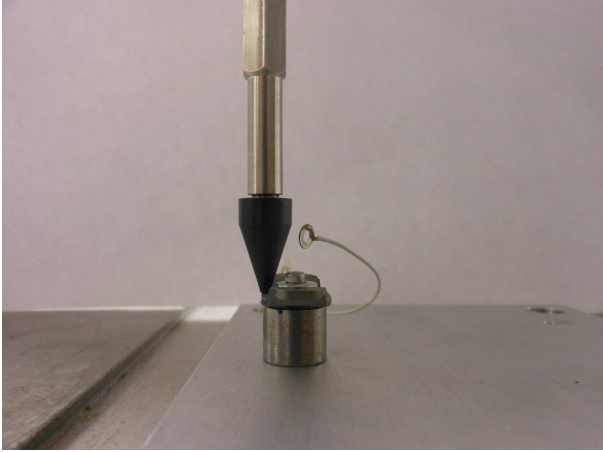


Figure 3.12 – Test setup, configuration A.

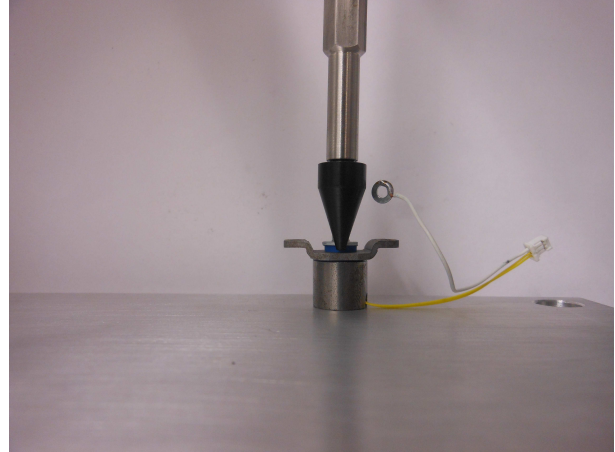


Figure 3.13 – Test setup, configuration B.

As depicted in Figure 3.12 and Figure 3.13, a conical probe is adopted.

The load is applied on two point symmetric with respect to the component longitudinal centerline plane.

For each configuration are collected:

- configuration A: 5 sets of data;
- configuration B: 3 sets of data.

These data are then manipulated in MATLAB in order to produce the characteristic curves of the device, showing the displacement [mm] on X-axis and the applied load [N] on Y-axis.

In Figure 3.14 and Figure 3.15 are presented the characteristic curves of the acquisition related to configuration A and B.

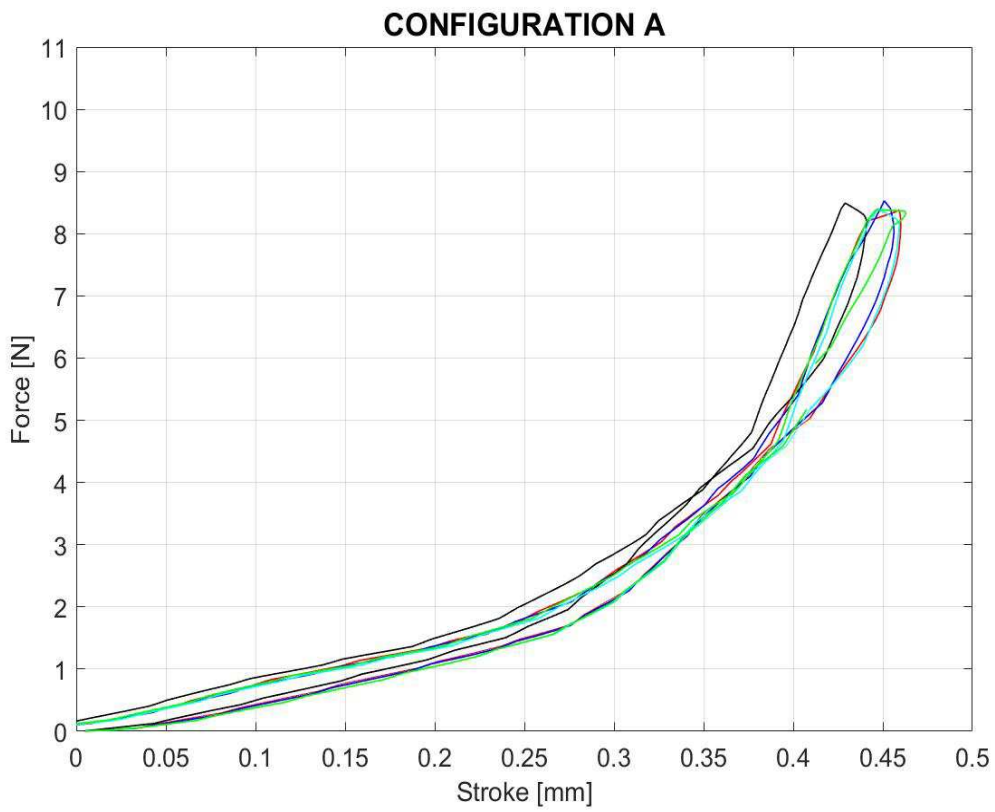


Figure 3.14 – Characteristic curve, configuration. A.

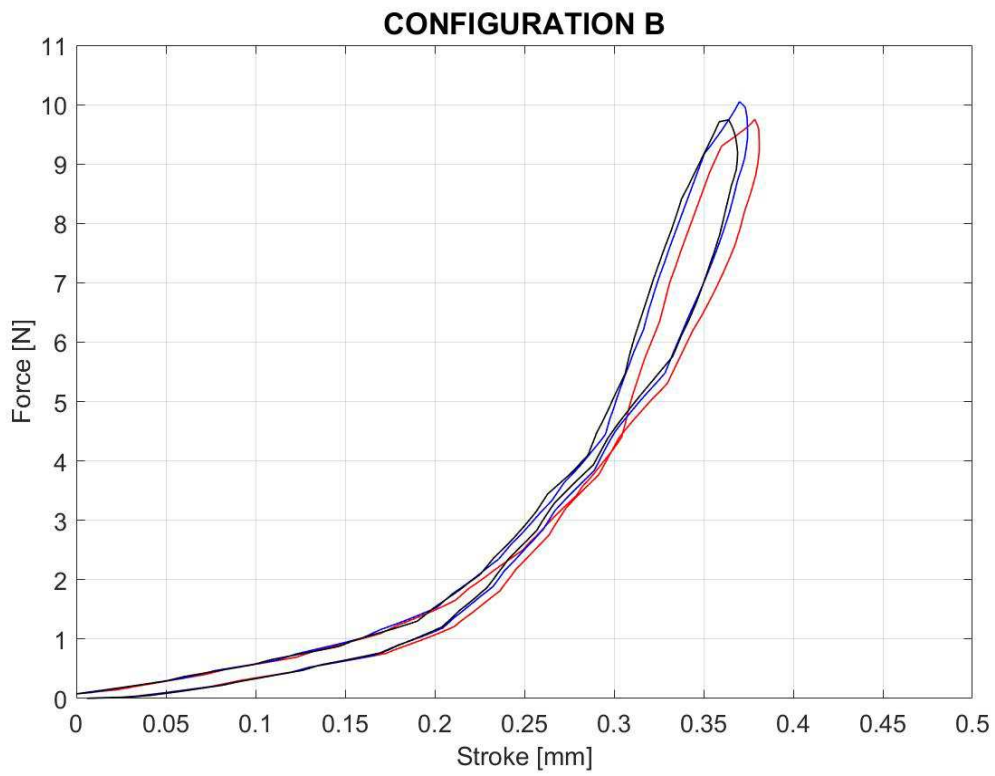


Figure 3.15 – Characteristic curve, configuration. B.

For analysis are considered only the charge strokes.

Being the analysis focused on the acquisition of the rotational stiffness, a transformation the of coordinates is required.

The transformation is computed considering Eq. 3.1 and 3.3, here briefly reported, and Eq. 3.5 which defines the lever arm value.

$$C = F \cdot b \quad (3.1)$$

$$\vartheta = \arcsin\left(\frac{z}{b}\right) \sim \frac{z}{b} \quad (\text{for small oscillations approximation}) \quad (3.3)$$

$$b = 6 \text{ mm} \quad (3.5)$$

where:

- C is the resulting torque [Nmm];
- F is the applied axial load [N];
- b is the arm of the applied torque [mm];
- z is the displacement along Z axis of the point where the force is applied [mm];
- ϑ is the angle corresponding to the axial displacement [rad].

The following characteristic curves are obtained.

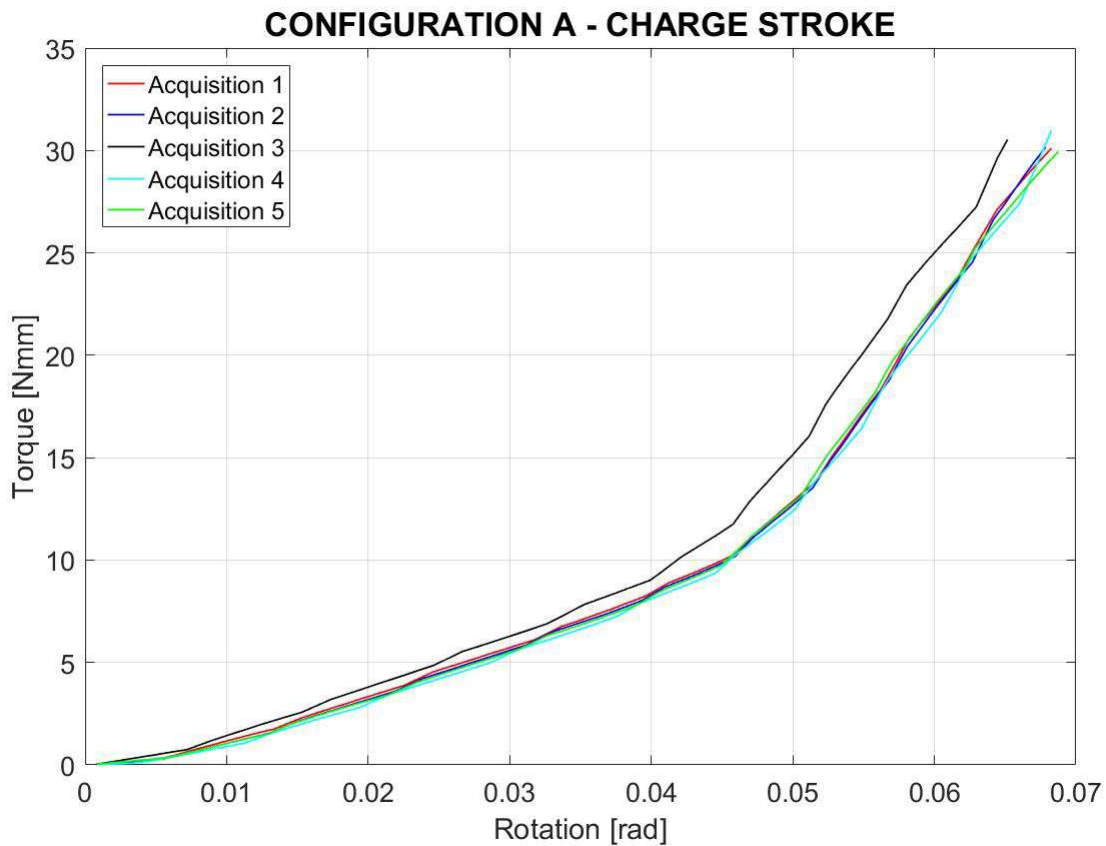


Figure 3.16 – Characteristic curve, configuration A, coordinates transformation.

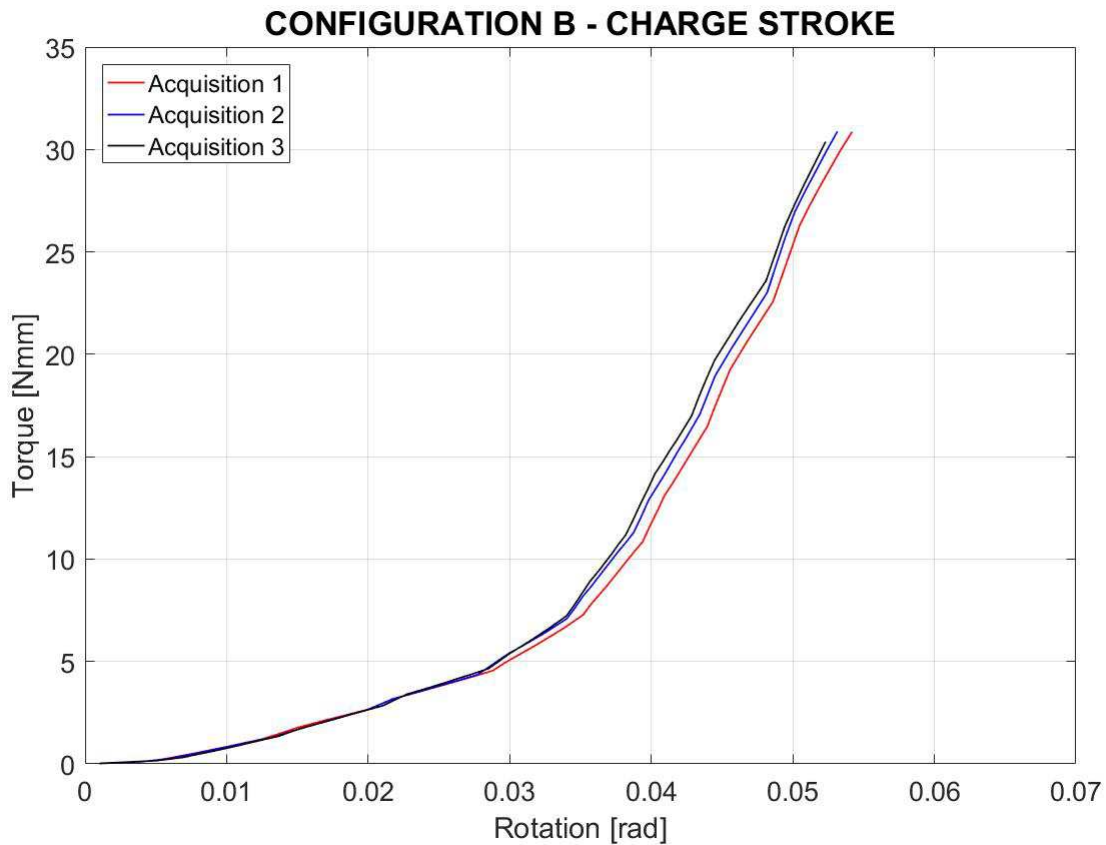


Figure 3.17 – Characteristic curve, configuration B, coordinates transformation.

It is important to note that, the range which is suitable for the stiffness computation is the linear one, which ranges between 0 - 0.04 rad approximately.

The increase in slope which takes place in the second parts of the characteristics is hypothesized to be caused by has to be ascribed to interferences/seizures within the device.

Furthermore, it can be highlighted the presence of an asymmetry in the behaviour of the device, which results in the fact that the linear range on one side of the Omega pad (configuration B) is lower than the other side (configuration A).

This asymmetric behaviour is experienced also during the pitch motion analysis, par. 3.1.1.1..

Considering the stiffness, the computation, is carried out considering the punctual derivative according to Eq. 3.4.

The stiffness trend for configuration A is presented in Figure 3.18.

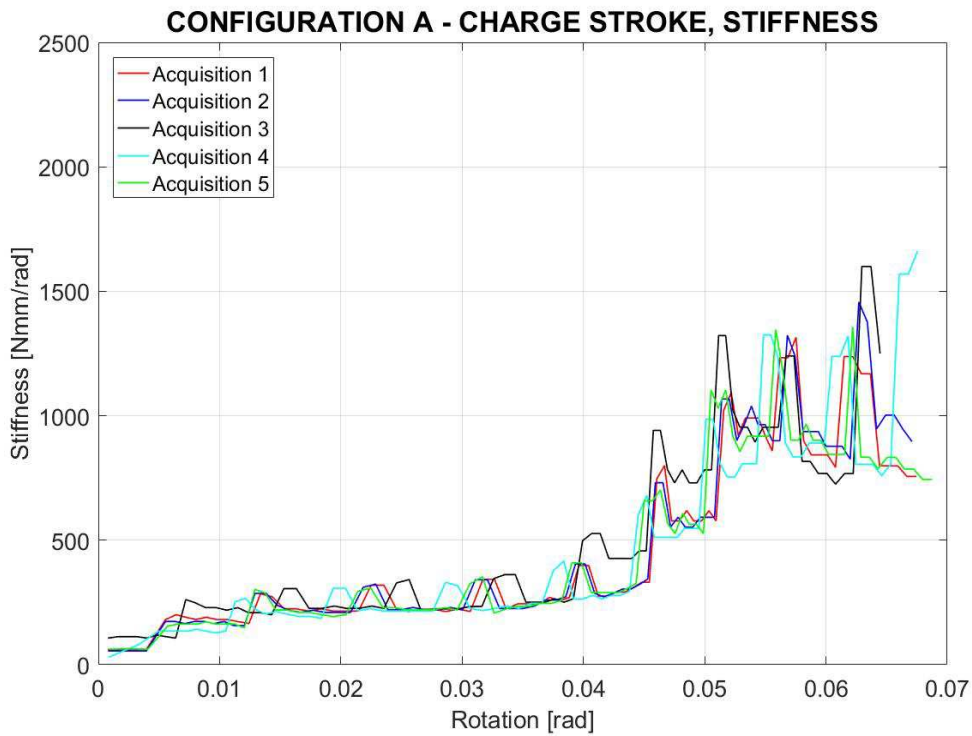


Figure 3.18 – Characteristic curve, configuration. A, stiffness trend.

As stated before, the significant displacement, useful for the stiffness computation, ranges between 0 rad and 0.04 rad. For rotations higher than 0.04 rad, the sudden increase of the stiffness value confirms the hypothesis of contacts/seizure within the device made in the previous pages. The significant range is presented in Figure 3.19.

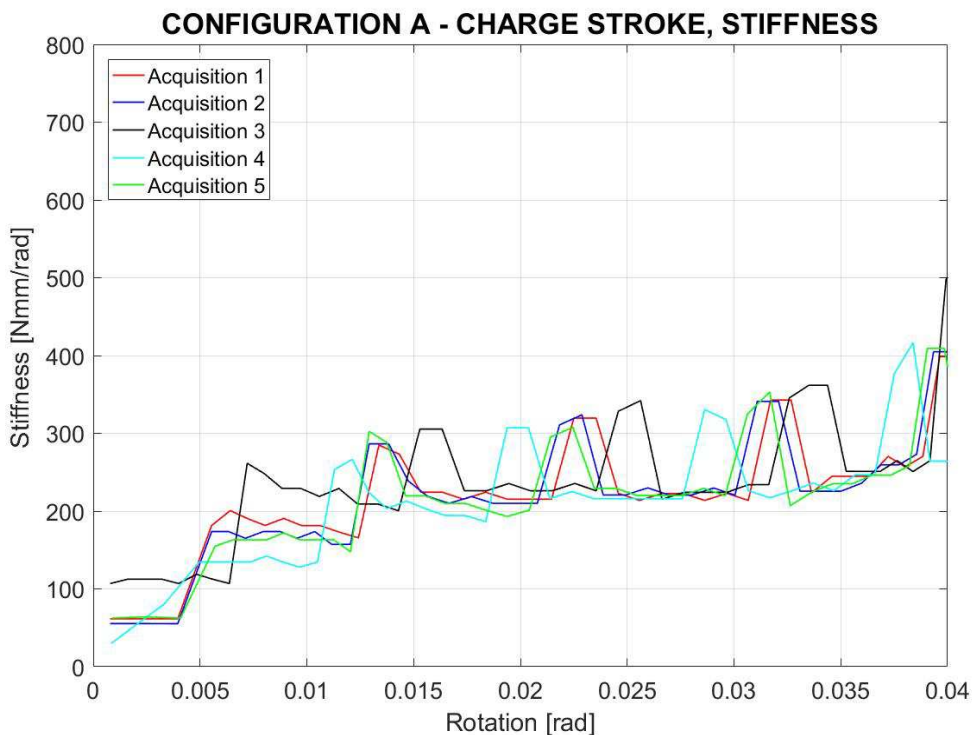


Figure 3.19 – Characteristic curve, configuration. A, stiffness trend within significant range.

The curves showing the stiffness trend for configuration B is presented in Figure 3.20.

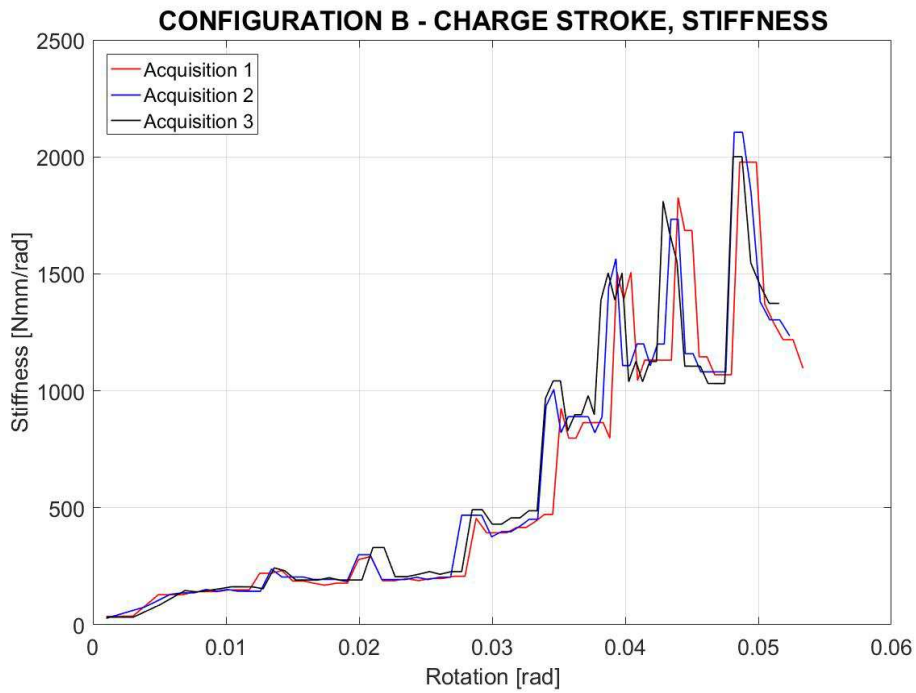


Figure 3.20 – Characteristic curve, configuration. B, stiffness trend.

A focus over the same significant displacement range 0 - 0.04 rad is presented in Figure 3.21.

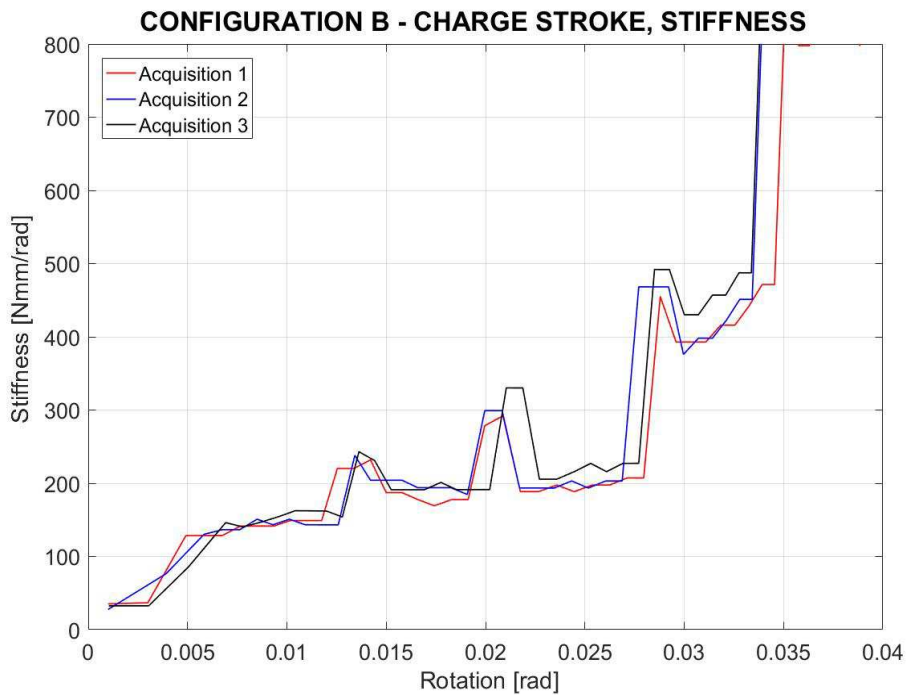


Figure 3.21 – Characteristic curve, configuration B, stiffness trend within significant range.

It is important to note that the asymmetry highlighted between the characteristic curves in Figures 3.16 and 3.17 results also in curves representing the stiffness. In this sense, a further curve-cleaning for configuration B is performed. The numerical values for rotational stiffness of both configuration, after the spikes removal, is presented in Table 3.3.

Table 3.3 – Results for rotational stiffness for roll motion.

Property	Unit of measurement	Value
Rotational stiffness, config. A	[Nmm/rad]	200.44
Rotational stiffness, config. B	[Nmm/rad]	177.31

3.2 Experimental analysis: axial stiffness

To characterize the equivalent stiffness of the axial spring, a similar procedure is adopted. The measuring machine is set up according to the parameters in Table 3.4:

Table 3.4 – Measuring machine set up parameters.

Characteristic	Property	Value
Force sensor	Gain	0.5
	Maximum Force [N]	5
	Offset [N]	- 0.03
Position sensor	Gain	0.005
	Maximum distance [mm]	5
	Offset [mm]	0
Supply voltage	Voltage [V]	24
Feeding speed	Speed [μm]	25

Two different configuration are considered:

- configuration A is based on a small probe that we will call probe type A;
- configuration B is based on a bigger probe that we will call probe type B.

In Figure 3.22 and Figure 3.23 are presented the configurations.

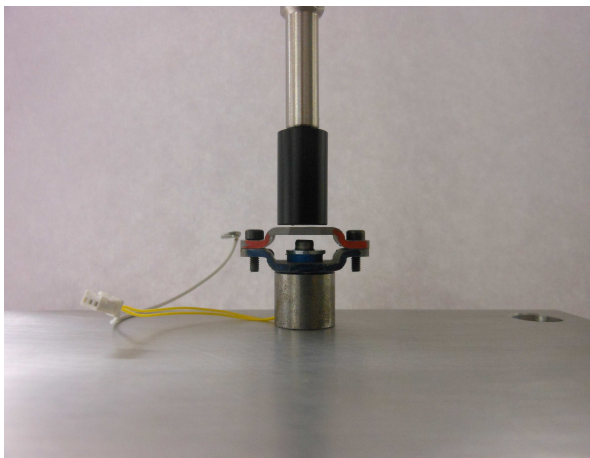


Figure 3.22 – Axial stiffness set up, probe type A.

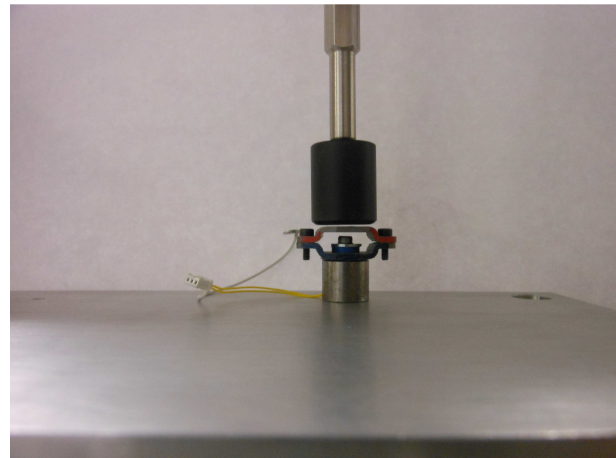


Figure 3.23 – Axial stiffness set up, probe type B.

For each configuration 2 sets of data are collected.

The data are then exported and elaborated on MATLAB in order to produce the force-stroke trend.

Figure 3.24 and 3.25 show the characteristics curves.

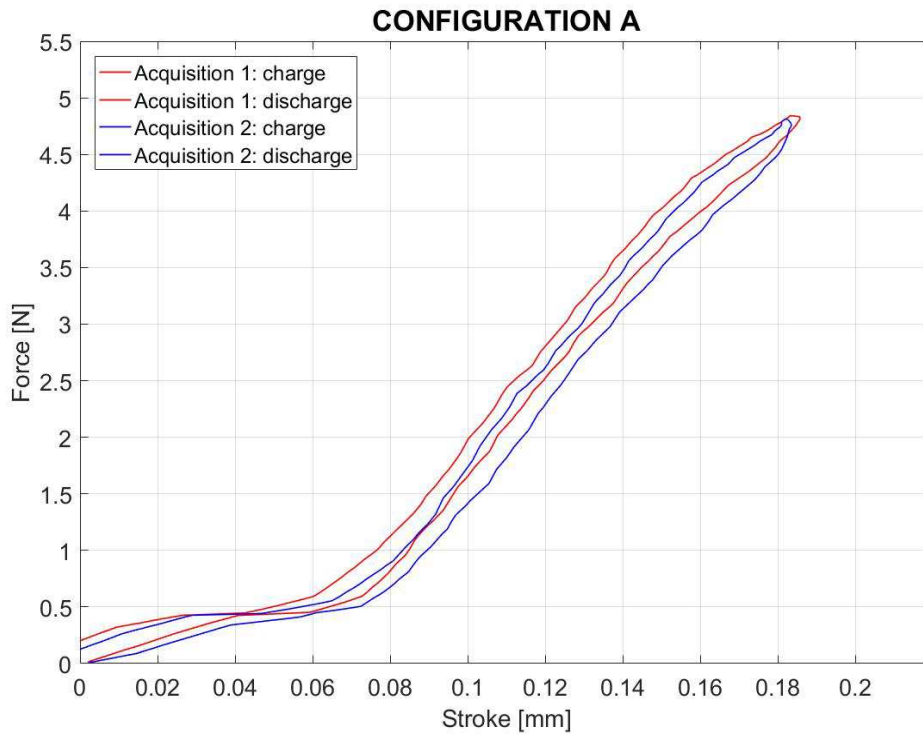


Figure 3.24 – Characteristic curve, probe type A.

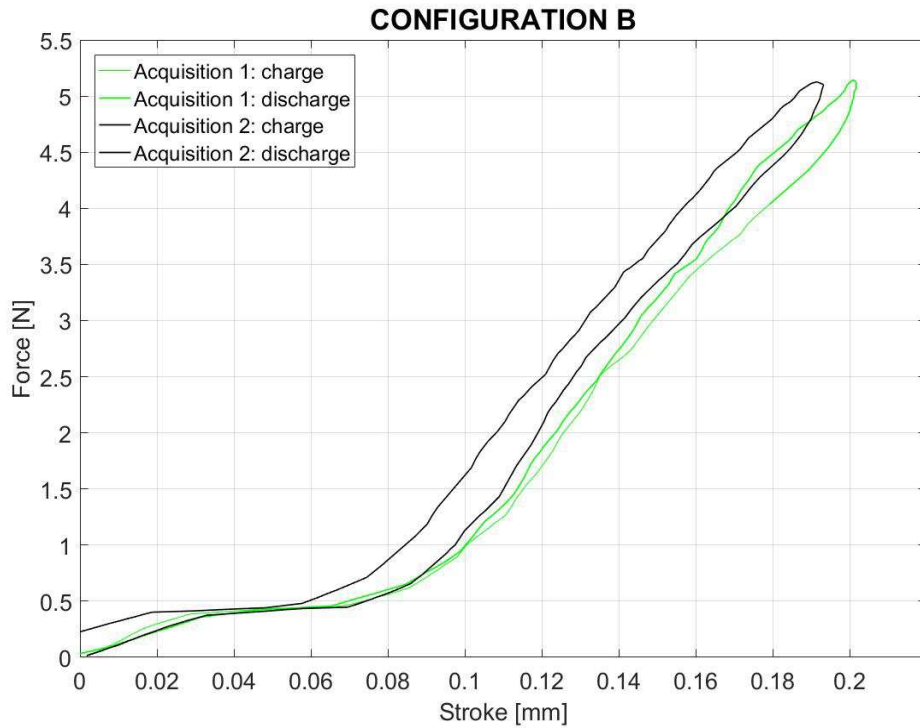


Figure 3.25 – Characteristic curve, probe type B.

Being the characteristic made by a charge and a discharge stroke it is possible to consider them separately. The charge-stroke trend is thus presented in Figure 3.26 for probe type A and Figure 3.27 for probe type B.

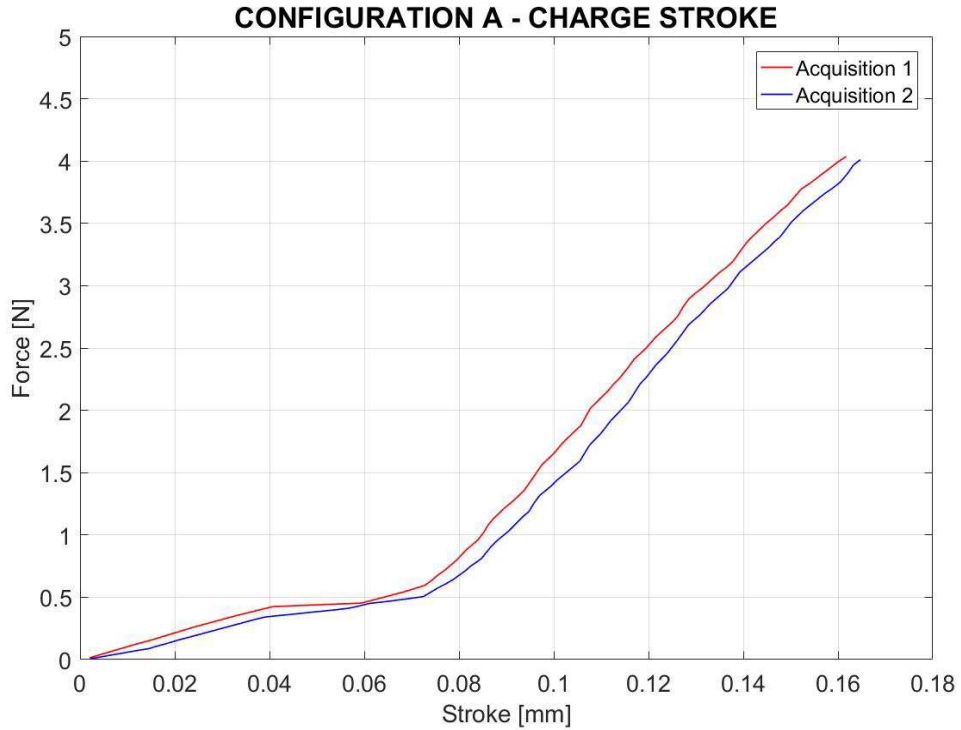


Figure 3.26 – Characteristic curve, charge stroke, probe type A.

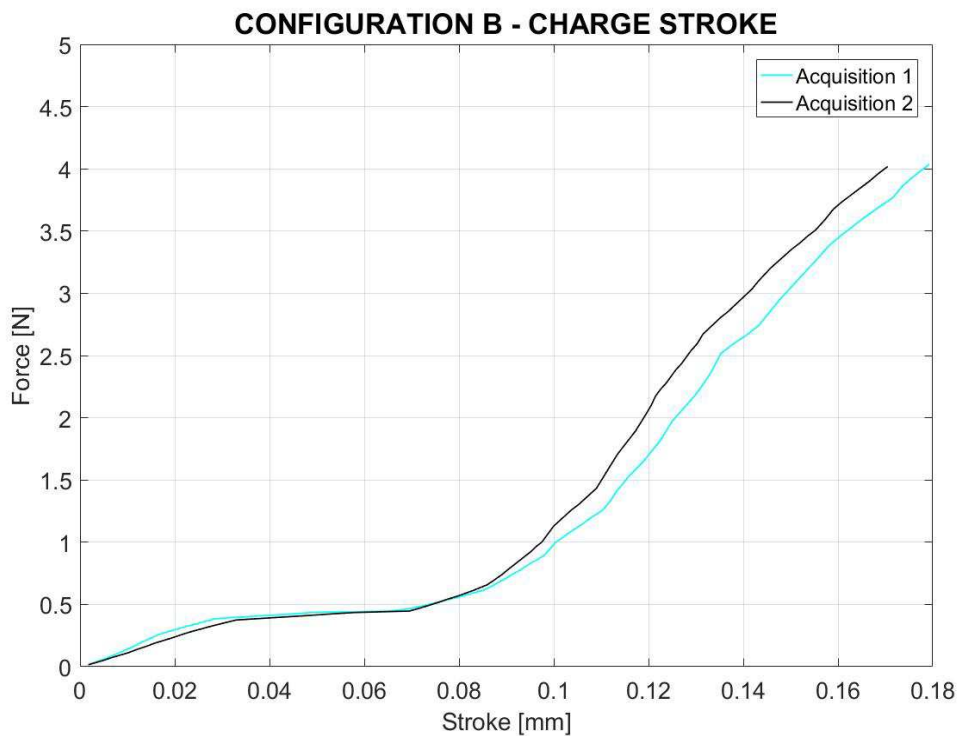


Figure 3.27 – Characteristic curve, charge stroke, probe type B.

Both characteristics show 2 main trends which displays a significant slope variation. The first one covers the stroke between 0 mm and 0.08 mm, the second one covers the stroke from 0.08 mm and 0.18 mm, the end of stroke point, where the limit load is reached.

The trends are connected each other through an inflection point where the slope is null.

This particular behaviour can be explained with a the mutual slipping between the probe and the omega pad and between the two omega pads.

Considering that, the part of the characteristic which is significant for the purpose of the computation of the stiffness is second one.

The stiffness computation requires the punctual derivative of each characteristic.

Results are presented in Figure 3.28 for configuration A and Figure 3.29 for configuration B.

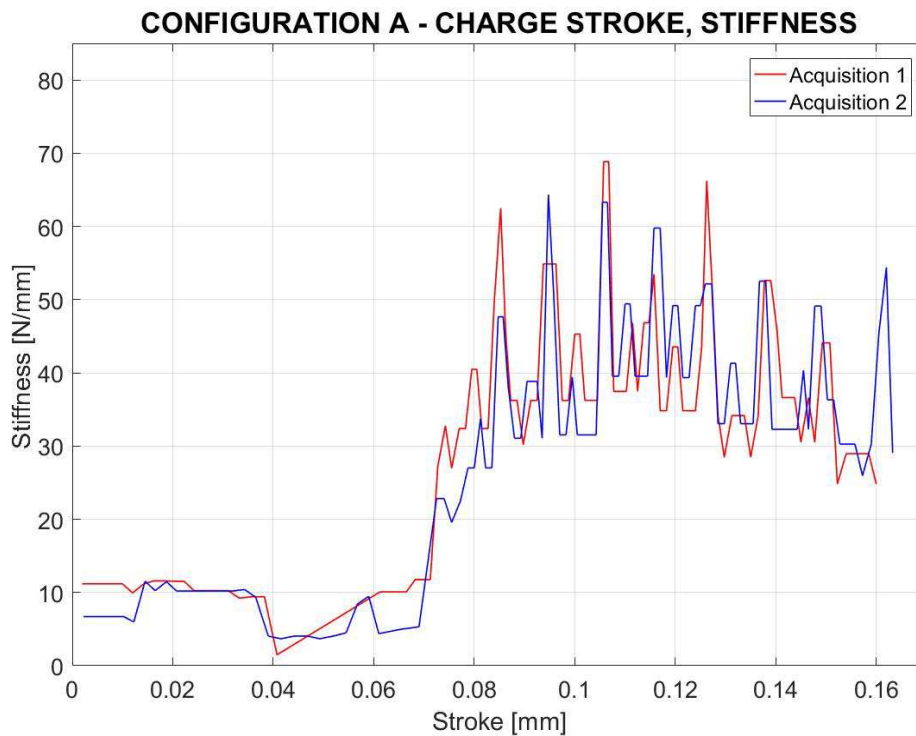


Figure 3.28 – Characteristic curve, probe type A, stiffness trend.

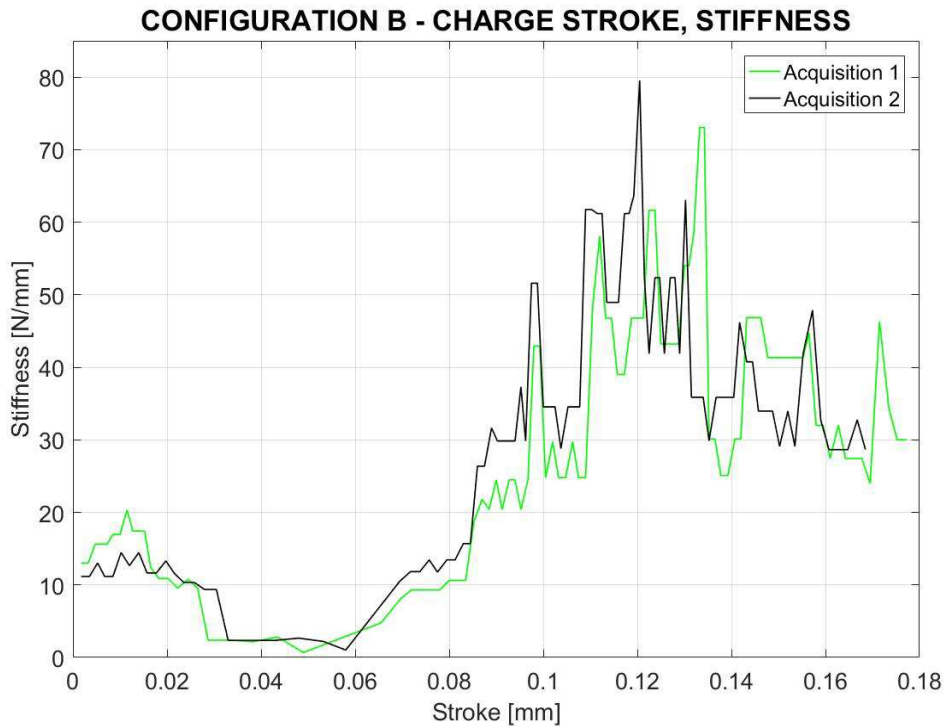


Figure 3.29 – Characteristic curve, probe type B, stiffness trend.

Both characteristics show spikes, probably caused by the measuring machine.

These spikes have to be removed in order to obtain a better approximation of the stiffness.

Furthermore, whereas configuration A shows a clear trend in the range between 0.08 mm and 0.16 mm, configuration B does not allow to compute any value for the stiffness.

Because of that, configuration B is discarded.

The value of the axial stiffness is thus computed on the charge and discharge strokes of configuration A for the significant range 0.08 - 0.16 mm

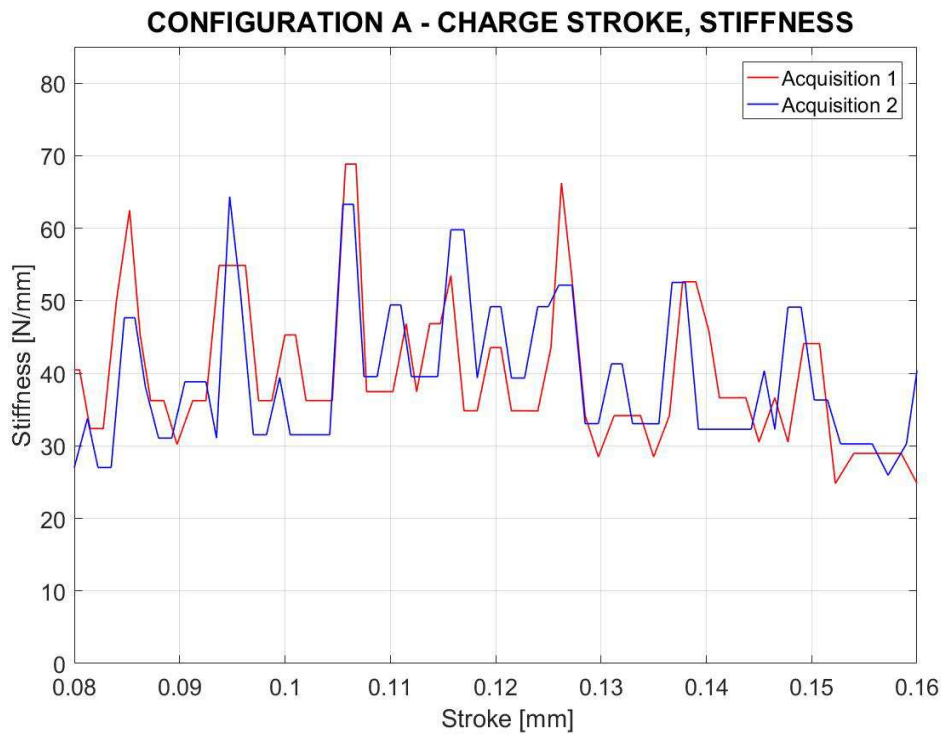


Figure 3.30 – Characteristic curve, probe type, charge stroke, significant range.

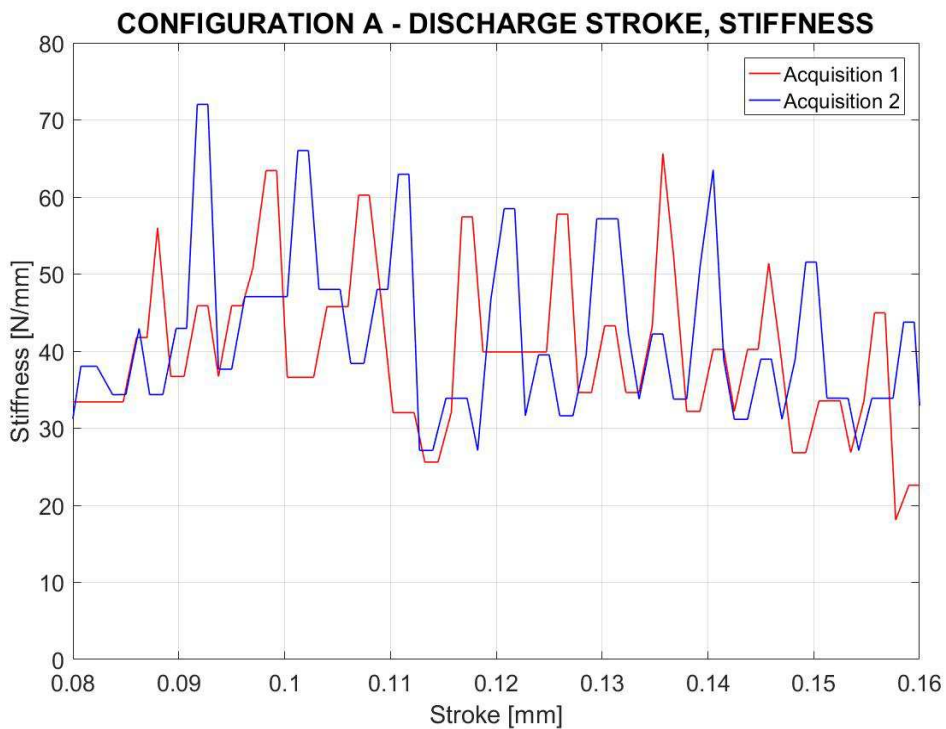


Figure 3.31 – Characteristic curve, probe type, discharge stroke, significant range

The value for the axial stiffness is computed eliminating the spikes from the characteristic and computing the average between the results of each set of data.

Results are presented in Table 3.5

Table 3.5 – Results, axial stiffness

Property	Unit of measurement	Value
Axial stiffness (A, charge, set 1)	[N/mm]	37.19
Axial stiffness (A, discharge, set 1)	[N/mm]	37.08
Axial stiffness (A, charge, set 2)	[N/mm]	37.40
Axial stiffness (A, discharge, set 2)	[N/mm]	38.09

The final value for axial stiffness is computed as the average between the previous results.

3.3 Conclusions

The objective of this chapter is to compute the axial and rotational stiffness of the physical device . Results shows the device has an asymmetric behaviour with respect to the transversal and longitudinal centerlines. This behaviour has to be ascribed most likely to the slip displacement over XY plane of the omega pad with respect the elastic elements. However, these displacements cannot be measured with this type of setup.

Furthermore, different stiffness values are computed between pitch and roll motion, which were expected to be similar. these differences suggests a possible misalignment of the system with respect to its normal configuration at steady state condition.

Considering that and reminding that the aim of this work is to highlight the method behind the modelling procedure of a physical body, the rotational stiffness is computed by averaging the values described in Table 3.2 and Table 3.3.

Axial stiffness is obtained by averaging the values described in Table 3.5.

Below are presented the results of the experimental static analyzes.

Table 3.6 – Results, stiffness values for experimental static analyzes.

Property	Unit of measurement	Value
Axial stiffness	[N/mm]	37.4
Rotational stiffness	[Nmm/rad]	223.9

4. Finite elements static analysis

To produce a model which is representative of the physical body, besides the geometry and the inertial properties, which are assigned in chapter 1 and 2, it is required to assign the elastic properties to the elastic elements of the model, which, in this case, are the spacer and the o-ring.

The objective of this chapter is to present the procedure through which are determined the Young modules of these elements and the numerical results.

It is a trial and error procedure involving FEM static analysis performed on Solidworks.

In the following paragraphs are presented the setup parameters and the relative numerical results concerning the computed stiffness of the model.

4.1 Results from experimental analyses

Experimental analyzes results, presented in Table 3.6 and here briefly reported, determines the values for the axial and rotational stiffness of the device.

Table 4.1 – Results, stiffness values for experimental static analyzes.

Characteristic	Property	Value
Axial stiffness	K, [N/mm]	37.4
Rotational stiffness	K, [Nmm/rad]	223.9

It is important to remind that these values are the results of an averaging process. Chapter 3 shows clearly that the range in which the stiffness values fall is significantly wide. This can be ascribed to different reasons:

- non linearity of the system;
- misalignment of the device under analysis;
- measurements errors.

Nevertheless, being this work mainly focused on the method, and considering the simplifications made previously, it is considered an average value for both axial and rotational stiffness.

4.2 Procedure

The objective of the analysis is to compute the value of the Young modulus (E) for the elastic elements, the spacer and the o-ring, that allow to best fit the behaviour of the physical body.

The Finite Element Analysis (FEA) gives the tool to reach the objective.

In order to perform a FEA, the following algorithm is required:

1. creation of mathematical model and clean-up procedure;
2. material properties and boundary definition;
3. parameter setting for the analysis;
4. test run;
5. results check: displacements along Z axis of specific points of the model
6. data comparison with experimental results;
7. elastic properties update: Young modulus

Being a trial and error process, the algorithm can be stopped when the error between experimental results and static analysis results is small enough to consider the mathematical model to be reliable.

4.2.1 Mathematical model

The body is modelled following the indications from the technical drawings, as presented in chapter 1 and 2.

Each component is designed and then the assembly is created, considering the various coupling constraints. This step is complete when the assembly is completely determined, so that no dof is left undefined.

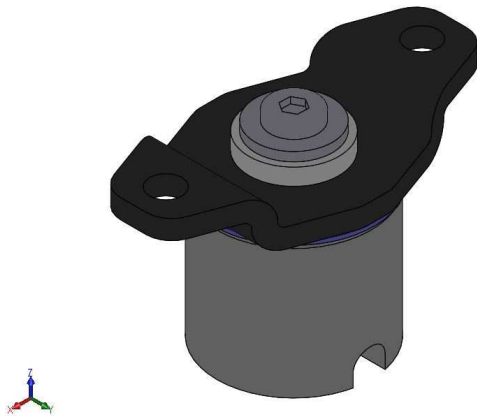


Figure 4.1 – Mathematical model, isometric view.

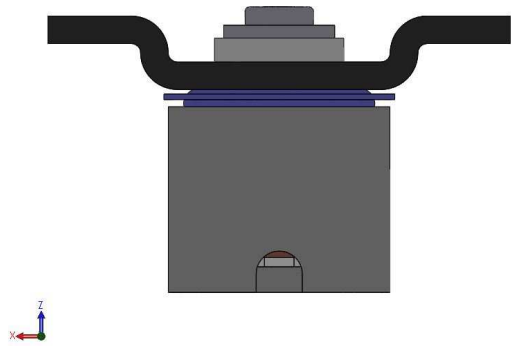


Figure 4.2 – Mathematical model, front view.

Considering that, the discrete model, defined in chapter 1, that approximates the physical body into a mass-spring-damper system, shows that the axial and rotational actions can be simplified as follows:

- axial behaviour related to o-ring only;
- rotational behaviour related to: oring and spacer, that act like a series of springs.

4.2.1.1 Clean up

This step is required in order to make the geometry suitable for the meshing process. In particular, each feature that displays high curvatures, edges with sharp angles, or infinitesimal contact areas has to be "simplified" in order to allow the correct discretisation.

A wrong meshing procedure of these areas would lead to error in the analysis results.

The clean-up procedures is required for the following components:

- o-ring;
- metallic body;
- flanged screw.

The o-ring circular section produces an infinitesimal contact area which has to be increased by flattening the cross section.

The metallic body and the screw are joined together through a threaded coupling, which produces errors during the mesh creation. In this way, the coupling is modified by considering a shaft-bore coupling through a common diameter between the two elements.

The mass variation due to the modified geometry can be neglected thanks to the fact that we're dealing with fixed component which does not take active actions in the analysis.

4.2.2 Material properties and boundary conditions

Once the geometry is fixed the model is updated with the materials.

Table 1.1, presented in chapter 1 and here briefly reported, shows the material of each component of the assembly.

Table 4.2 – Materials and components.

Material	Sub component
11SMn30 (1.0715, AISI 1213)	Metallic ELM body
	Omega Pad
Copper	Coil
PA6 GF30	Plastic body
Silicone 20 ShA*	O-Ring
Silicone 80 ShA*	Spacer
Alloy Steel	Flanged screw

The marked* materials are the ones which are going to be updated by tuning the Young modulus.

Speaking about the boundary conditions, we have to set both constraints and external loads.

Considering the constraints, a fixed joint is defined at the base of the metallic body, locking all dofs. In this way the device, and in particular the omega pad, is allowed to have 3 principal motions already presented in chapter 3, here briefly reported:

- pitch, rotation around transversal Y-axis;
- roll, rotation around longitudinal X-axis;
- axial, displacement along its Z-axis.

These motions are presented in Figure 4.3.

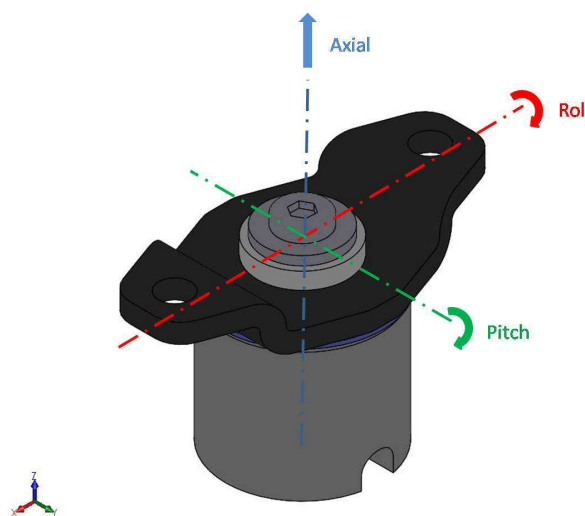


Figure 4.3 – Omega pad principal motions.

The external loads are applied considering the setup configurations of the experimental static analysis. The body is tested considering 3 load conditions which aim to study the principal motions.

As stated in paragraph 4.2.1, the axial behaviour is considered to characterize the o-ring only, while pitch and roll behaviour are considered in order to study the spacer, freezing the o-ring elastic properties.

In particular, the roll motion is tested to check the results from the pitch motion once the young modules of the elastic elements are determined.

In the next paragraphs are presented the configurations and the applied load together with the results of the analyses.

4.3 Axial motion analysis

The axial motion is analyzed in order to investigate the elastic modulus for the o-ring element.

The objective of the analysis is to obtain a value of the stiffness around 37 N/mm, coming from the averaging of the data from experimental analysis.

Each analysis is associated with a report in which are presented the input parameters and the results concerning the displacement along Z axis of the specific points.

The stiffness is then computed as follows:

$$k = \frac{F}{z} \left[\frac{N}{mm} \right] \quad (4.1)$$

where:

- F is the applied load [N];
- z is the absolute value of displacement along Z axis [mm].

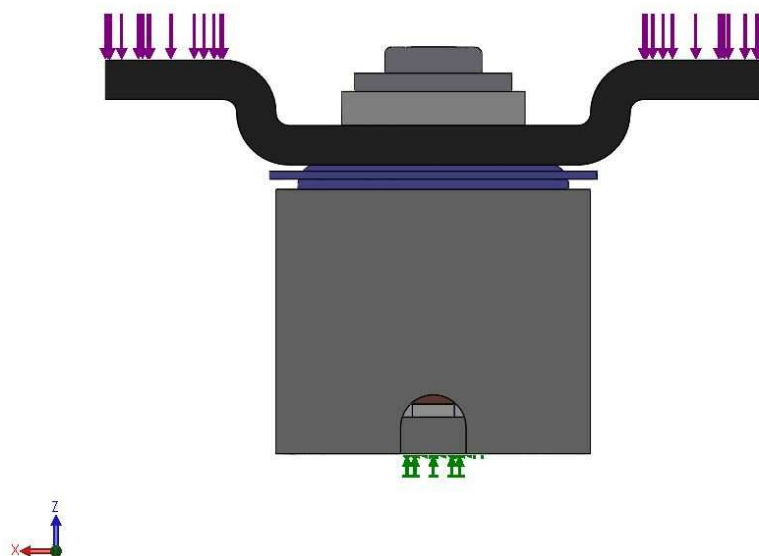


Figure 4.4 – Axial motion analysis, model setup, <X,Z> plane.

4.3.1 Mathematical model refinements

Considering the loads acting on the system, an additional refinements to the mathematical model is performed, reducing the computation time and limiting possible errors due to contacts and interferences that could occur between the spacer and the omega pad.

In particular, it is possible to state that in this specific configuration, which implies an axial load along Z negative, the spacer does not take action. According to this, the spacer is deactivated from the analysis.

The refines model is presented in FIGURE 4.5.

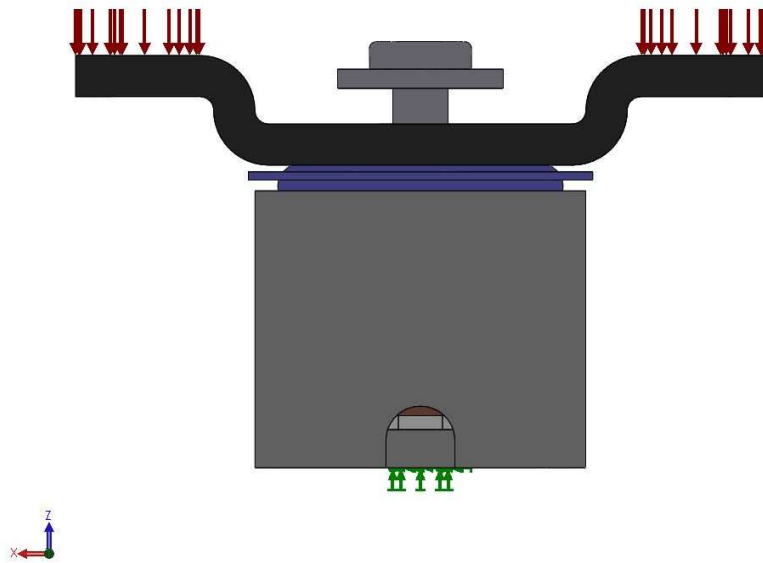


Figure 4.5 – Refined mathematical model, $\langle X, Z \rangle$ plane.

4.3.2 Results

In the following paragraphs each analysis is presented and described with a short report.

4.3.2.1 Static analysis 1 - axial

The first analysis is performed considering the non-refined model, with the spacer as an active element.

Table 4.3 – Mesh parameters.

Parameter	Units of measurements	Value
Type of mesh	-	Tetraedric elements
Mesher	-	Curvature based
Number of Jacobian points	-	4
Max dimension	[mm]	1.594
Min dimension	[mm]	0.319
Nodes	-	31090
Elements	-	18246
AR<3	-	92.5
AR>10	-	0.159
AR max	-	22.41
Jacobian (distorted elements)	%	0

Table 4.4 – Analysis parameters.

Parameter	Units of measurements	Value
DOF	-	91980
Solver	-	FFE Plus
Spacer Young modulus	[N/m ²]	50000000
O-ring Young modulus	[N/m ²]	50000000
External load	[N]	1
Load application point		Omega pad wings
Restraints	-	Fixed geometry applied to the base of metallic body

A "no penetration contact type" between the following couples of elements is considered:

- flanged screw and spacer;
- spacer and omega pad;
- omega pad and o-ring;
- o-ring and plastic body

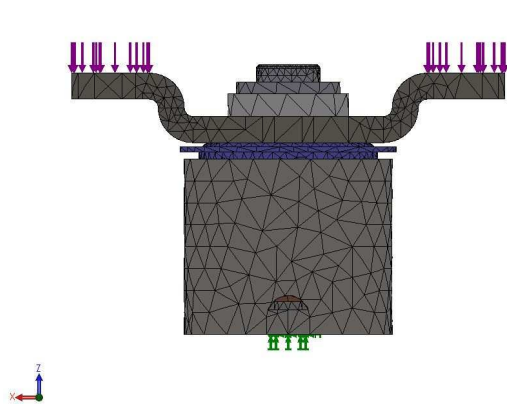


Figure 4.6 – Mathematical model, $\langle X,Z \rangle$ plane.

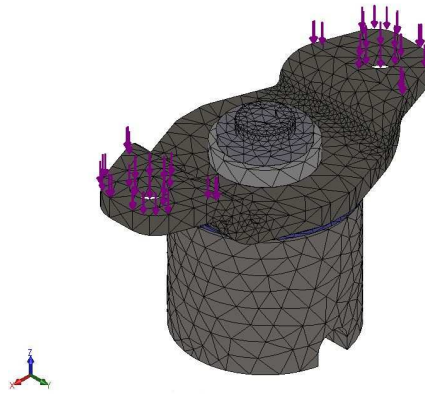


Figure 4.7 – Mathematical model, isometric view.

The current configuration does not allow any result for the analysis: an error concerning the failed preconditioning and the impossibility to compute any results is displayed. The refined model is thus considered for the next analyses.

4.3.2.2 Static analysis 2 - axial

In the following tables are presented the setup parameters.

Table 4.5 – Mesh parameters.

Parameter	Units of measurements	Value
Type of mesh	-	Tetraedric elements
Mesher	-	Curvature based
Number of Jacobian points	-	4
Max dimension	[mm]	1.594
Min dimension	[mm]	0.319
Nodes	-	29568
Elements	-	17368
AR<3	-	93
AR>10	-	0.173
AR max	-	23.961
Jacobian (distorted elements)	%	0

Table 4.6 – Analysis parameters.

Parameter	Units of measurements	Value
DOF	-	87438
Solver	-	FFE Plus
Spacer Young modulus	[N/m ²]	-
O-ring Young modulus	[N/m ²]	50000000
External load	[N]	1
Load application point		Omega pad wings
Restraints	-	Fixed geometry applied to the base of metallic body

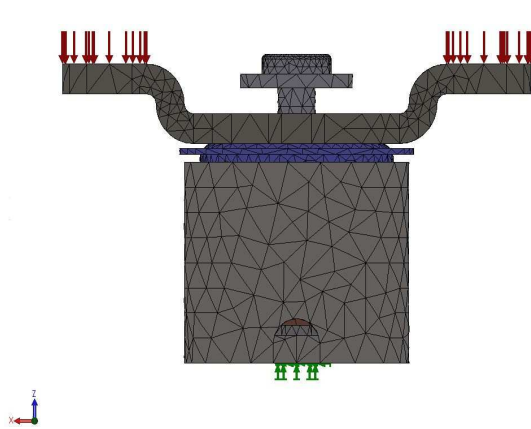


Figure 4.12 – Mathematical model, <X,Z> plane.

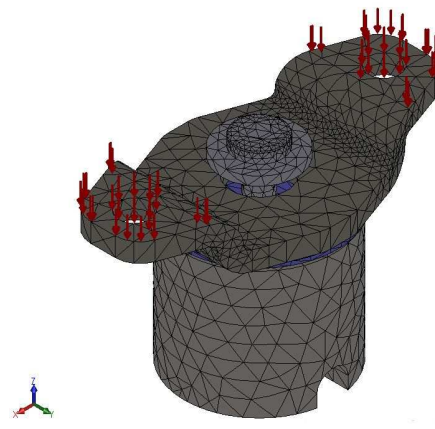


Figure 4.13 – Mathematical model, isometric view

It has to be noted that:

- In order to get rid from the previous analysis failed pre-conditioning, the spacer is excluded from the analysis. This new configuration does not affect the final results because the spacer contribution along axial displacement is null;
- No penetration contact type between the following elements is considered:
 - omega pad and o-ring;
 - o-ring and plastic body.
- Computation of FB forces parameter is enabled.

The results are presented in Table 4.7.

Table 4.7 – Static analysis 2 - axial, results.

Parameter	Units of measurements	Value
Time of computation	[s]	00:05:05
UZ	[mm]	-3.003E-3
Computed stiffness	[N/mm]	333
Error	[%]	790

Note that the measure relative to the displacements along Z (UZ) is computed taking as reference nodes 16314 and 16303.

Note that, during the experimental analysis, in order to be able to apply the load it was used an additional omega pad. Figure 4.14 shows the displacement graph of the device,

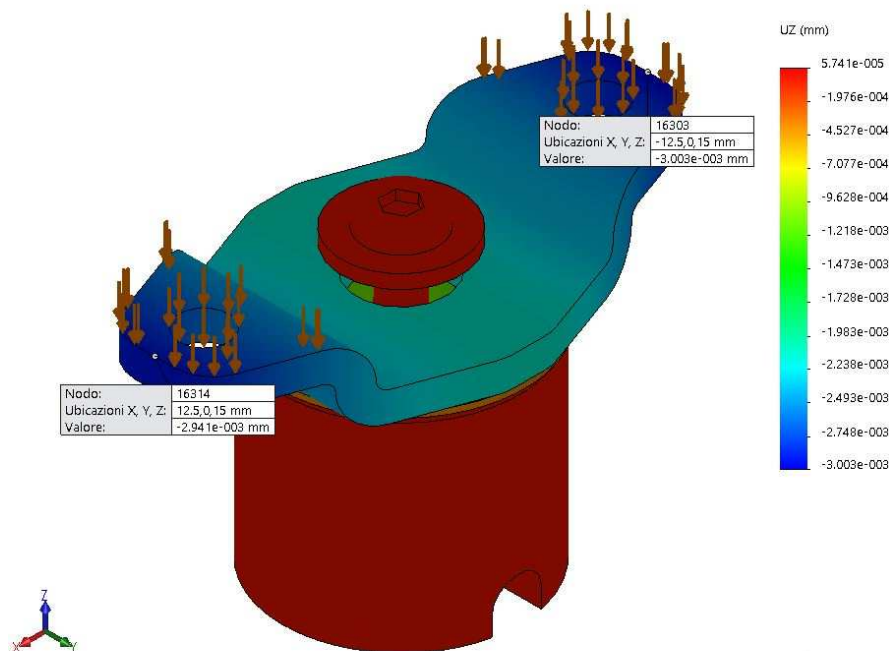


Figure 4.14 – Static analysis 2 - axial, displacement values.

Considering the results from the analysis, the value for the elastic modulus of the o-ring is lowered by 50%, down to $E = 25\text{MPa}$ (25000000N/m^2).

4.3.2.3 Static analysis 3 - axial

In the following tables are presented the setup parameters.

Table 4.8 – Mesh parameters.

Parameter	Units of measurements	Value
Type of mesh	-	Tetraedric elements
Mesher	-	Curvature based
Number of Jacobian points	-	4
Max dimension	[mm]	1.594
Min dimension	[mm]	0.319
Nodes	-	29568
Elements	-	17368
AR<3	-	93
AR>10	-	0.173
AR max	-	23.961
Jacobian (distorted elements)	%	0

Table 4.9 – Analysis parameters.

Parameter	Units of measurements	Value
DOF	-	87438
Solver	-	FFE Plus
Spacer Young modulus	[N/m ²]	-
O-ring Young modulus	[N/m ²]	25000000
External load	[N]	1
Load application point		Omega pad wings
Restraints	-	Fixed geometry applied to the base of metallic body

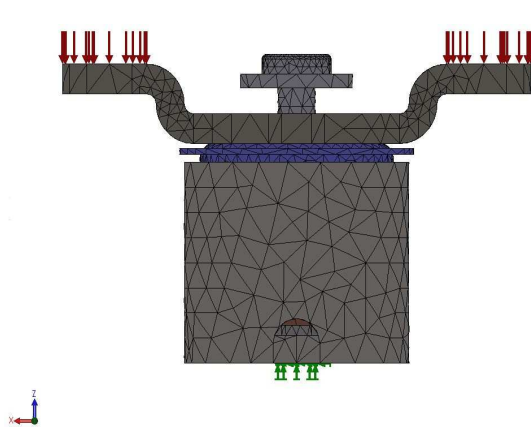


Figure 4.15 – Mathematical model, <X,Z> plane.

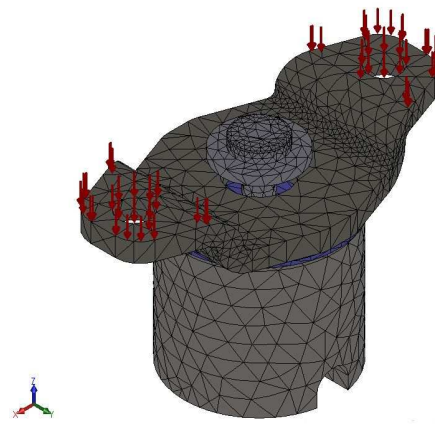


Figure 4.16 – Mathematical model, isometric view

It has to be noted that:

- the spacer is excluded from the analysis. This new configuration does not affect the final results because the spacer contribution along axial displacement is null.
- No penetration contact type between:
 - omega pad and o-ring;
 - o-ring and plastic body.
- Computation of FB forces parameter is enabled.

The results are presented in Table 4.10.

Table 4.10 – Static analysis 3 - axial, results.

Parameter	Units of measurements	Value
Time of computation	[s]	00:06:40
UZ	[mm]	-5.230E-3
Computed stiffness	[N/mm]	191.2
Error	[%]	411

In the following Figure is presented the displacement chart and the displacement value for nodes 16314 and 16303.

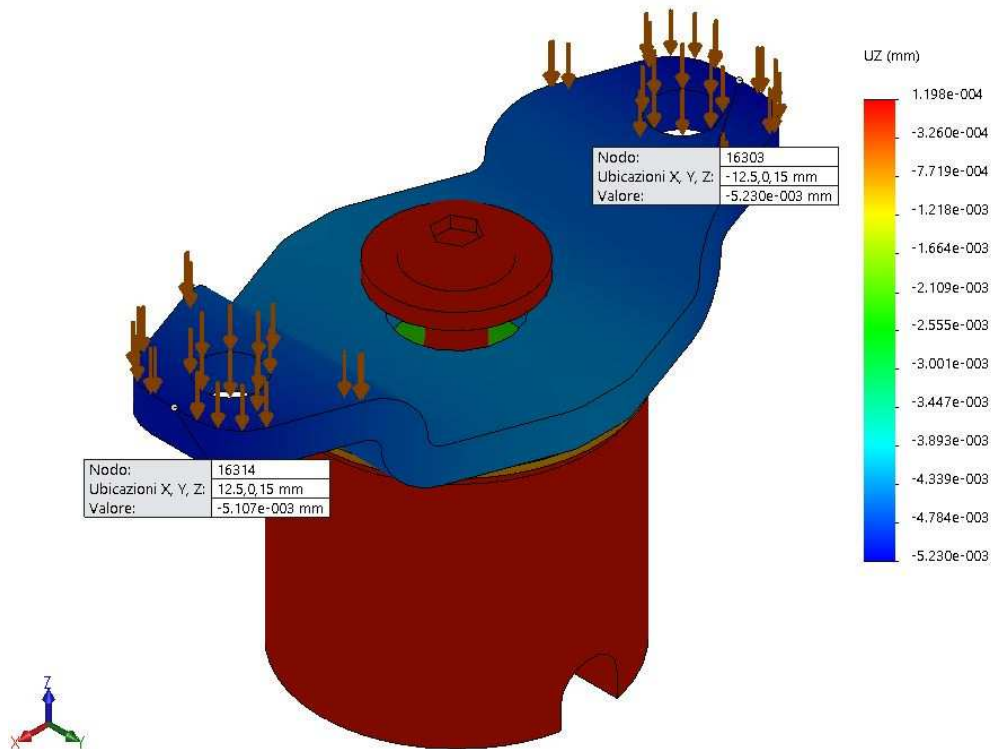


Figure 4.17 – Static analysis 3 - axial, displacement values.

Considering the results from the analysis the value for the elastic modulus of the o-ring is lowered by 60%, down to $E = 10 \text{ MPa}$ (10000000 N/m^2).

4.3.2.4 Static analysis 4 - axial

In the following tables are presented the setup parameters.

Table 4.11 – Mesh parameters.

Parameter	Units of measurements	Value
Type of mesh	-	Tetraedric elements
Mesher	-	Curvature based
Number of Jacobian points	-	4
Max dimension	[mm]	1.594
Min dimension	[mm]	0.319
Nodes	-	29568
Elements	-	17368
AR<3	-	93
AR>10	-	0.173
AR max	-	23.961
Jacobian (distorted elements)	%	0

Table 4.12 – Analysis parameters.

Parameter	Units of measurements	Value
DOF	-	87438
Solver	-	FFE Plus
Spacer Young modulus	[N/m ²]	-
O-ring Young modulus	[N/m ²]	10000000
External load	[N]	1
Load application point		Omega pad wings
Restraints	-	Fixed geometry applied to the base of metallic body

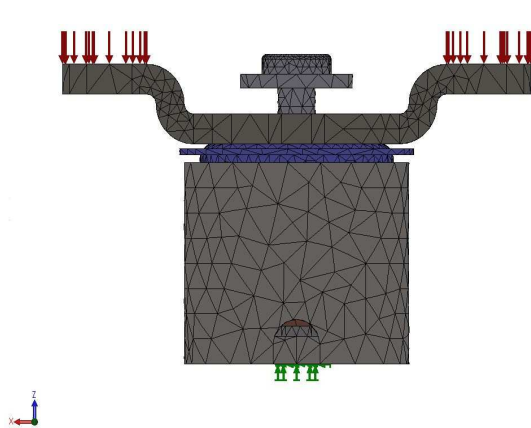


Figure 4.18 – Mathematical model, <X,Z> plane.

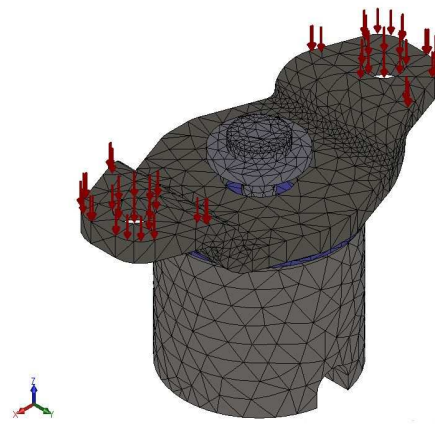


Figure 4.19 – Mathematical model, isometric view

As defined before:

- the spacer is excluded from the analysis. This new configuration does not affect the final results because the spacer contribution along axial displacement is null.
- No penetration contact type between:
 - omega pad and o-ring;
 - o-ring and plastic body.
- Computation of FB forces parameter is enabled.

The results are presented in Table 4.13.

Table 4.13 – Static analysis 4 - axial, results.

Parameter	Units of measurements	Value
Time of computation	[s]	00:06:27
UZ	[mm]	-1.191E-2
Computed stiffness	[N/mm]	52.3

In the following Figure is presented the displacement chart and the displacement value for nodes 16314 and 16303.

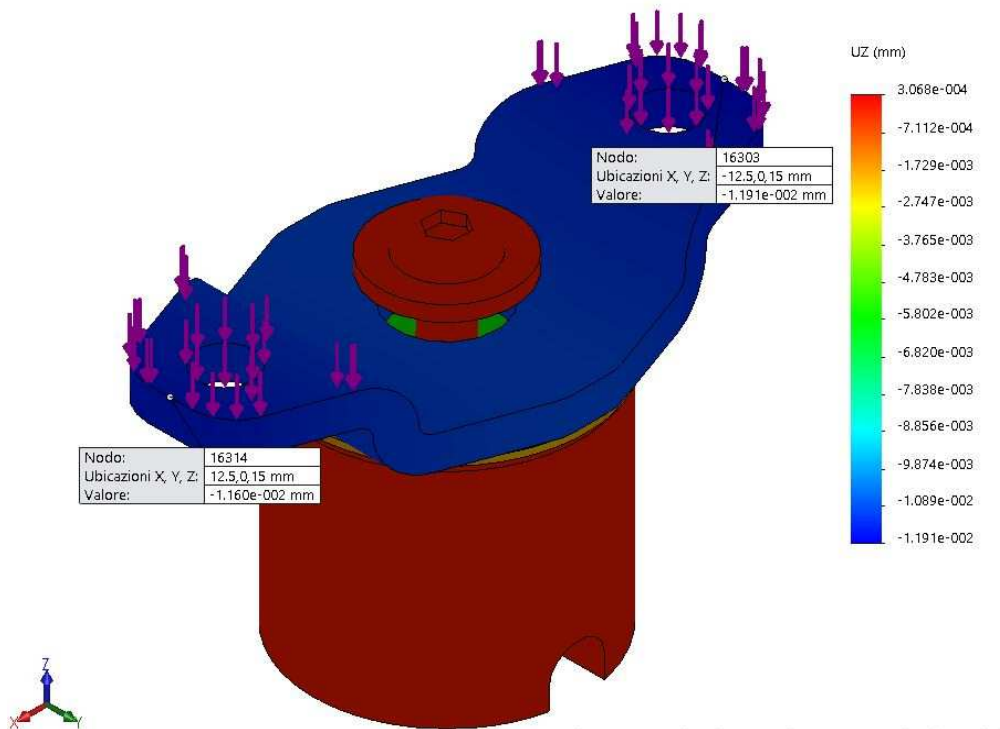


Figure 4.20 – Static analysis 4 - axial, displacement values.

Considering the results from the analysis the value for the elastic modulus of the oring is lowered by 55%, down to $E = 4.5 \text{ MPa}$ (4500000 N/m^2).

4.3.2.5 Static analysis 5 - axial

In the following tables are presented the setup parameters.

Table 4.14 – Mesh parameters.

Parameter	Units of measurements	Value
Type of mesh	-	Tetraedric elements
Mesher	-	Curvature based
Number of Jacobian points	-	4
Max dimension	[mm]	1.594
Min dimension	[mm]	0.319
Nodes	-	29568
Elements	-	17368
AR<3	-	93
AR>10	-	0.173
AR max	-	23.961
Jacobian (distorted elements)	%	0

Table 4.15 – Analysis parameters.

Parameter	Units of measurements	Value
DOF	-	87438
Solver	-	FFE Plus
Spacer Young modulus	[N/m ²]	-
O-ring Young modulus	[N/m ²]	4500000
External load	[N]	1
Load application point		Omega pad wings
Restraints	-	Fixed geometry applied to the base of metallic body

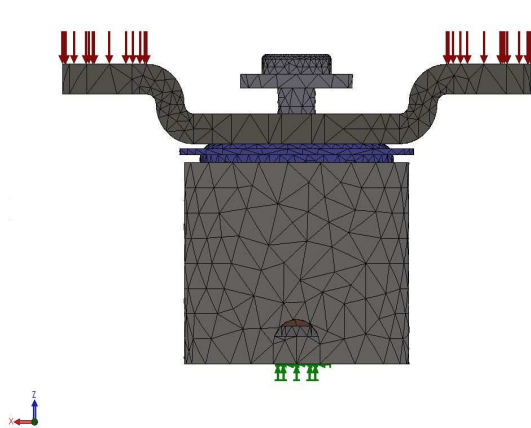


Figure 4.21 – Mathematical model, <X,Z> plane.

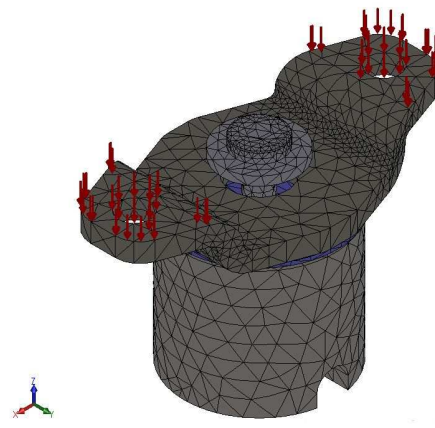


Figure 4.22 – Mathematical model, isometric view

As defined before:

- the spacer is excluded from the analysis. This new configuration does not affect the final results because the spacer contribution along axial displacement is null.
- No penetration contact type between:
 - omega pad and o-ring;
 - o-ring and plastic body.
- Computation of FB forces parameter is enabled.

The results are presented in Table 4.16.

Table 4.16 – Static analysis 5 - axial, results.

Parameter	Units of measurements	Value
Time of computation	[s]	00:04:36
UZ	[mm]	-2.552E-2
Computed stiffness	[N/mm]	39.2
Error	[%]	5

In the following Figure is presented the displacement chart and the displacement value for nodes 16314 and 16303.

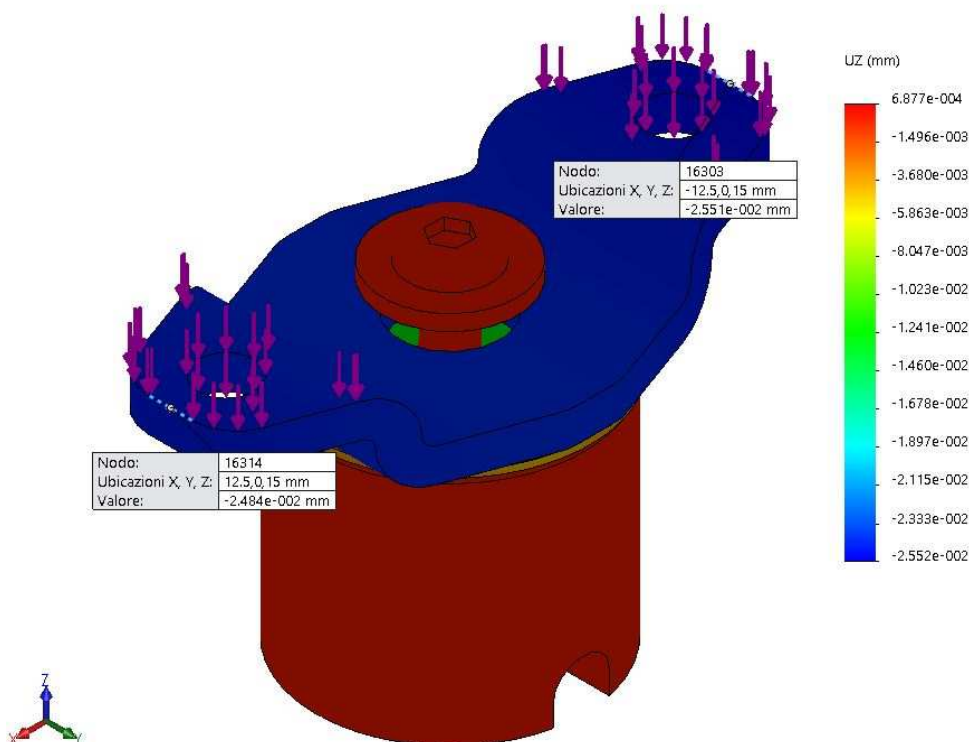


Figure 4.23 – Static analysis 5 - axial, displacement values.

In order to double-check the values from this analysis, a revision 1 is presented, where the parameter concerning the computation of FB forces is disabled

4.3.2.6 Static analysis 5 rev1 - axial

In the following tables are presented the setup parameters.

Table 4.17 – Mesh parameters.

Parameter	Units of measurements	Value
Type of mesh	-	Tetraedric elements
Mesher	-	Curvature based
Number of Jacobian points	-	4
Max dimension	[mm]	1.594
Min dimension	[mm]	0.319
Nodes	-	29568
Elements	-	17368
AR<3	-	93
AR>10	-	0.173
AR max	-	23.961
Jacobian (distorted elements)	%	0

Table 4.18 – Analysis parameters.

Parameter	Units of measurements	Value
DOF	-	87438
Solver	-	FFE Plus
Spacer Young modulus	[N/m ²]	-
O-ring Young modulus	[N/m ²]	4500000
External load	[N]	1
Load application point		Omega pad wings
Restraints	-	Fixed geometry applied to the base of metallic body

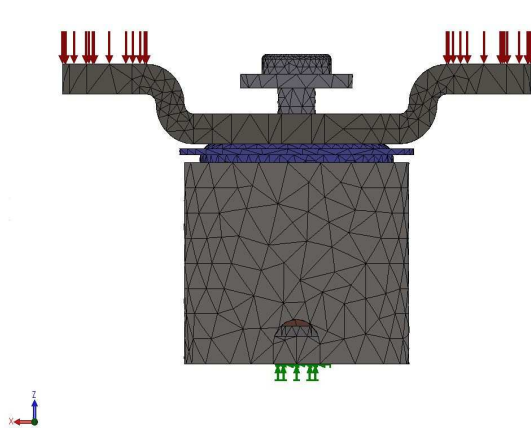


Figure 4.24 – Mathematical model, <X,Z> plane.

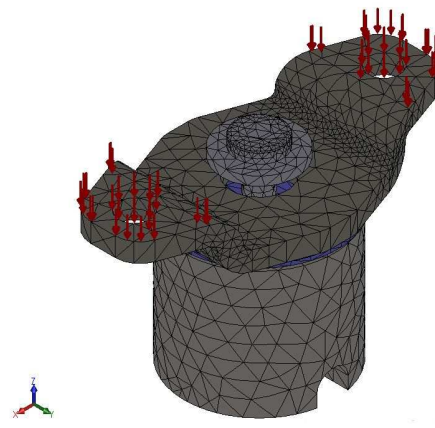


Figure 4.25 – Mathematical model, isometric view

As defined in previous analyses:

- the spacer is excluded from the analysis. This new configuration does not affect the final results because the spacer contribution along axial displacement is null.
- No penetration contact type between:
 - omega pad and o-ring;
 - o-ring and plastic body.

The results are presented in Table 4.19.

Table 4.19 – Static analysis 5 rev1 - axial, results.

Parameter	Units of measurements	Value
Time of computation	[s]	00:04:36
UZ	[mm]	-2.552E-2
Computed stiffness	[N/mm]	39.2
Error	[%]	5

In the following Figure is presented the displacement chart and the displacement value for nodes 16314 and 16303.

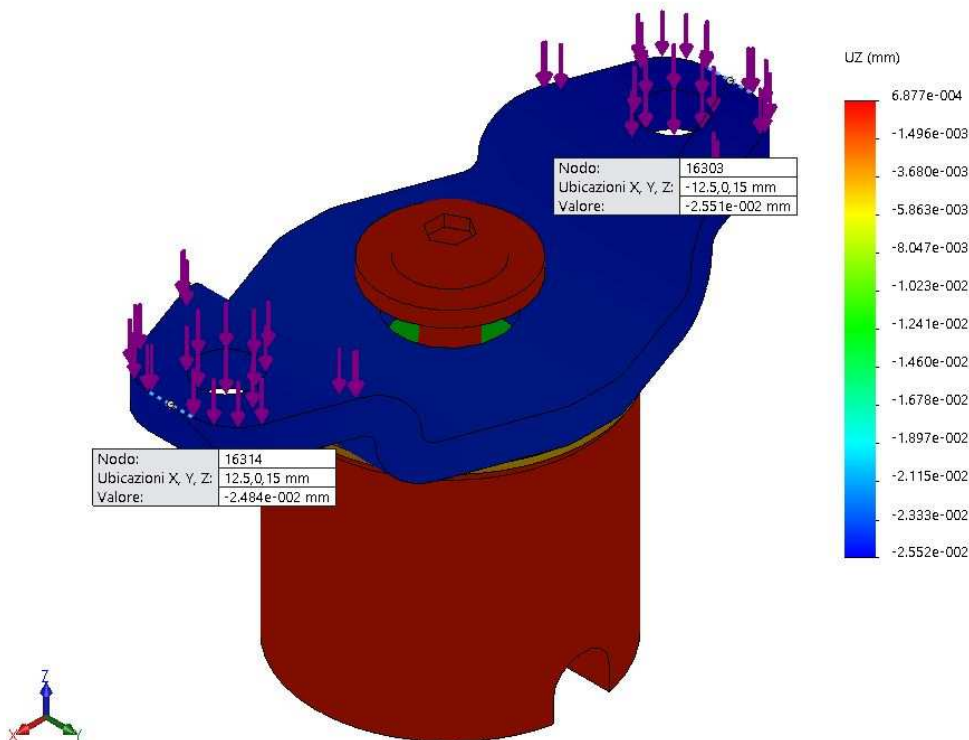


Figure 4.26 – Static analysis 5 rev1 - axial, displacement values.

Same values of previous analysis are obtained

Considering the results from the analysis the value for the elastic modulus of the oring is lowered by 5%, down to $E = 4.25 \text{ MPa}$ (4250000 N/m^2).

4.3.2.7 Static analysis 6 - axial

In the following tables are presented the setup parameters.

Table 4.20 – Mesh parameters.

Parameter	Units of measurements	Value
Type of mesh	-	Tetraedric elements
Mesher	-	Curvature based
Number of Jacobian points	-	4
Max dimension	[mm]	1.594
Min dimension	[mm]	0.319
Nodes	-	29568
Elements	-	17368
AR<3	-	93
AR>10	-	0.173
AR max	-	23.961
Jacobian (distorted elements)	%	0

Table 4.21 – Analysis parameters.

Parameter	Units of measurements	Value
DOF	-	87438
Solver	-	FFE Plus
Spacer Young modulus	[N/m ²]	-
O-ring Young modulus	[N/m ²]	4250000
External load	[N]	1
Load application point		Omega pad wings
Restraints	-	Fixed geometry applied to the base of metallic body

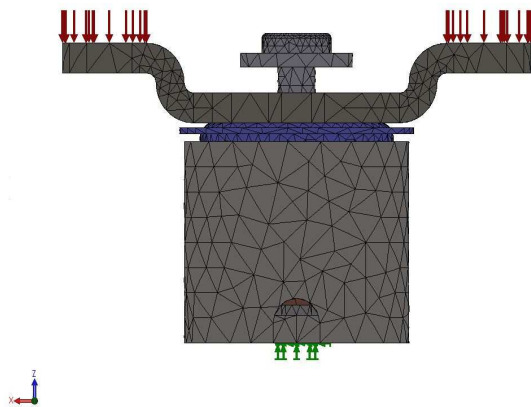


Figure 4.27 – Mathematical model, <X,Z> plane.

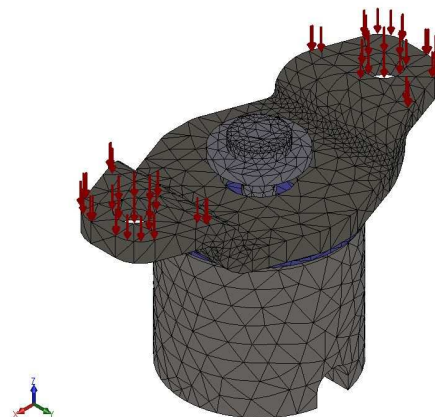


Figure 4.28 – Mathematical model, isometric view

As defined in previous analyses:

- the spacer is excluded from the analysis. This new configuration does not affect the final results because the spacer contribution along axial displacement is null.
- No penetration contact type between:
 - omega pad and o-ring;
 - o-ring and plastic body.

The results are presented in Table 4.22.

Table 4.22 – Static analysis 6 - axial, results.

Parameter	Units of measurements	Value
Time of computation	[s]	00:07:20
UZ	[mm]	-2.698 E-2
Computed stiffness	[N/mm]	37.1
Error	[%]	1

In the following Figure is presented the displacement chart and the displacement value for nodes 16314 and 16303.

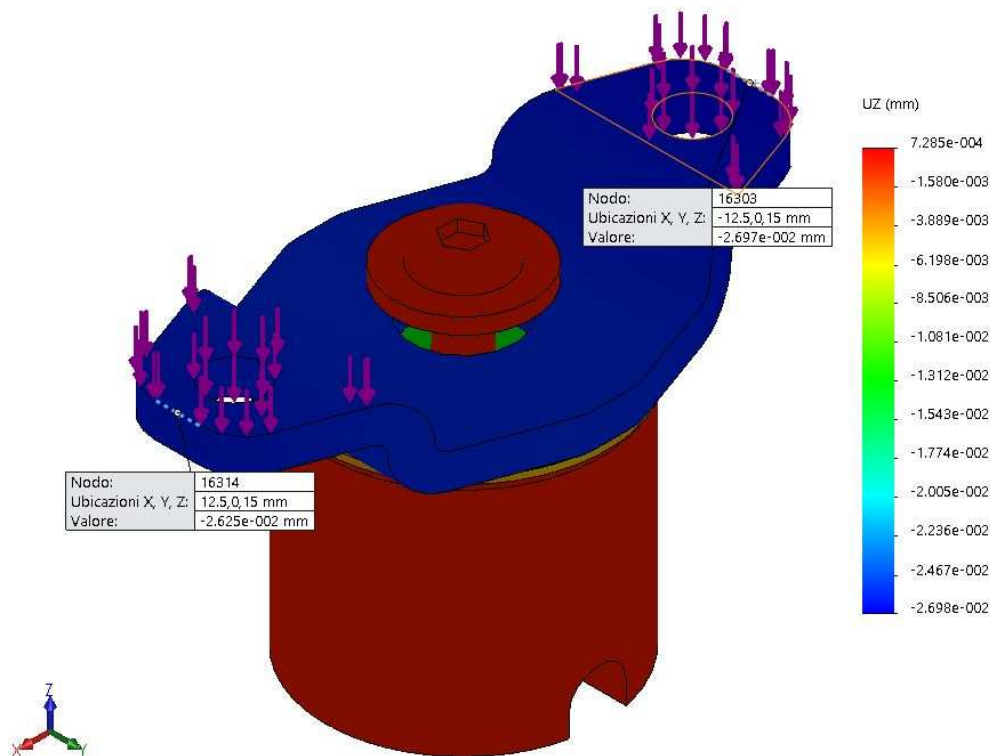


Figure 4.29 – Static analysis 6 - axial, displacement values.

Considering the result obtained from the static analysis, the computed stiffness is equal to 37.1 N/mm, which successfully approximates the values computed from experimental tests. The Young modulus for the o-ring is thus set to $E = 4.25 \text{ MPa}$ (4250000 N/m^2). Further analyses are carried at different applied loads in order to check the linearity of the stiffness behaviour.

4.3.2.8 Static analysis 7 - axial

In the following tables are presented the setup parameters.

Table 4.23 – Mesh parameters.

Parameter	Units of measurements	Value
Type of mesh	-	Tetraedric elements
Mesher	-	Curvature based
Number of Jacobian points	-	4
Max dimension	[mm]	1.594
Min dimension	[mm]	0.319
Nodes	-	29568
Elements	-	17368
AR<3	-	93
AR>10	-	0.173
AR max	-	23.961
Jacobian (distorted elements)	%	0

Table 4.24 – Analysis parameters.

Parameter	Units of measurements	Value
DOF	-	87438
Solver	-	FFE Plus
Spacer Young modulus	[N/m ²]	-
O-ring Young modulus	[N/m ²]	4250000
External load	[N]	2
Load application point		Omega pad wings
Restraints	-	Fixed geometry applied to the base of metallic body

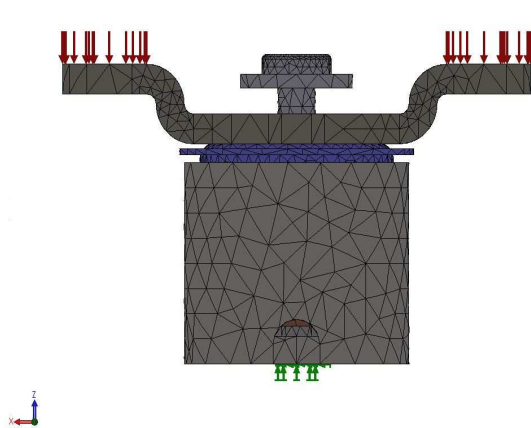


Figure 4.30 – Mathematical model, <X,Z> plane.

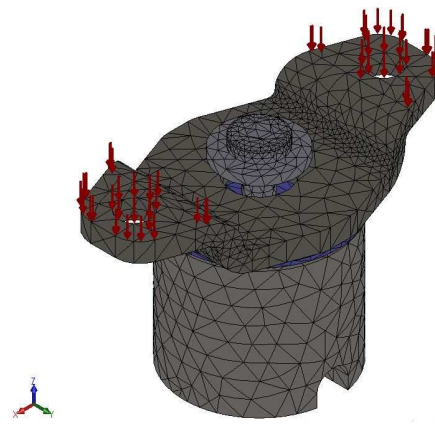


Figure 4.31 – Mathematical model, isometric view

As defined in previous analyses:

- the spacer is excluded from the analysis. This new configuration does not affect the final results because the spacer contribution along axial displacement is null.
- No penetration contact type between:
 - omega pad and o-ring;
 - o-ring and plastic body.

The results are presented in Table 4.25.

Table 4.25 – Static analysis 7 - axial, results.

Parameter	Units of measurements	Value
Time of computation	[s]	00:06:55
UZ	[mm]	-5.395 E-2
Computed stiffness	[N/mm]	37.1
Error	[%]	1

In the following Figure is presented the displacement chart and the displacement value for nodes 16314 and 16303.

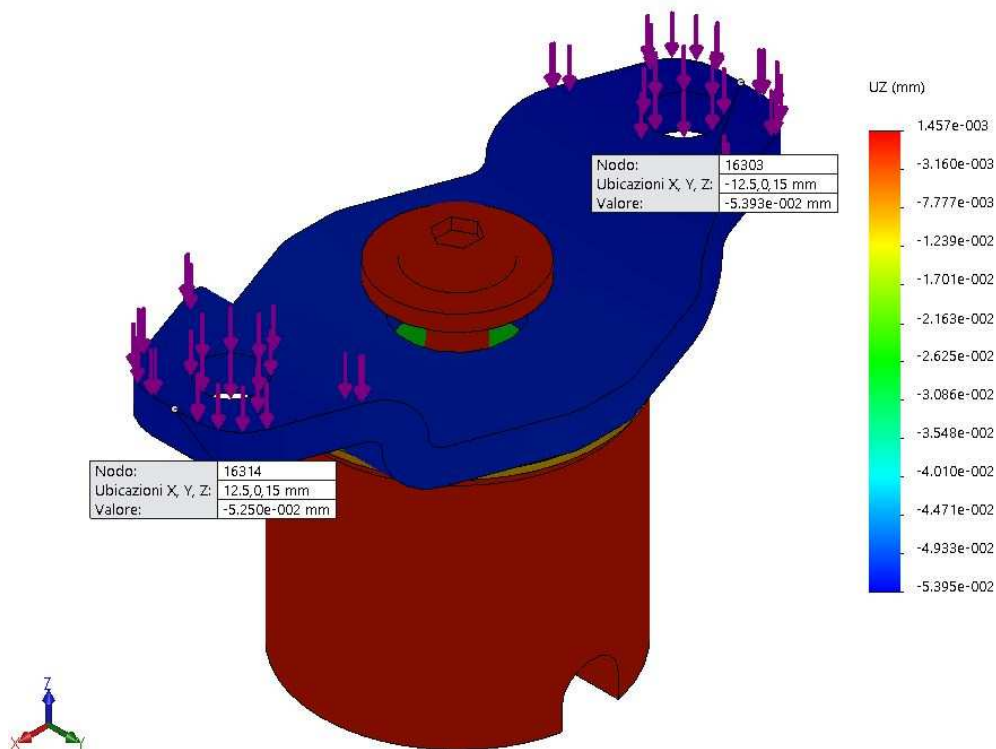


Figure 4.32 – Static analysis 7 - axial, displacement values.

The analysis show that the application of an external load of 2 N, applied along Z direction in the same points of previous analyses, produces a displacement that leads to a stiffness value of 37.1 N/mm, which corresponds to the one presented in Table 4.22.

4.3.2.9 Static analysis 8 - axial

In the following tables are presented the setup parameters.

Table 4.26 – Mesh parameters.

Parameter	Units of measurements	Value
Type of mesh	-	Tetraedric elements
Mesher	-	Curvature based
Number of Jacobian points	-	4
Max dimension	[mm]	1.594
Min dimension	[mm]	0.319
Nodes	-	29568
Elements	-	17368
AR<3	-	93
AR>10	-	0.173
AR max	-	23.961
Jacobian (distorted elements)	%	0

Table 4.27 – Analysis parameters.

Parameter	Units of measurements	Value
DOF	-	87438
Solver	-	FFE Plus
Spacer Young modulus	[N/m ²]	-
O-ring Young modulus	[N/m ²]	4250000
External load	[N]	3
Load application point		Omega pad wings
Restraints	-	Fixed geometry applied to the base of metallic body

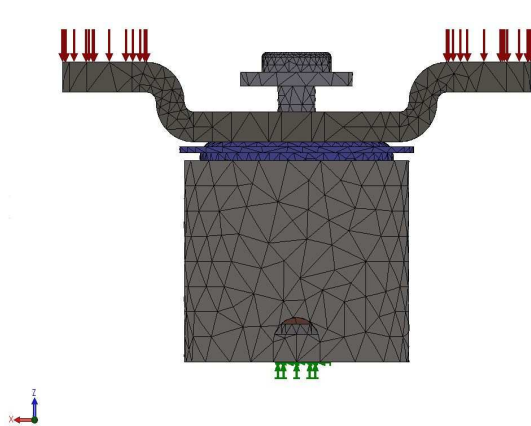


Figure 4.33 – Mathematical model, <X,Z> plane.

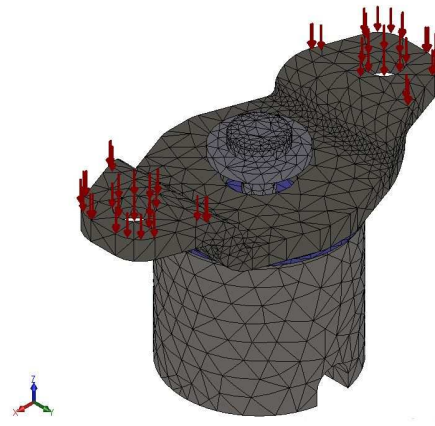


Figure 4.34 – Mathematical model, isometric view

As defined in previous analyses:

- the spacer is excluded from the analysis. This new configuration does not affect the final results because the spacer contribution along axial displacement is null.
- No penetration contact type between:
 - omega pad and o-ring;
 - o-ring and plastic body.

The results are presented in Table 4.28.

Table 4.28 – Static analysis 8 - axial, results.

Parameter	Units of measurements	Value
Time of computation	[s]	00:04:25
UZ	[mm]	-8.085 E-2
Computed stiffness	[N/mm]	37.1
Error	[%]	1

In the following Figure is presented the displacement chart and the displacement value for nodes 16314 and 16303.

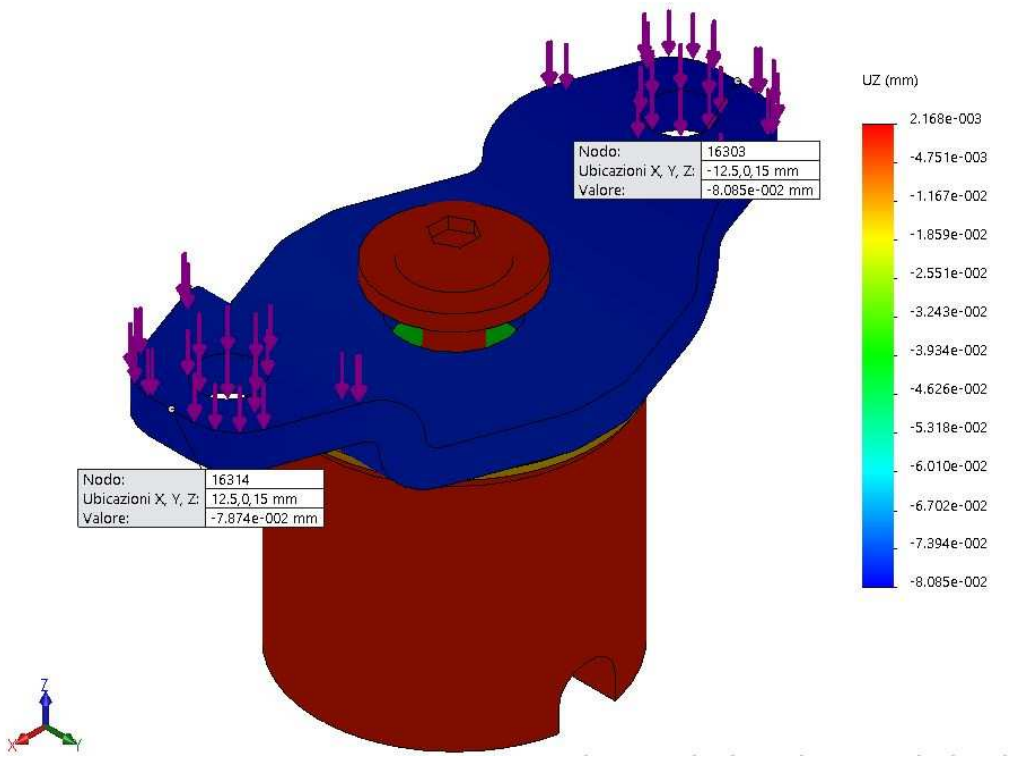


Figure 4.35 – Static analysis 8 - axial, displacement values.

The analysis show that the application of an external load of 3 N, applied along Z direction in the same points of previous analyses, produces a displacement that leads to a stiffness value of 37.1 N/mm, which corresponds to the one presented in Table 4.22.

4.3.2.10 Results for axial static analysis

The following table shows briefly the Young modulus and the related stiffness for the o-ring.

Table 4.29 – Static analysis - axial, results.

Young modulus [MPa]	Displacement [mm]	Stiffness [N/mm]	Error [%]
50	-3.00E-3	333	790
25	-5.23E-3	191.2	411
10	-1.19E-2	83.96	125
4.5	-2.55E-2	39.21	5
4.25	-2.70E-2	37.06	1
4.25	-5.40E-2	37.07	1
4.25	-8.09E-2	37.10	1

From the analyses it results that the best value for the Young modulus for the o-ring , that allow to reach a good approximation of the experimental stiffness, is equal to 4.25MPa.

4.4 Pitch and roll motion analyses

The rotational motion is analyzed in order to investigate the elastic modulus for the spacer element. The objective of the analysis is to obtain a value of the stiffness which is affected by a reasonable small error with respect the expected value, 224N/mm, coming from the averaging of the data from experimental analysis.

Analyses and results of pitch and roll motion are presented in the following paragraphs.

4.4.1 Mathematical model for pitch motion

The pitch motion is analyzed in order to investigate the elastic modulus value for the spacer element: the objective of the analysis is to obtain a value of the rotational stiffness similar to the one coming from experimental analysis: 2

Each analysis is associated with a report in which are presented the input parameters and the results concerning the displacement along Z axis of the specific points.

The rotational stiffness is then computed and compared with the one from the experimental analysis.

It is import to highlight that the rotational stiffness is computed as:

$$k = \frac{C}{\vartheta} \left[\frac{Nmm}{rad} \right] \quad (4.2)$$

considering that:

$$C = F \cdot b \quad (4.3)$$

$$b = 12.50 \text{ mm} \quad (4.4)$$

$$\vartheta = \arcsin\left(\frac{z}{b}\right) \sim \frac{z}{b} \quad (\text{for small oscillations approximation}) \quad (4.5)$$

where:

- C is the resulting torque [Nmm];
- F is the applied axial load [N];
- b is the arm of the applied torque [mm];
- z is the displacement along Z axis of the point where the force is applied [mm];
- ϑ is the angle corresponding to the axial displacement [rad].

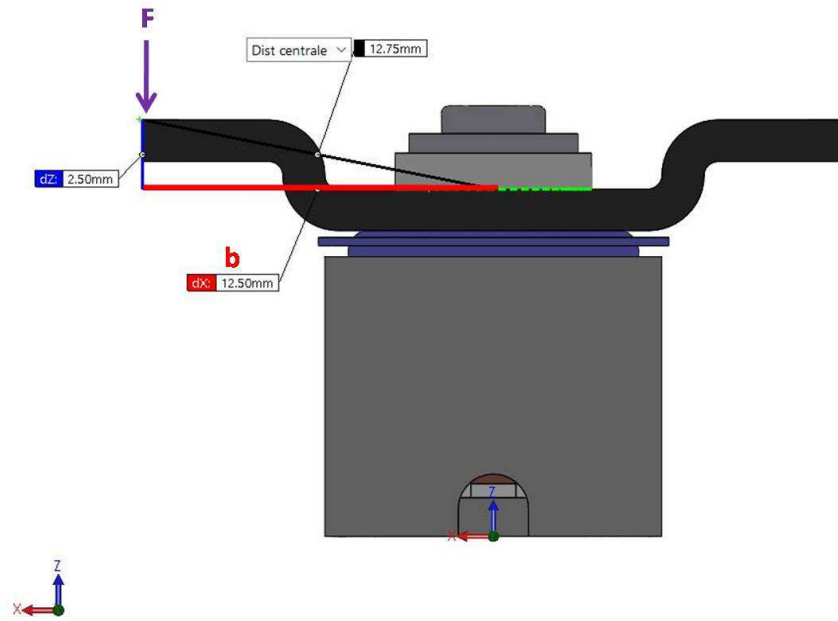


Figure 4.36 – Pitch motion analysis, applied load an lever arm.

4.4.1.1 Static analysis 1 - pitch

In the following tables are presented the setup parameters.

Table 4.30 – Mesh parameters.

Parameter	Units of measurements	Value
Type of mesh	-	Tetraedric elements
Mesher	-	Curvature based
Number of Jacobian points	-	4
Max dimension	[mm]	1.565
Min dimension	[mm]	0.313
Nodes	-	31273
Elements	-	18329
AR<3	-	91.9
AR>10	-	0.153
AR max	-	18.55
Jacobian (distorted elements)	%	0

Table 4.31 – Analysis parameters.

Parameter	Units of measurements	Value
DOF	-	92541
Solver	-	FFE Plus
Spacer Young modulus	[N/m ²]	50000000
O-ring Young modulus	[N/m ²]	4250000
External load	[N]	1
Load application point		Omega pad, left wing
Restraints	-	Fixed geometry applied to the base of metallic body

The load is applied on the edge of the omega pad so that to reproduce the experimental analysis. The difference is in the lever arm value, 12.5 mm against 11.875 mm of the experimental analysis, which, anyway, does not affect the stiffness computation process.

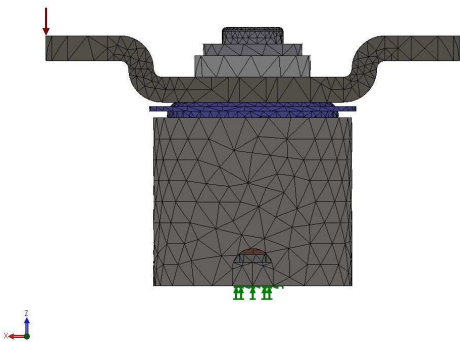


Figure 4.37 – Mathematical model, <X,Z> plane.

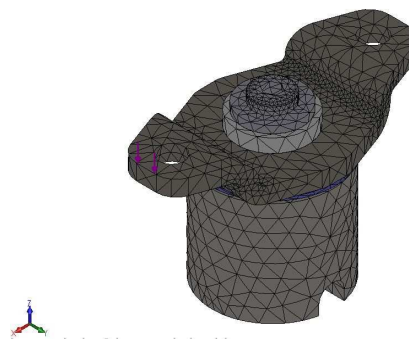


Figure 4.38 – Mathematical model, isometric view.

It has to be noted that no penetration contact type between the following couples of elements is set:

- flanged screw and spacer;
- spacer and omega pad;
- omega pad and o-ring;
- o-ring and plastic body.

The results are presented in Table 4.32.

Table 4.32 – Results.

Parameter	Units of measurements	Value
Time of computation	[s]	00:02:43
UZ	[mm]	-2.047 E-1
UX	[mm]	-
UY	[mm]	-
Computed stiffness	[Nmm/rad]	763.3
Error	[%]	241

Note that the measure relative to the displacements along Z (UZ) is computed taking as reference the extreme node 166640 on the omega pad wing, corresponding to the load application point.

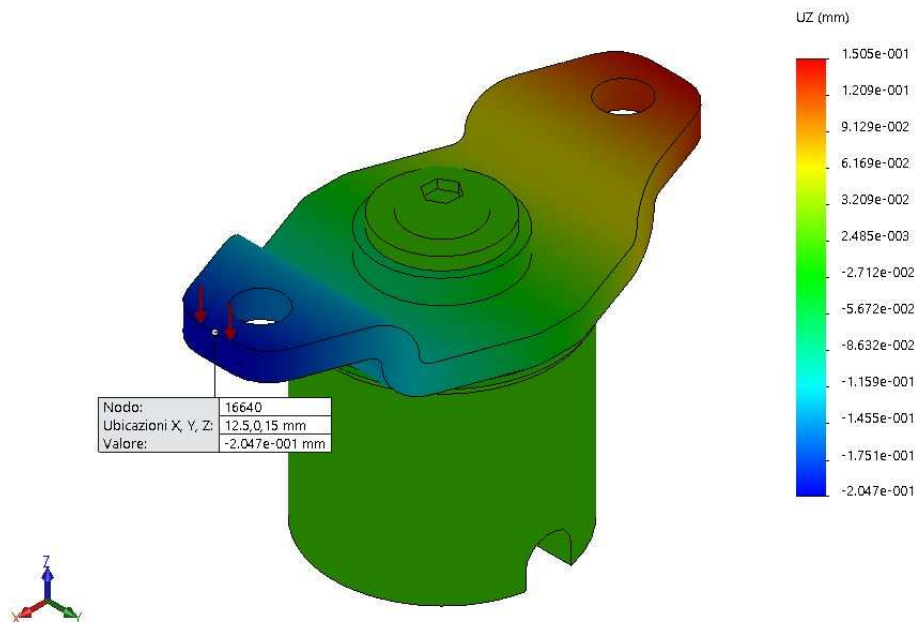


Figure 4.39 – Static analysis 1 - pitch, displacement values.

The analysis shows an asymmetric behaviour of the omega pad wings. In fact, the displacement along Z of the right wing is, in module, lower than the one of the left wing (1.5 E-1 versus 2.047 E-1). This shows that the center of rotation of the omega pad does not coincide with the symmetry axis. Furthermore, the error on the computed stiffness is 241%, which requires E to be lowered.

4.4.1.2 Static analysis 2 - pitch

In the following tables are presented the setup parameters.

Table 4.33 – Mesh parameters.

Parameter	Units of measurements	Value
Type of mesh	-	Tetraedric elements
Mesher	-	Curvature based
Number of Jacobian points	-	4
Max dimension	[mm]	1.565
Min dimension	[mm]	0.313
Nodes	-	31273
Elements	-	18329
AR<3	-	91.9
AR>10	-	0.153
AR max	-	18.55
Jacobian (distorted elements)	%	0

Table 4.34 – Analysis parameters.

Parameter	Units of measurements	Value
DOF	-	92541
Solver	-	FFE Plus
Spacer Young modulus	[N/m ²]	5000000
O-ring Young modulus	[N/m ²]	4250000
External load	[N]	1
Load application point		Omega pad, left wing
Restraints	-	Fixed geometry applied to the base of metallic body

In the following Figures is presented the meshed model and the application point of applied load.

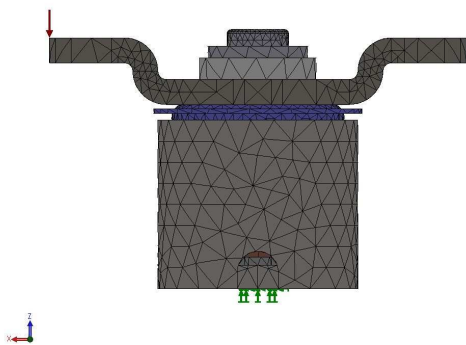


Figure 4.40 – Mathematical model, <X,Z> plane.

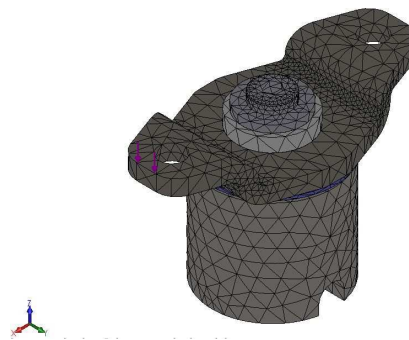


Figure 4.41 – Mathematical model, isometric view.

As previously defined, no penetration contact type is adopted between:

- flanged screw and spacer;
- spacer and omega pad;
- omega pad and o-ring;
- o-ring and plastic body.

The results are presented in Table 4.35.

Table 4.35 – Results.

Parameter	Units of measurements	Value
Time of computation	[s]	00:02:11
UZ	[mm]	-2.966 E-1
UX	[mm]	-
UY	[mm]	-
Computed stiffness	[Nmm/rad]	526.8
Error	[%]	135

Note that the measure relative to the displacements along Z (UZ) is computed taking as reference the extreme node on the omega pad wing, corresponding to the load application point.

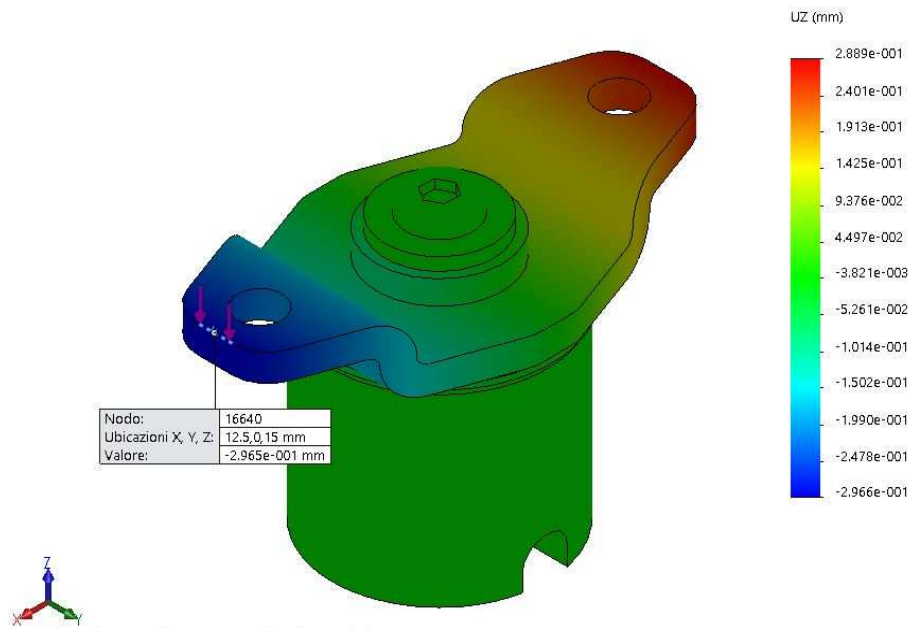


Figure 4.42 – Static analysis 2 - pitch, displacement values

The analysis shows a non-symmetric behaviour of the omega pad wings due to a misalignment of the center of rotation of the omega pad. The computed stiffness has an error of 135% which requires the E value to be lowered.

4.4.1.3 Static analysis 3 - pitch

In the following tables are presented the setup parameters.

Table 4.36 – Mesh parameters.

Parameter	Units of measurements	Value
Type of mesh	-	Tetraedric elements
Mesher	-	Curvature based
Number of Jacobian points	-	4
Max dimension	[mm]	1.594
Min dimension	[mm]	0.319
Nodes	-	31090
Elements	-	18246
AR<3	-	92.5
AR>10	-	0.159
AR max	-	22.41
Jacobian (distorted elements)	%	0

Table 4.37 – Analysis parameters.

Parameter	Units of measurements	Value
DOF	-	91980
Solver	-	FFE Plus
Spacer Young modulus	[N/m ²]	2050000
O-ring Young modulus	[N/m ²]	4250000
External load	[N]	1
Load application point		Omega pad, left wing
Restraints	-	Fixed geometry applied to the base of metallic body

The load is applied on the edge of the omega pad so that to reproduce the experimental analysis. The difference is in the lever arm value, 12.5 mm against 11.875 mm of the experimental analysis, which, anyway, does not affect the stiffness computation process.

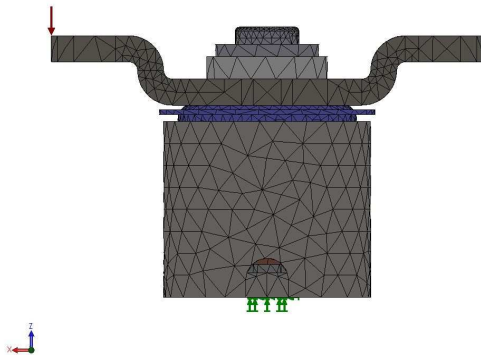


Figure 4.43 – Mathematical model, <X,Z> plane.

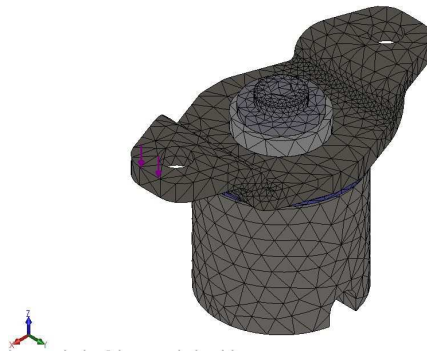


Figure 4.44 – Mathematical model, isometric view.

As previously defined, no penetration contact type is adopted between:

- flanged screw and spacer;
- spacer and omega pad;
- omega pad and o-ring;
- o-ring and plastic body.

The results are presented in Table 4.38.

Table 4.38 – Results.

Parameter	Units of measurements	Value
Time of computation	[s]	00:02:10
UZ	[mm]	-3.917 E-1
UX	[mm]	-
UY	[mm]	-
Computed stiffness	[Nmm/rad]	398.9
Error	[%]	78

Note that the measure relative to the displacements along Z (UZ) is computed taking as reference the extreme node on the omega pad wing, corresponding to the load application point.

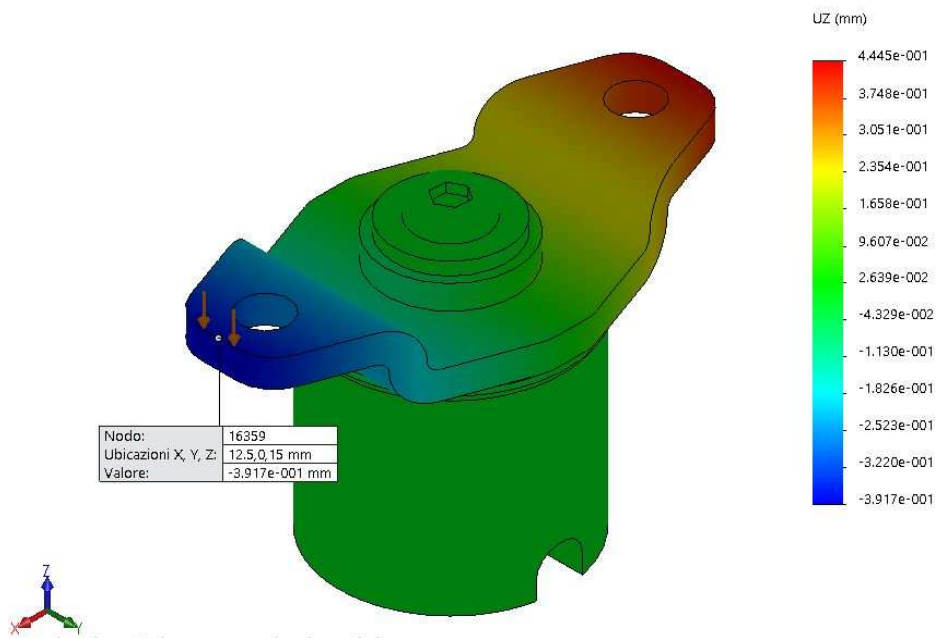


Figure 4.45 – Static analysis 3 - pitch, displacement values.

The analysis shows an asymmetric behaviour of the omega pad wings due to the misalignment of center of rotation of the omega pad. The computed stiffness results to be affected by a significant error: a decrease in Young modulus value for the spacer is required.

4.4.1.4 Static analysis 4 - pitch

In the following tables are presented the setup parameters.

Table 4.39 – Mesh parameters.

Parameter	Units of measurements	Value
Type of mesh	-	Tetraedric elements
Mesher	-	Curvature based
Number of Jacobian points	-	4
Max dimension	[mm]	1.565
Min dimension	[mm]	0.313
Nodes	-	31273
Elements	-	18329
AR<3	-	91.9
AR>10	-	0.153
AR max	-	18.55
Jacobian (distorted elements)	%	0

Table 4.40 – Analysis parameters.

Parameter	Units of measurements	Value
DOF	-	92541
Solver	-	FFE Plus
Spacer Young modulus	[N/m ²]	1250000
O-ring Young modulus	[N/m ²]	4250000
External load	[N]	1
Load application point		Omega pad, left wing
Restraints	-	Fixed geometry applied to the base of metallic body

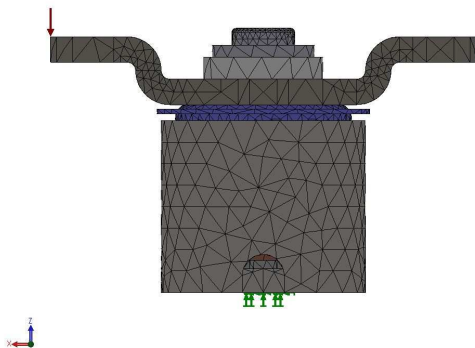


Figure 4.46 – Mathematical model, <X,Z> plane.

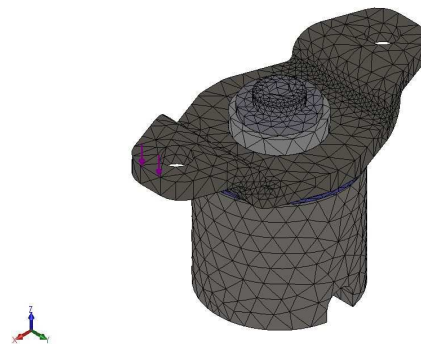


Figure 4.47 – Mathematical model, isometric view.

As previously defined, no penetration contact type is adopted between:

- flanged screw and spacer;
- spacer and omega pad;
- omega pad and o-ring;
- o-ring and plastic body.

The results are presented in Table 4.41.

Table 4.41 – Results.

Parameter	Units of measurements	Value
Time of computation	[s]	00:03:15
UZ	[mm]	-4.54 E-1
UX	[mm]	-
UY	[mm]	-
Computed stiffness	[Nmm/rad]	344.4
Error	[%]	54

Note that the measure relative to the displacements along Z (UZ) is computed taking as reference the extreme node on the omega pad wing, corresponding to the load application point.

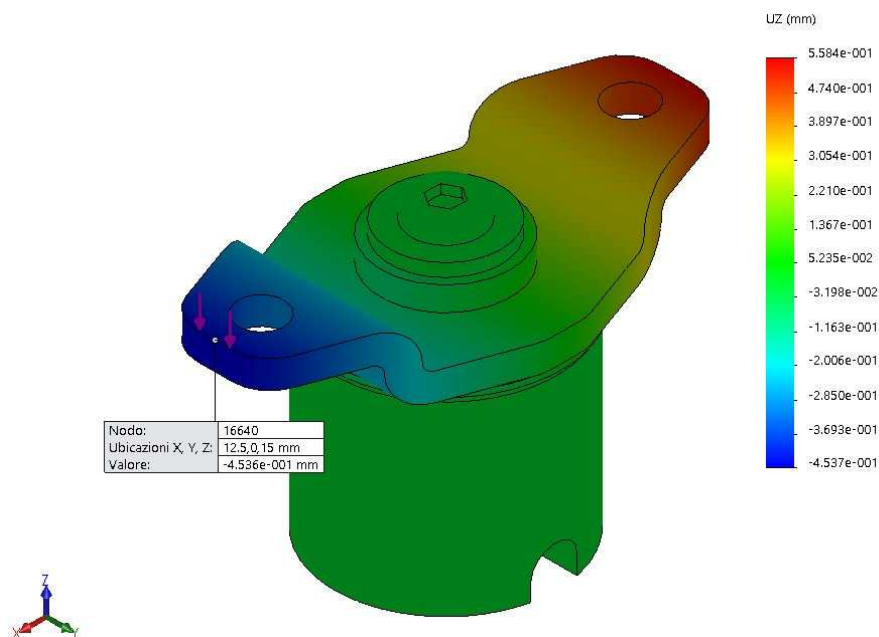


Figure 4.48 – Static analysis 4 - pitch, displacement values.

The asymmetry between the wings displacements can be spotted in Figure 4.48. The computed stiffness is decreasing with respect previous analyses, but still higher than the expected value. A further reduction in Young modulus of spacer is performed in the next analysis.

4.4.1.5 Static analysis 5 - pitch

In the following tables are presented the setup parameters.

Table 4.42 – Mesh parameters.

Parameter	Units of measurements	Value
Type of mesh	-	Tetraedric elements
Mesher	-	Curvature based
Number of Jacobian points	-	4
Max dimension	[mm]	1.565
Min dimension	[mm]	0.313
Nodes	-	31273
Elements	-	18329
AR<3	-	91.9
AR>10	-	0.153
AR max	-	18.55
Jacobian (distorted elements)	%	0

Table 4.43 – Analysis parameters.

Parameter	Units of measurements	Value
DOF	-	92541
Solver	-	FFE Plus
Spacer Young modulus	[N/m ²]	970000
O-ring Young modulus	[N/m ²]	4250000
External load	[N]	1
Load application point		Omega pad, left wing
Restraints	-	Fixed geometry applied to the base of metallic body

The load is at the edge of the right wing of the omega pad so that to reproduce the experimental analysis configuration.

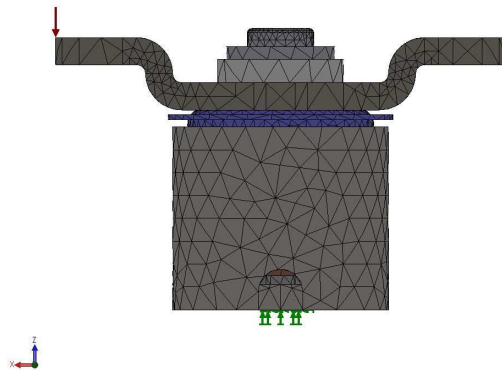


Figure 4.49 – Mathematical model, <X,Z> plane.

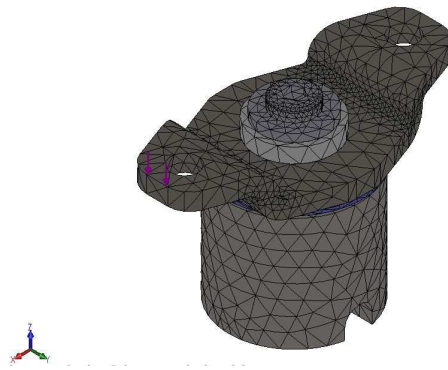


Figure 4.50 – Mathematical model, isometric view.

As previously defined, no penetration contact type is adopted between:

- flanged screw and spacer;
- spacer and omega pad;
- omega pad and o-ring;
- o-ring and plastic body.

The results are presented in Table 4.44.

Table 4.44 – Results.

Parameter	Units of measurements	Value
Time of computation	[s]	00:03:08
UZ	[mm]	-5.086 E-1
UX	[mm]	-
UY	[mm]	-
Computed stiffness	[Nmm/rad]	307.22
Error	[%]	37

Note that the measure relative to the displacements along Z (UZ) is computed taking as reference the extreme node on the omega pad wing, corresponding to the load application point.

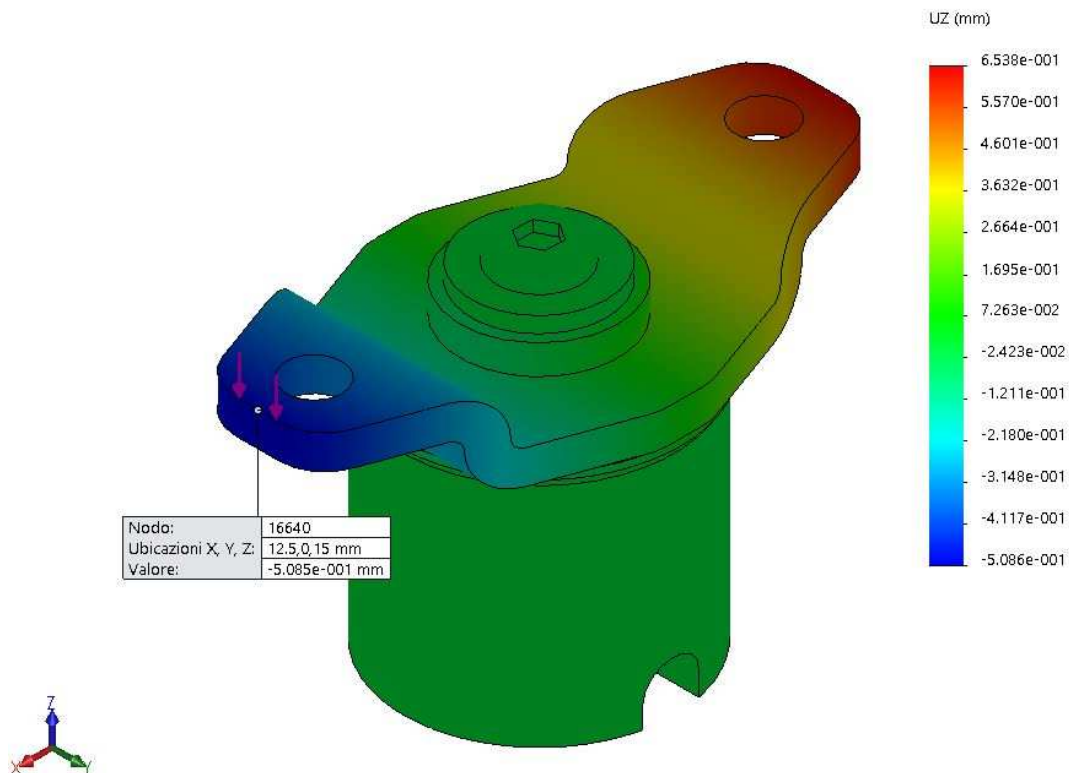


Figure 4.51 – Static analysis 5 - pitch, displacement values.

Asymmetry between wings displacement is still present due to the sliding of the omega pad along x axis, which changes the centre of rotation. As presented in Table 4.43, the stiffness is still high. A further reduction in Young modulus value is required.

4.4.1.6 Static analysis 6 - pitch

In the following tables are presented the setup parameters.

Table 4.45 – Mesh parameters.

Parameter	Units of measurements	Value
Type of mesh	-	Tetraedric elements
Mesher	-	Curvature based
Number of Jacobian points	-	4
Max dimension	[mm]	1.681
Min dimension	[mm]	0.336
Nodes	-	29238
Elements	-	17036
AR<3	-	91.2
AR>10	-	0.205
AR max	-	18.175
Jacobian (distorted elements)	%	0

Table 4.46 – Analysis parameters.

Parameter	Units of measurements	Value
DOF	-	86427
Solver	-	FFE Plus
Spacer Young modulus	[N/m ²]	900000
O-ring Young modulus	[N/m ²]	4250000
External load	[N]	0.5
Load application point		Omega pad, left wing
Restraints	-	Fixed geometry applied to the base of metallic body

A lower applied load, together with a more coarse mesh with bigger tetraedric elements are adopted in order to reduce the time required for the analysis.

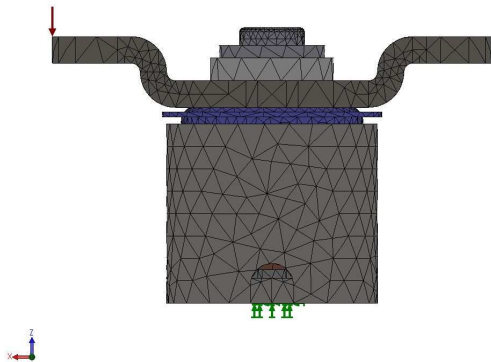


Figure 4.52 – Mathematical model, <X,Z> plane.

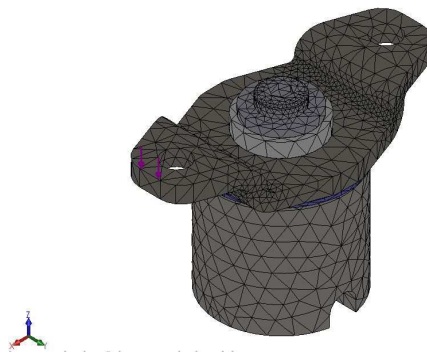


Figure 4.53 – Mathematical model, isometric view

As previously defined, no penetration contact type is adopted between:

- flanged screw and spacer;
- spacer and omega pad;
- omega pad and o-ring;
- o-ring and plastic body.

The results are presented in Table 4.47.

Table 4.47 – Results.

Parameter	Units of measurements	Value
Time of computation	[s]	00:02:00
UZ	[mm]	-2.785 E-1
UX	[mm]	-
UY	[mm]	-
Computed stiffness	[Nmm/rad]	280.52
Error	[%]	25

Note that the measure relative to the displacements along Z (UZ) is computed taking as reference the extreme node on the omega pad wing, corresponding to the load application point.

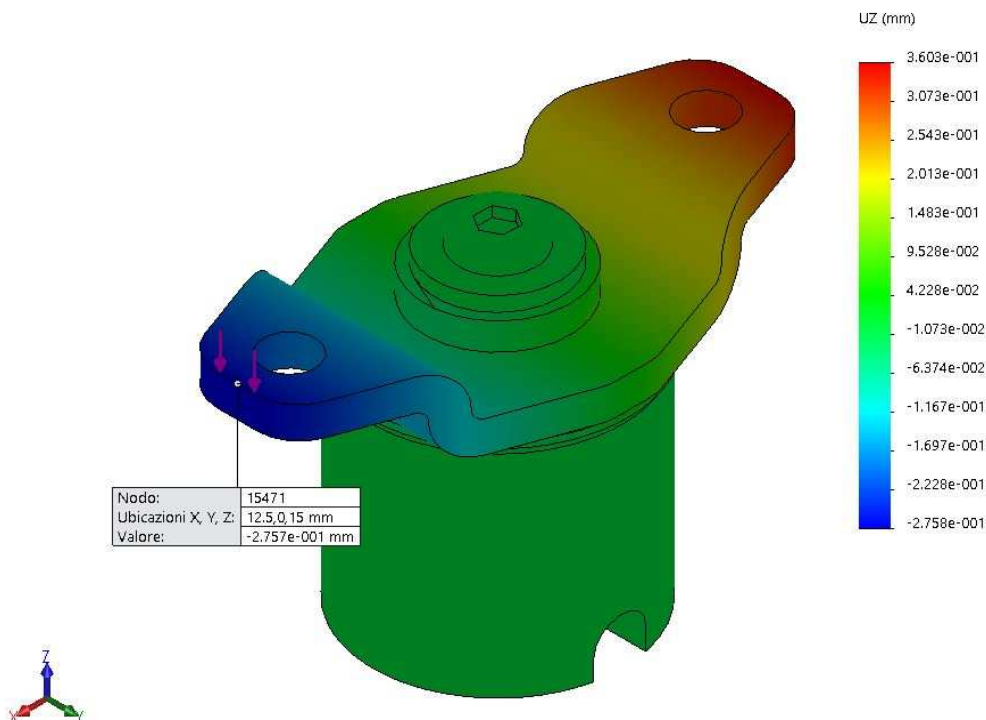


Figure 4.54 – Static analysis 6 - pitch, displacement values.

In Figure 4.54 is possible to note the difference in displacement between left and right wings of the omega pad. This shows that the center of rotation of the omega pad does not coincide with the symmetry axis. The stiffness computed with respect to node 15.471 is still higher, affected by an error of 25%. A further reduction in Young modulus of the spacer is required.

4.4.1.7 Static analysis 7 - pitch

In the following tables are presented the setup parameters.

Table 4.48 – Mesh parameters.

Parameter	Units of measurements	Value
Type of mesh	-	Tetraedric elements
Mesher	-	Curvature based
Number of Jacobian points	-	4
Max dimension	[mm]	2.086
Min dimension	[mm]	0.412
Nodes	-	26103
Elements	-	15177
AR<3	-	89.4
AR>10	-	0.191
AR max	-	23.734
Jacobian (distorted elements)	%	0

Table 4.49 – Analysis parameters.

Parameter	Units of measurements	Value
DOF	-	77052
Solver	-	FFE Plus
Spacer Young modulus	[N/m ²]	750000
O-ring Young modulus	[N/m ²]	4250000
External load	[N]	0.3
Load application point		Omega pad, left wing
Restraints	-	Fixed geometry applied to the base of metallic body

The applied load is further reduced down to 0.3N. Furthermore, a more coarse is adopted. This can be seen in Figure 4.55 and 4.56, through the bigger dimensions of the tetraedric elements.

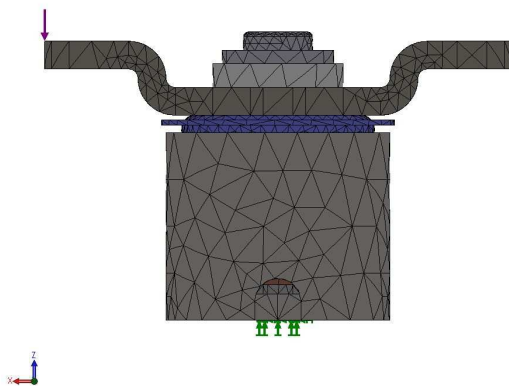


Figure 4.55 – Mathematical model, <X,Z> plane.

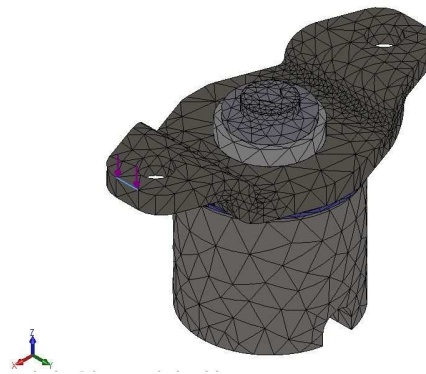


Figure 4.56 – Mathematical model, isometric view.

As previously defined, no penetration contact type is adopted between:

- flanged screw and spacer;
- spacer and omega pad;
- omega pad and o-ring;
- o-ring and plastic body.

The results are presented in Table 4.50.

Table 4.50 – Results.

Parameter	Units of measurements	Value
Time of computation	[s]	00:02:09
UZ	[mm]	-1.812 E-1
UX	[mm]	-
UY	[mm]	-
Computed stiffness	[Nmm/rad]	258.7
Error	[%]	15

The measurement relative to the displacements along Z (UZ) is computed taking as reference node 13709, at the edge of the omega pad wing, corresponding to the load application point.

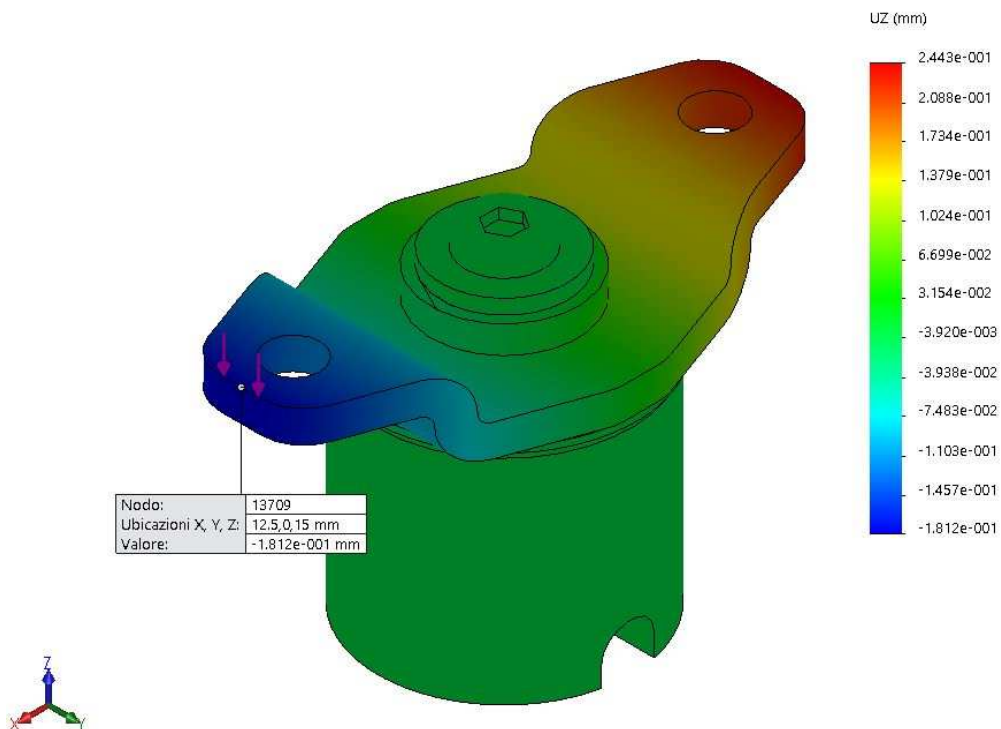


Figure 4.57 – Static analysis 7 - pitch, displacement values.

In this analysis the applied load is reduced down to 0.3 N. The computed stiffness, presented in Table 4.50 is still affected by an relevant error. A further reduction in spacer Young modulus is required.

4.4.1.8 Static analysis 8 - pitch

In the following tables are presented the setup parameters.

Table 4.51 – Mesh parameters.

Parameter	Units of measurements	Value
Type of mesh	-	Tetraedric elements
Mesher	-	Curvature based
Number of Jacobian points	-	4
Max dimension	[mm]	2.17
Min dimension	[mm]	0.435
Nodes	-	24339
Elements	-	14037
AR<3	-	88.2
AR>10	-	0.242
AR max	-	25.538
Jacobian (distorted elements)	%	0

Table 4.52 – Analysis parameters.

Parameter	Units of measurements	Value
DOF	-	71943
Solver	-	FFE Plus
Spacer Young modulus	[N/m ²]	650000
O-ring Young modulus	[N/m ²]	4250000
External load	[N]	0.3
Load application point		Omega pad, left wing
Restraints	-	Fixed geometry applied to the base of metallic body

A further increase mesh dimensions is required. The resulting mesh is presented in the following figures

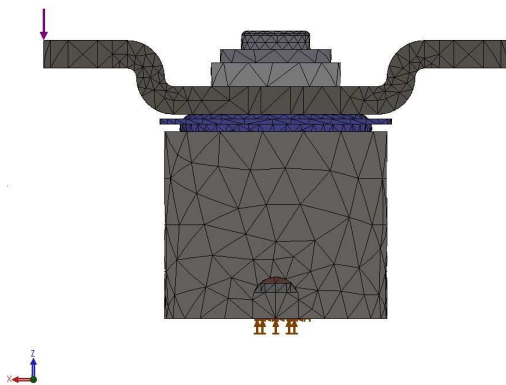


Figure 4.58 – Mathematical model, <X,Z> plane.

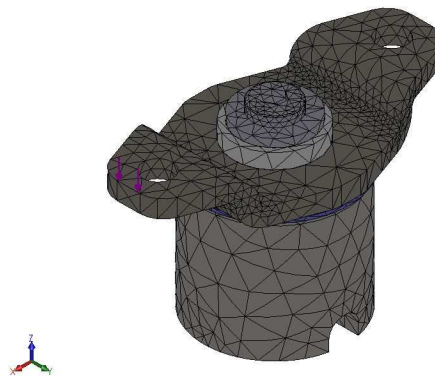


Figure 4.59 – Mathematical model, isometric view.

As previously defined, no penetration contact type is adopted between:

- flanged screw and spacer;
- spacer and omega pad;
- omega pad and o-ring;
- o-ring and plastic body.

The results are presented in Table 4.53.

Table 4.53 – Results.

Parameter	Units of measurements	Value
Time of computation	[s]	00:09:09
UZ	[mm]	-1.984 E-1
UX	[mm]	-
UY	[mm]	-
Computed stiffness	[Nmm/rad]	236.26
Error	[%]	5

The measurement relative to the displacements along Z (UZ) is computed taking as reference node 13117, at the edge of the omega pad wing, corresponding to the load application point.

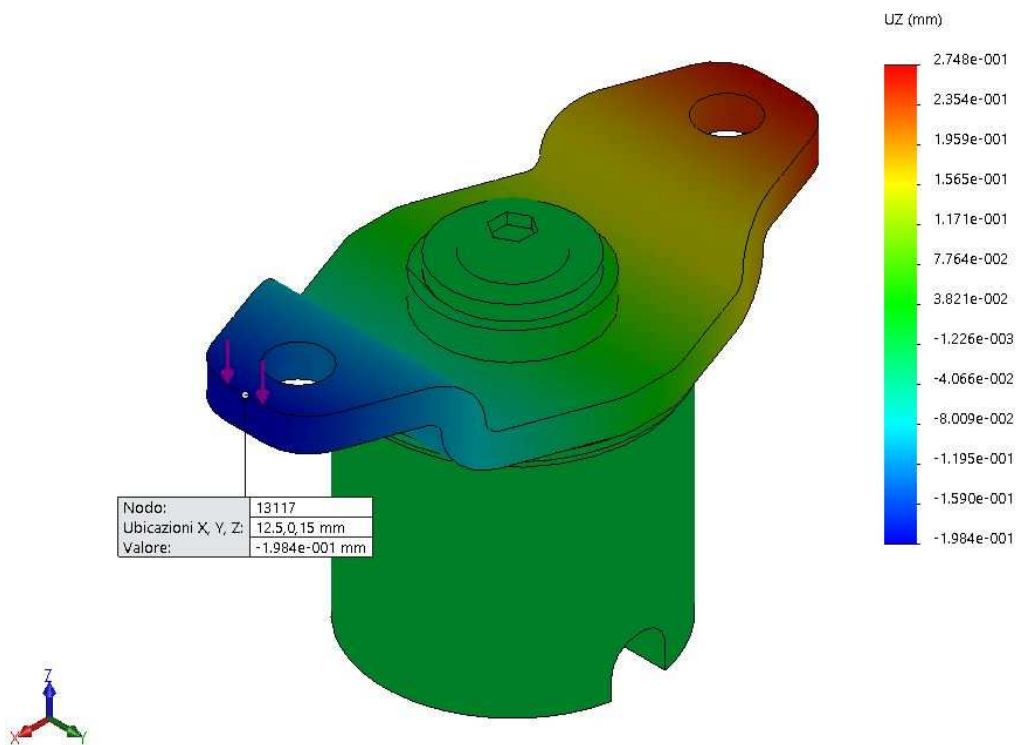


Figure 4.60 – Static analysis 8 - pitch, displacement values.

The error between the computed and the expected stiffness is reduced down to 5%, as presented in Table 4.53. The asymmetry is still affecting the analysis. . A further reduction in spacer Young modulus is required.

4.4.1.9 Static analysis 9 - pitch

In the following tables are presented the setup parameters.

Table 4.54 – Mesh parameters.

Parameter	Units of measurements	Value
Type of mesh	-	Tetraedric elements
Mesher	-	Curvature based
Number of Jacobian points	-	4
Max dimension	[mm]	2.086
Min dimension	[mm]	0.417
Nodes	-	26103
Elements	-	15177
AR<3	-	89.4
AR>10	-	0.191
AR max	-	23.734
Jacobian (distorted elements)	%	0

Table 4.55 – Analysis parameters.

Parameter	Units of measurements	Value
DOF	-	77052
Solver	-	FFE Plus
Spacer Young modulus	[N/m ²]	565000
O-ring Young modulus	[N/m ²]	4250000
External load	[N]	0.3
Load application point		Omega pad, left wing
Restraints	-	Fixed geometry applied to the base of metallic body

The mathematical model and the related meshed model is presented in the following figures.

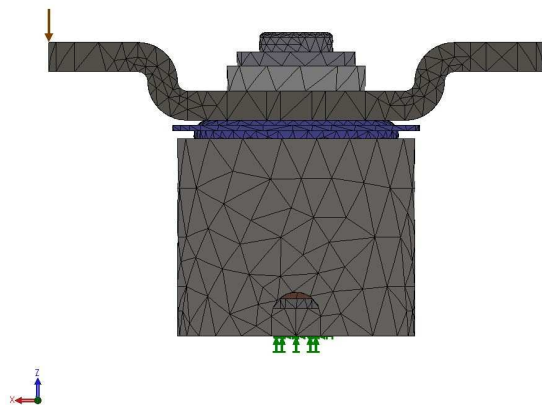


Figure 4.61 – Mathematical model, <X,Z> plane.

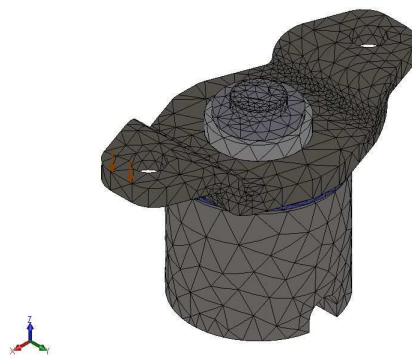


Figure 4.62 – Mathematical model, isometric view.

No penetration contact type is adopted between the following elements:

- flanged screw and spacer;
- spacer and omega pad;
- omega pad and o-ring;
- o-ring and plastic body.

Table 4.56 – Results.

Parameter	Units of measurements	Value
Time of computation	[s]	00:02:03
UZ	[mm]	-2.104 E-1
UX	[mm]	-
UY	[mm]	-
Computed stiffness	[Nmm/rad]	222.79
Error	[%]	1

The displacement along Z axis is measured with respect to node13709, as presented in Figure 4.63

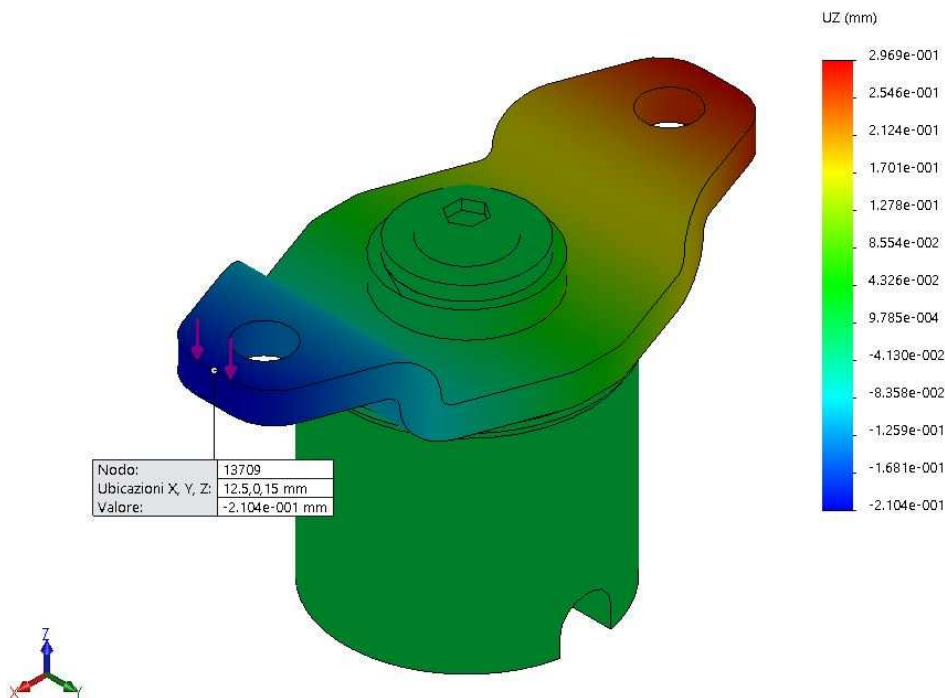


Figure 4.63 – Static analysis 9 - pitch, displacement values.

As presented in Table 4.56, the computed stiffness differs from experimental one only by 1%, which can be considered a good approximation. The Young modulus for the spacer is thus fixed at 565000 N/m². One more analysis is required in order to check the linearity of the stiffness trend with decreasing applied load. A refinement in mesh is also performed to get a more precise result.

4.4.1.10 Static analysis 10 - pitch

In the following tables are presented the setup parameters.

Table 4.57 – Mesh parameters.

Parameter	Units of measurements	Value
Type of mesh	-	Tetraedric elements
Mesher	-	Curvature based
Number of Jacobian points	-	4
Max dimension	[mm]	1.65
Min dimension	[mm]	0.330
Nodes	-	29871
Elements	-	17427
AR<3	-	91.7
AR>10	-	0.149
AR max	-	19.632
Jacobian (distorted elements)	%	0

Table 4.58– Analysis parameters.

Parameter	Units of measurements	Value
DOF	-	88311
Solver	-	FFE Plus
Spacer Young modulus	[N/m ²]	565000
O-ring Young modulus	[N/m ²]	4250000
External load	[N]	0.2
Load application point		Omega pad, left wing
Restraints	-	Fixed geometry applied to the base of metallic body

A mesh refinement, together with a lower applied load are defined in order to perform the analysis

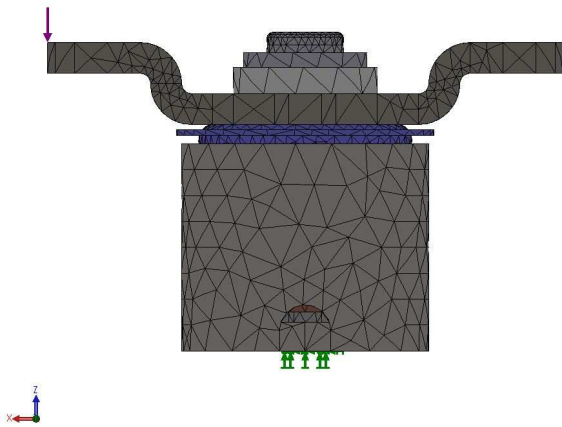


Figure 4.64 – Mathematical model, <X,Z> plane.

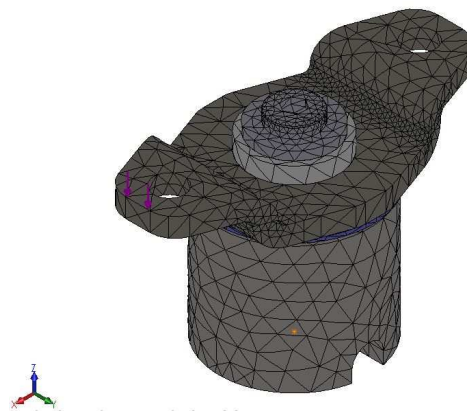


Figure 4.65 – Mathematical model, isometric view.

No penetration contact type is adopted between the following elements:

- flanged screw and spacer;
- spacer and omega pad;
- omega pad and o-ring;
- o-ring and plastic body
- .

Results are presented below.

Table 4.59 – Results.

Parameter	Units of measurements	Value
Time of computation	[s]	00:01:53
UZ	[mm]	-1.148 E-1
UX	[mm]	-
UY	[mm]	-
Computed stiffness	[Nmm/rad]	220.38
Error	[%]	2

The displacement along Z axis is measured with respect to node15688, as presented in Figure 4.63

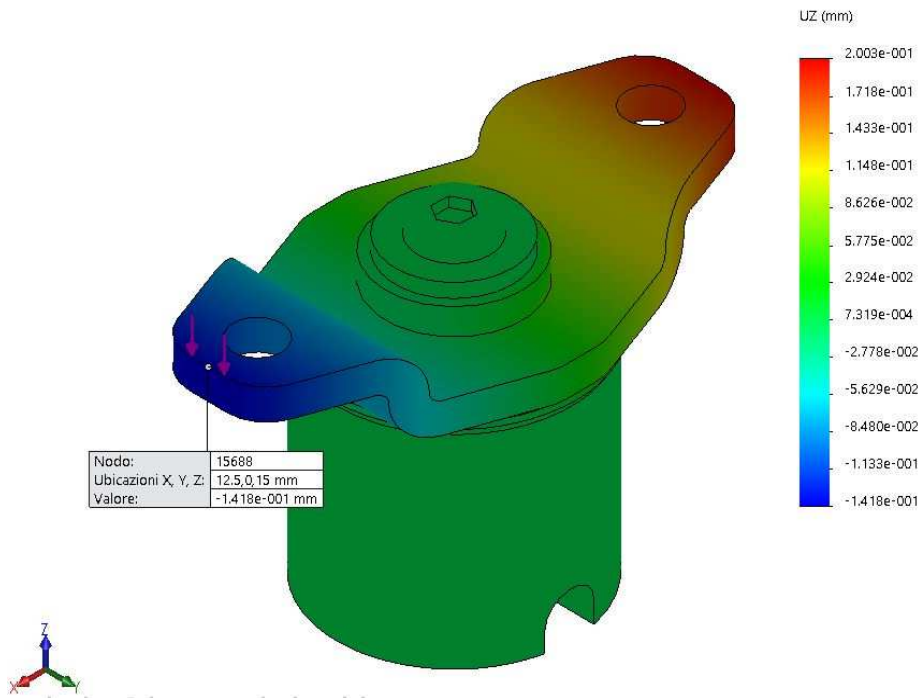


Figure 4.66 – Static analysis 10 - pitch, displacement values.

The computed stiffness differs from previous result only by 1%, thus, the behaviour can be considered linear. The Young modulus for the spacer is thus fixed at 565000 N/m².

4.4.1.11 Static analysis for pitch motion: results

Results of previous analyses is here summarized in Table 4.60

Table 4.60 – Results.

Young modulus [N/m ²]	Displacement [mm]	Stiffness [Nmm/rad]	Error [%]
50000000	-2.047 E-1	763.2	241
5000000	-2.966 E-1	526.8	135
2050000	-3.9170 E-1	398.9	78
1250000	-2.966 E-1	334.4	54
970000	-4.537 E-1	398.9	37
900000	-5.086E-1	307.2	25
750000	-2.785 E-1	280.5	15
650000	-1.984 E-1	236.3	5
565000	-2.104 E-1	222.8	1
565000	-1.418 E-1	220.4	2

The Young modulus for spacer element is thus set to 565000 N/m², being the error with respect to experimental analysis equal to 2%.

4.4.2 Mathematical model for roll motion

The roll motion is analyzed in order to check the results obtained from pitch motion. In particular, being the Young modules of the elastic elements fixed, this analysis is performed in order to check the quality of the model.

A single analysis is performed considering that, for roll behaviour, the stiffness is computed as:

$$k = \frac{C}{\vartheta} \left[\frac{Nmm}{rad} \right] \quad (4.6)$$

where:

$$C = F \cdot b \quad (4.7)$$

$$b = 6.50 \text{ mm} \quad (4.8)$$

$$\vartheta = \arcsin\left(\frac{z}{b}\right) \sim \frac{z}{b} \quad (\text{for small oscillations approximation}) \quad (4.9)$$

where:

- C is the resulting torque [Nmm];
- F is the applied axial load [N];
- b is the arm of the applied torque [mm];
- z is the displacement along Z axis of the point where the force is applied [mm];
- ϑ is the angle corresponding to the axial displacement [rad].

The applied load and the lever arm relative to roll motion are presented in Figure 4.67.

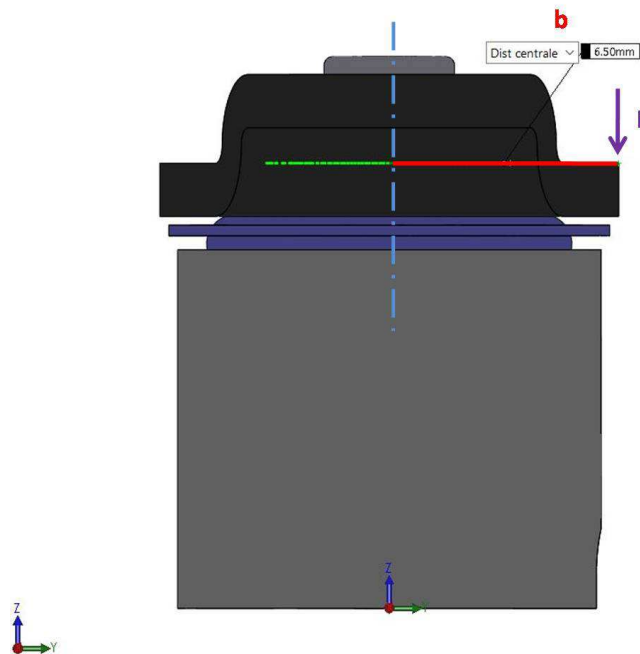


Figure 4.67 – Mathematical model, applied load and lever arm.

4.4.2.1 Static analysis 1 - roll

In the following tables are presented the setup parameters.

Table 4.61 – Mesh parameters.

Parameter	Units of measurements	Value
Type of mesh	-	Tetraedric elements
Mesher	-	Curvature based
Number of Jacobian points	-	4
Max dimension	[mm]	1.59
Min dimension	[mm]	0.319
Nodes	-	31090
Elements	-	18246
AR<3	-	92.5
AR>10	-	0.159
AR max	-	22.41
Jacobian (distorted elements)	%	0

Table 4.62 – Analysis parameters.

Parameter	Units of measurements	Value
DOF	-	91980
Solver	-	FFE Plus
Spacer Young modulus	[N/m ²]	565000
O-ring Young modulus	[N/m ²]	4250000
External load	[N]	0.3
Load application point		Omega pad, left side
Restraints	-	Fixed geometry applied to the base of metallic body

The load is applied on the edge of the omega pad so that to reproduce the experimental analysis. The difference is in the lever arm value, 6.5 mm against 6 mm of the experimental analysis, which, anyway, does not affect the stiffness computation process.

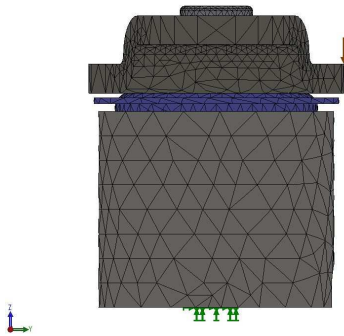


Figure 4.68 – Mathematical model, <Y,Z> plane.

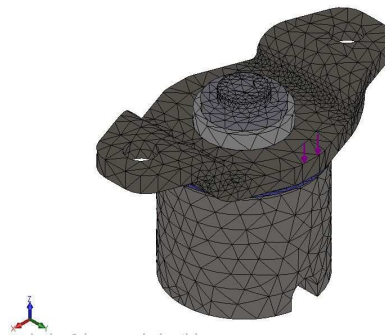


Figure 4.69 – Mathematical model, isometric view.

No penetration contact type is adopted between the following elements:

- flanged screw and spacer;
- spacer and omega pad;
- omega pad and o-ring;
- o-ring and plastic body.
-

Results are presented below.

Table 4.63 – Results.

Parameter	Units of measurements	Value
Time of computation	[s]	00:02:48
UZ	[mm]	-4.525E-2
UX	[mm]	-
UY	[mm]	-
Computed stiffness	[Nmm/rad]	280.11
Error	[%]	25

The displacement along Z axis is measured with respect to node16424, as presented in Figure 4.70.

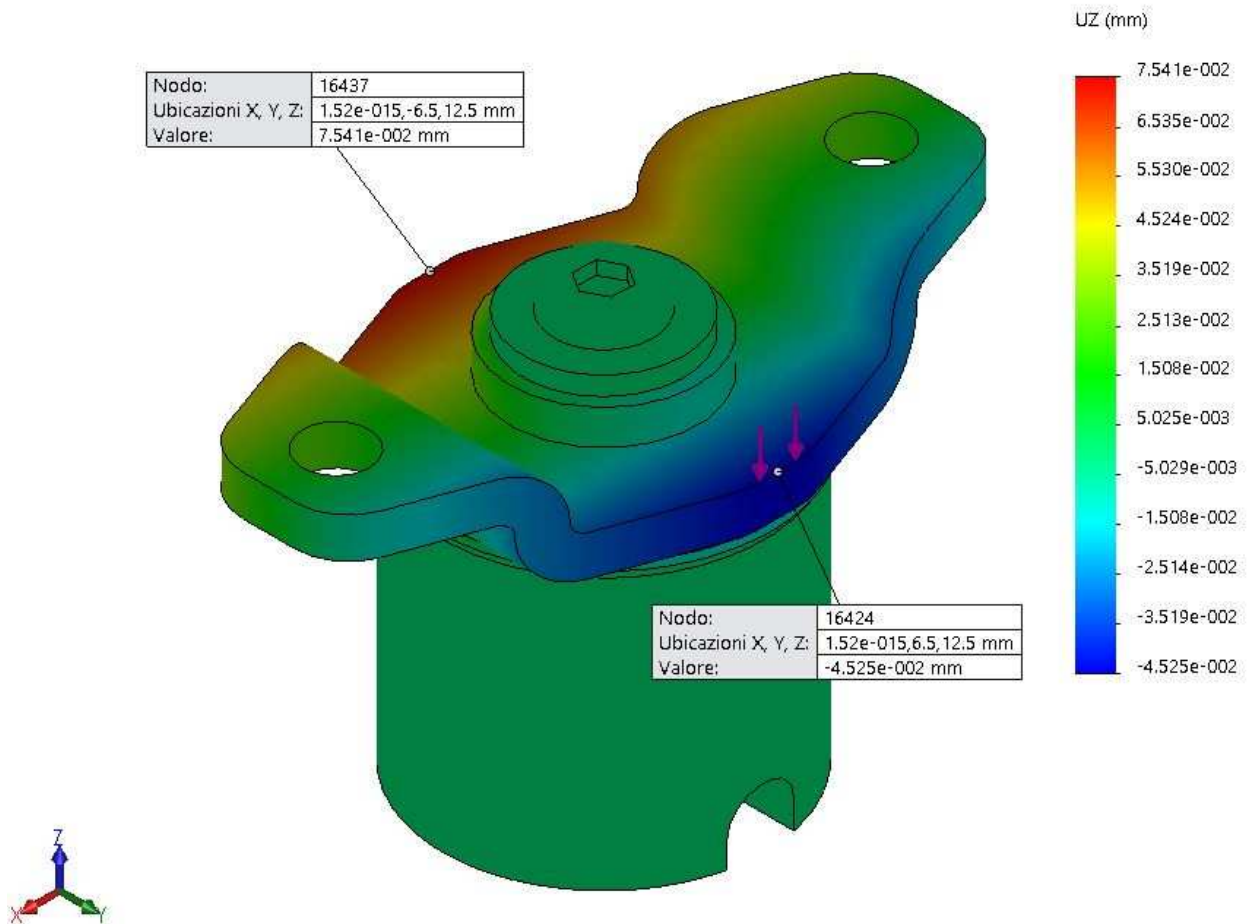


Figure 4.70 – Static analysis 8 - axial, displacement values.

A strong asymmetry is affecting the model between the displacement of the sides of the omega pad:

- -4.525 E-2 mm for node 16424,
- 7.541 E-2 mm for node 16437.

Considering the results of Table 4.63, the computed stiffness differs from the results relative to pitch motion analysis by 25%. However, considering the range within the experimental stiffness falls, 177Nmm/rad up to 284 Nmm/rad, the results is still within the range.

4.5 Conclusions

The objective of the presented analyses is to produce a model that reproduces the physical device. The method through which this is accomplished is based on a trial and error procedure, which requires the continuous update of the model parameters, in this case the Young modules of the elastic elements.

Due to the complexity of the physical device, the procedure it is decided to split the test between the o-ring characterization, which is performed through the FE static analysis in axial displacement, and the spacer characterization, which is performed through the pitch FE static analysis of the pitch motion. A double check is performed with the FE static analysis of the roll motion, where it is expected the results to fall within the range of the experimental data.

From the computed results it can be observed that:

- the Young modules of the elastic elements which satisfy the requirements on the stiffness, and in particular the one of the spacer, are low compared to the ones of a typical elastomeric rubber element;
- the results between the pitch and roll motion, which are expected to be similar, present a discrepancy of about 25%, even though the value falls within the experimental computed range presented in chapter 2;
- even if small, FE static analyses shows that there are present slip motions of the omega pad along X and Y. These motion were not characterized during experimental tests because of the impossibility to physically measure them. In this sense, the obtained results are for sure affected by these "physiological" slip displacements. but there is no numerical evidence upon which we can rely on.

By stating that, the achieved results are anyhow meaningful with respect the objective of this thesis work, which aim mostly to show a method and a practical case study through which the mathematical modelling procedure of a physical device is done.

As a further step, it can be considered to model the elastic elements as assemblies of multiples sub-elements, each of one characterized with its own elastic properties, in order to achieve a more precise approximation of the experimental data.

Furthermore, a wider experimental background is preferable, which however would involve a different work load, that is beyond the scope of this master's thesis work.

5. Modal experimental analysis

In the following chapter are presented the experimental analyzes carried out at DIMEAS laboratory of the Politecnico di Torino.

The objective of this test is the dynamic characterization of the device and, in particular, to estimate and identify the modal parameter of the system, which are:

- natural frequencies,
- damping factors,
- mode shapes.

The main characteristics of the analysis are:

- the acquisition system;
- type of excitation;
- the measured parameters;
- the identification methods.

5.1 Test definition

The analysis is conducted by exciting the model through a vibrating bench using a sweep excitation. The measurements are collected thanks an acquisition system made by:

- signal generator;
- amplifier;
- excitation system (electromagnetic shaker);
- structure;
- transducers;
- analyzer.

These device allow to excite the structure, read and transform the physical quantities into electrical signals and process the response of the system to the excitation (FRF).

In Figure 5.1 is presented a scheme of the acquisition system.

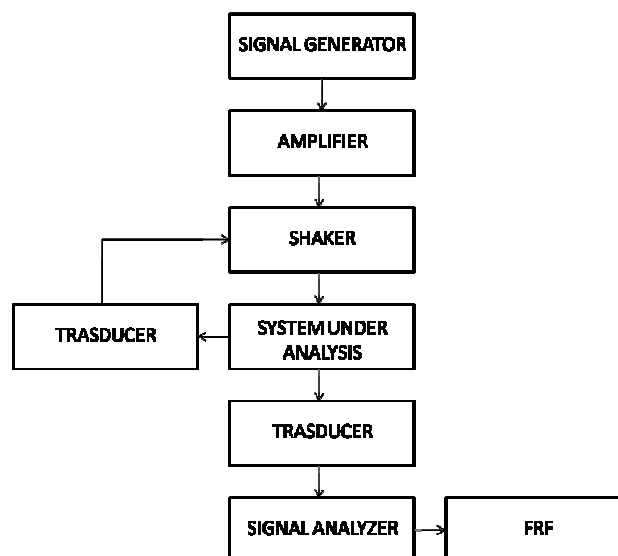


Figure 5.1 – Acquisition system scheme.

In particular:

- the signal generator is the device that determines the type of force and excitation that the system has to undergo;
- the amplifier amplifies the signal from the generator and sends it to the excitation generator;
- the shaker is an electromechanical device that converts the electrical signal delivered from the amplifier into a physical signal, the excitation;
- the system under analysis undergoes the excitation and provides a physical output that is read by the transducers;
- the transducers, usually accelerometers, read and convert the output into an electrical signal. We have two sets of transducers, one of which sends feedback of the input excitation signal and the others that actually collect the output from the device under test.
- finally the signal analyzer collects the electrical signal from the transducers and compute the FRF.

Speaking about the type of excitation, modal parameters can be detected using different input signals, one of which consists in the sine wave excitation.

This type of excitation test has the purpose to give an overall understanding of the device behaviour. The input signal is so described in time as a sinusoidal function:

$$y(t) = A \cdot \sin(\omega t) \quad (5.1)$$

where A is the input amplitude and ω is the vibration frequency [rad/s].

These parameters are given during the test setup.

The sweep over a range of excitation frequencies is achieved thanks to the fact that the argument of the sinusoidal function varies in time, increasing or decreasing in this way the excitation frequency.

Note that, at different time instants, the system is excited by a single frequency.

The main parameters to be set are:

- acceleration of excitation, given in G;
- frequency domain [minimum frequency; maximum frequency];
- amplitude displacement, limit of the shaker (peak-peak, zero-peaks), given in millimeters;
- type of sweep rate;
- type of cycle (increasing excitation, decreasing excitation, combined).

Given the setup, the test is run and the output signal is detected and analyzed, producing the FRF, Frequency Response Function of the system.

Once the FRF is computed a suitable method for the modal parameter extraction has to be chosen.

For modal parameter extraction is intended a method based process through which we manipulate the FRF and are able to identify the modes of the system together with its natural frequencies and damping factors.

In this analysis we rely on PolyMAX, that stands for "Polyreference least-squares complex frequency-domain method".

5.2 System setup

The setup concerning the structure, measuring device, measured coordinates and test configurations are herein presented.

5.2.1 System setup: accelerometers and structure

The tests are conducted in the DIMEAS laboratory of the Politecnico di Torino.

The equipments consists in:

- electromechanical shaker;
- 3 laser accelerometers: LK-H 150, LK-H 80, LK-H 50;
- workbench;
- assembled structure to constrain the accelerometers.

In order to fully define the system 2 coordinates are required:

- ϑ which is the rotation angle about the axes of symmetry, in both X and Y directions;
- x_G which is the axial displacement along Z axis of the omega pad.

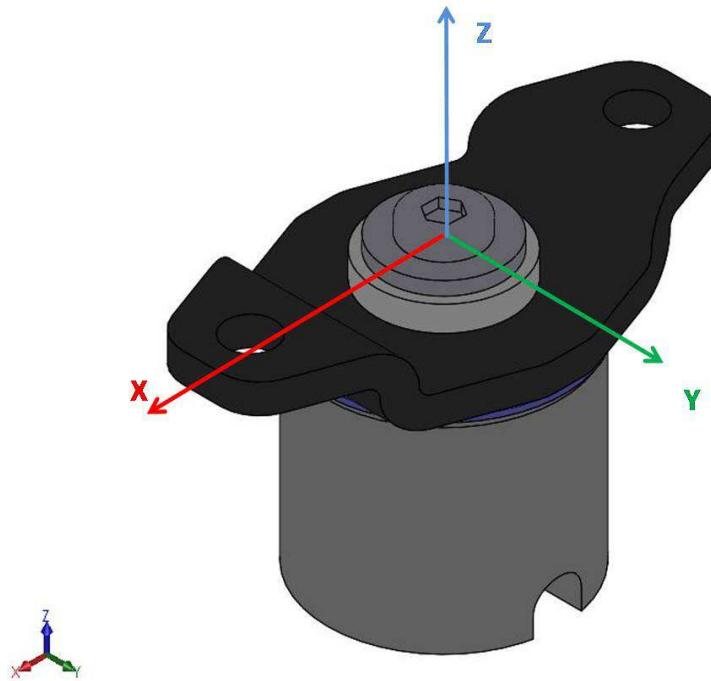


Figure 5.1 – Reference system.

In order to be able to define the previous displacements, considering that we're dealing with accelerometers that measure axial displacement, 3 axial coordinates, along Z axis, are required to be measured:

$$\left\{ \begin{array}{l} \vartheta = \arcsin\left(\frac{x_B - x_A}{L}\right) \sim \left(\frac{x_B - x_A}{L}\right) \\ x_G = \left(\frac{x_B - x_A}{2} - x_P\right) \end{array} \right\} \quad (5.1)$$

where:

- x_A and x_B are the axial displacements of two points on the omega pad;
- x_P is the rigid axial displacement of the base upon which the niceclick is constrained to. It's equal to the displacement imposed by the shaker;
- L is the distance between the x_A and x_B .

As mentioned in the chapter 3, Figure 3.1, being the component described according to its 3 main motions, axial shaking, roll and pitch, measurements are conducted along both X and Y axes by keeping the same sets of coordinates, by simply changing the value for L parameter.

5.2.2 System setup: accelerometers and structure

The initial setup consists in defining a suitable structure upon which the measuring transducers are constrained to.

For the tests are adopted 3 laser accelerometers, corresponding to the 3 measured outputs, operating at 3 different relative distances from the measuring points:

- LK H - 50 mm;
- LK H - 80 mm;
- LK H - 150 mm.

In Figure 5.2 is presented the structure and the laser configuration.



Figure 5.2 – Clamped free configuration.

Considering the measured coordinates, the laser arrangement corresponds to the following outputs, presented in Table 5.1.

Table 5.1 – Laser setup.

Measured output	Laser	Measured coordinate
Output1	LK H - 50	x_A
Output 2	LK H - 150	x_B
Output 3	LK H - 80	x_P

Considering the device under test, a clamped-free configuration is defined, in which the device is fixed to the shaker from its metallic body as presented in Figure 5.3.

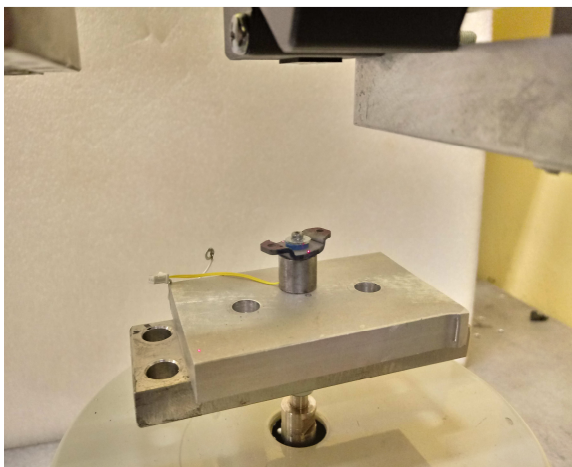


Figure 5.3 – Clamped free configuration.

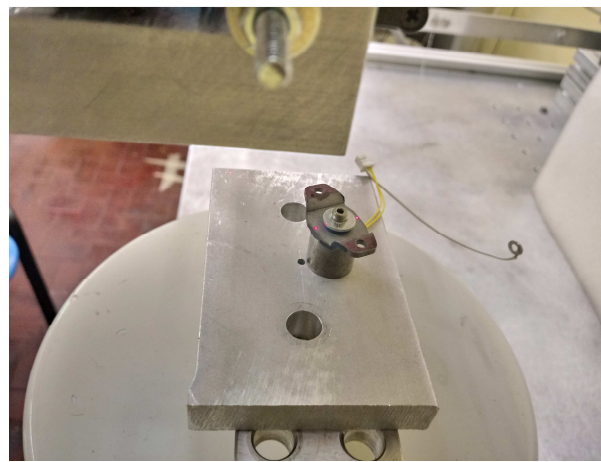


Figure 5.4 – Laser beam.

A preliminary test performed to check the configuration highlights that it is not possible to obtain repeatable results between the frequency response functions.

In particular, by exciting the system several times over the frequency range 0 - 1000 Hz and setting different input amplitudes, 0.1 mm, 0.01 mm and 0.005 mm, it is not possible to obtain FRFs which are comparable with each other. A possible explanation to this effect is attributed to the following main reasons:

- the omega pad reduced weight;
- the omega pad available surface too small to guarantee the laser beam to measure the displacement over the complete frequency domain;

According to these indications, the configuration is updated adding 2 metal plates, of the total weight of 60.6g, and fixing them on the omega pad, as presented in Figure 5.5 and 5.6.

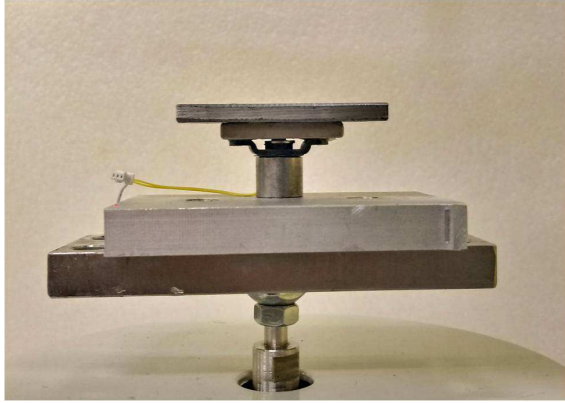


Figure 5.5 – Updated configuration: additional masses.



Figure 5.6 – Updated configuration: additional masses.

The measured points are defined as follows. As defined in previous chapters, the main characteristic motions of the device are the axial and the rotational ones, relatively pitch and roll. In order to study all these behaviours and to acquire an exhaustive amount of data which can fully describe the motion of the omega, the following measured points are defined:

- axial and pitch behaviour characterization:
 - x_A : point 8;
 - x_B : point 7;
 - x_P : point 6.

- axial and roll behaviour characterization:
 - x_A : point 9;
 - x_B : point 10;
 - x_P : point 6;

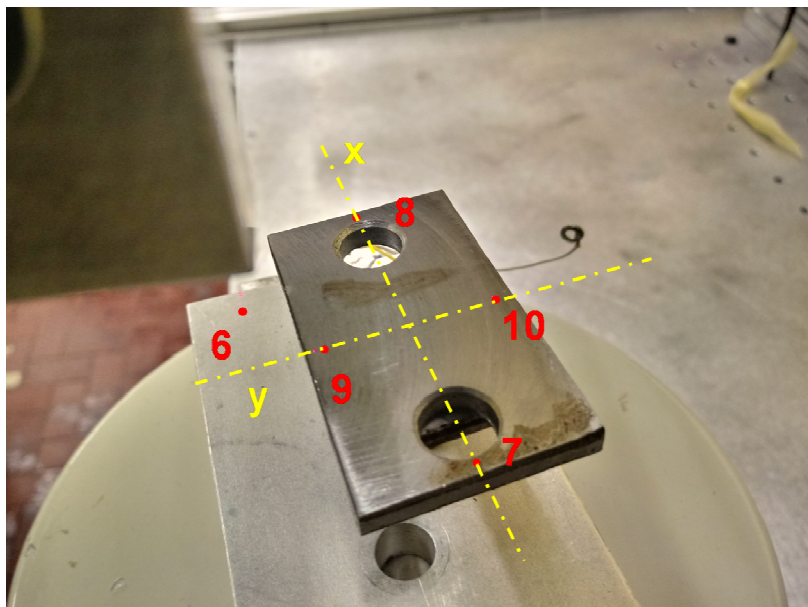


Figure 5.7 – Measured points.

5.2.3 Test setup: input parameters and configurations

The main parameters of the test are presented in Table 5.2

Table 5.2 – Test parameters.

Property	Unit of measurement	Value
Minimum frequency (sweep)	[Hz]	30
Maximum frequency (sweep)	[Hz]	500
Resolution	[Hz]	0.1
Sweep direction	-	up
Rate	[Hz/s]	1
Input vibration amplitude	[mm]	0.01
		0.005
Additional mass	[g]	60.6

As presented in Figure 5.7, in order to fully define the motion of the omega pad it is necessary to be able to measure the defined points. In this sense, being the acquisition system made by 3 measuring laser, that measure x_A , x_B and x_P , and being the points to be measured 5, are required 2 configurations reported below.

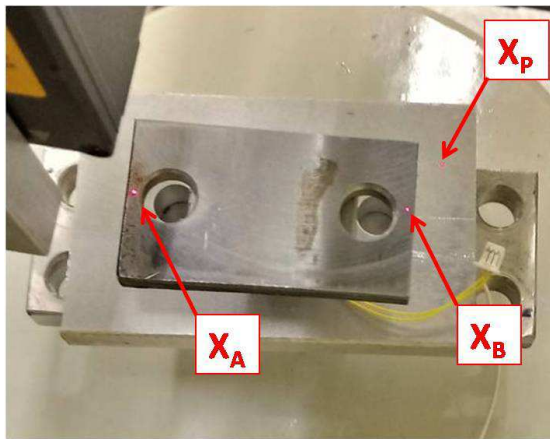


Figure 5.8 – Configuration A.

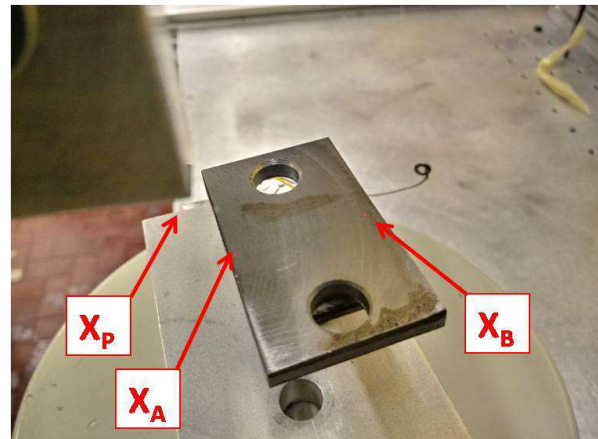


Figure 5.9 – Configuration B.

Each configuration is tested for the two input vibration amplitude.

5.3 Results

In this paragraph are presented the results, which consists, for each amplitude, in:

- FRF and relative synthesized FRF for each point, for each amplitude;
- BODE plot for each amplitude;
- Computed natural frequencies;
- Mode shapes.

5.3.1 Input vibration amplitude: 0.01 mm

The device is tested according to the parameters presented in Table 5.2, with an input amplitude equal to 0.01 mm.

As presented in Figure 5.8 and 5.9, configurations A and B are tested separately.

They generates the following FRFs:

- FRF 7 and FRF 8;
- FRF 9 and FRF 10.

These results and the relative synthesis are presented in the following Figures.

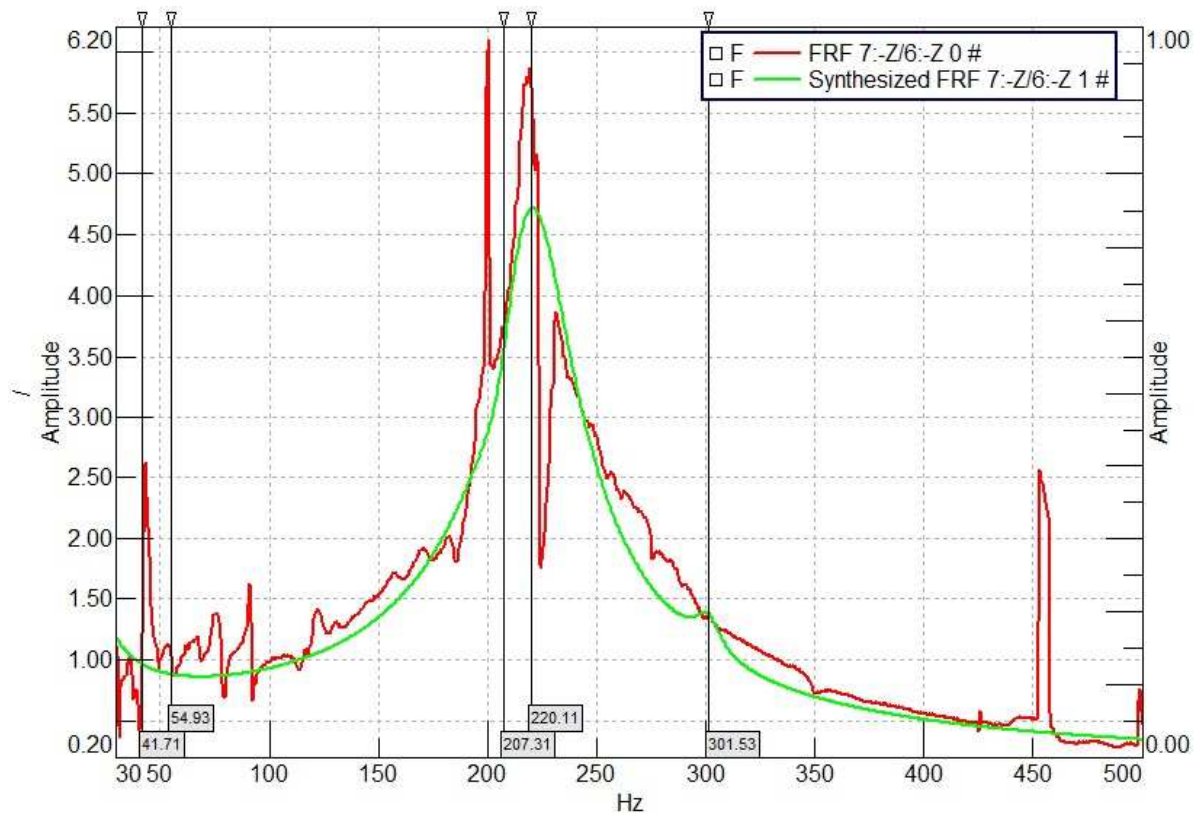


Figure 5.10 – FRF and synthesis of point 7.

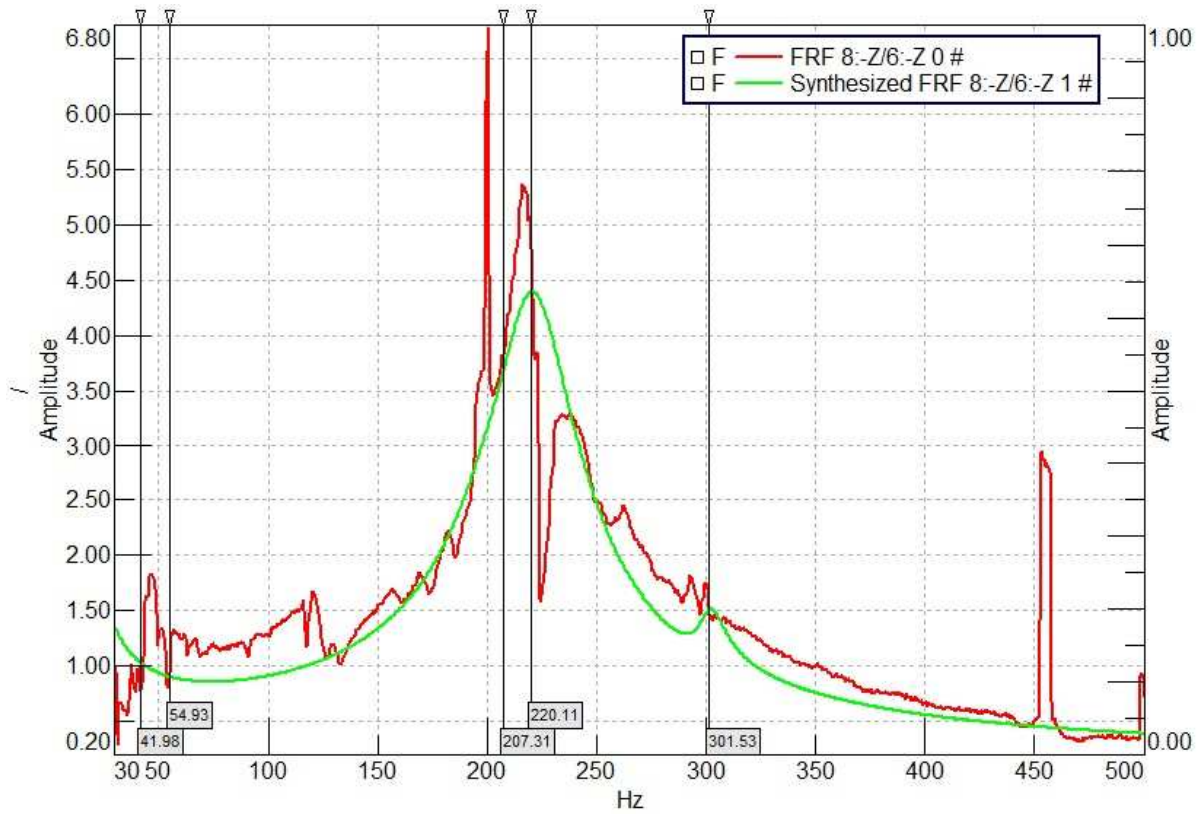


Figure 5.11 – FRF and synthesis of point 8.

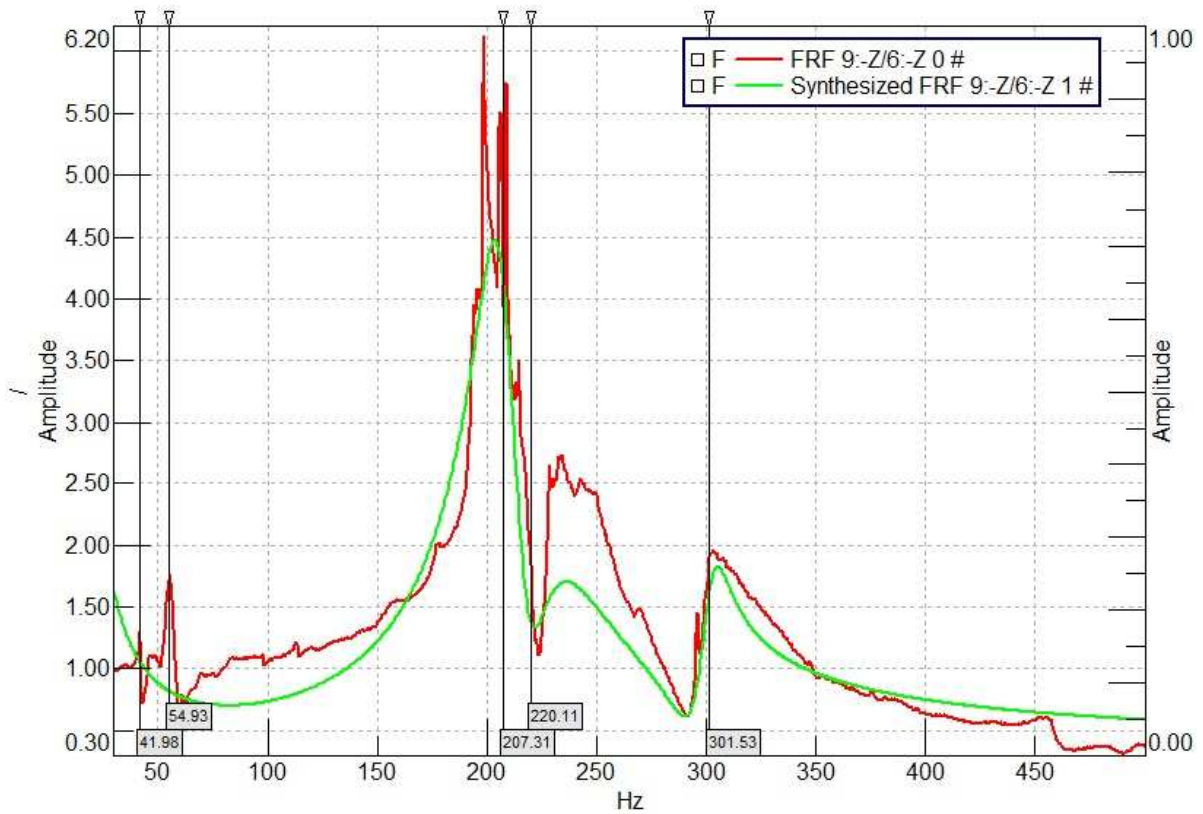


Figure 5.12 – FRF and synthesis of point 9.

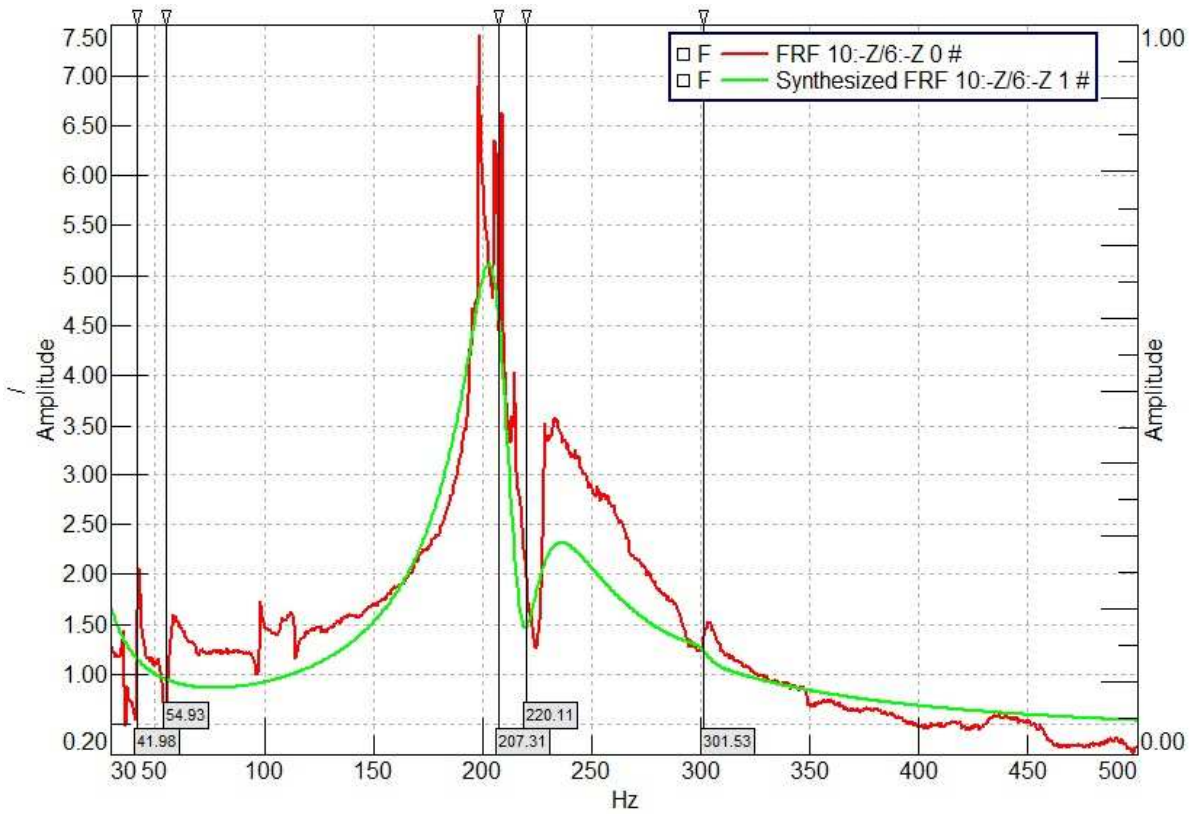


Figure 5.13 – FRF and synthesis of point 10.

The Bode plot, consisting in the diagram representing amplitude and phase of the system response with respect the frequency range, is presented in Figure 5.14.

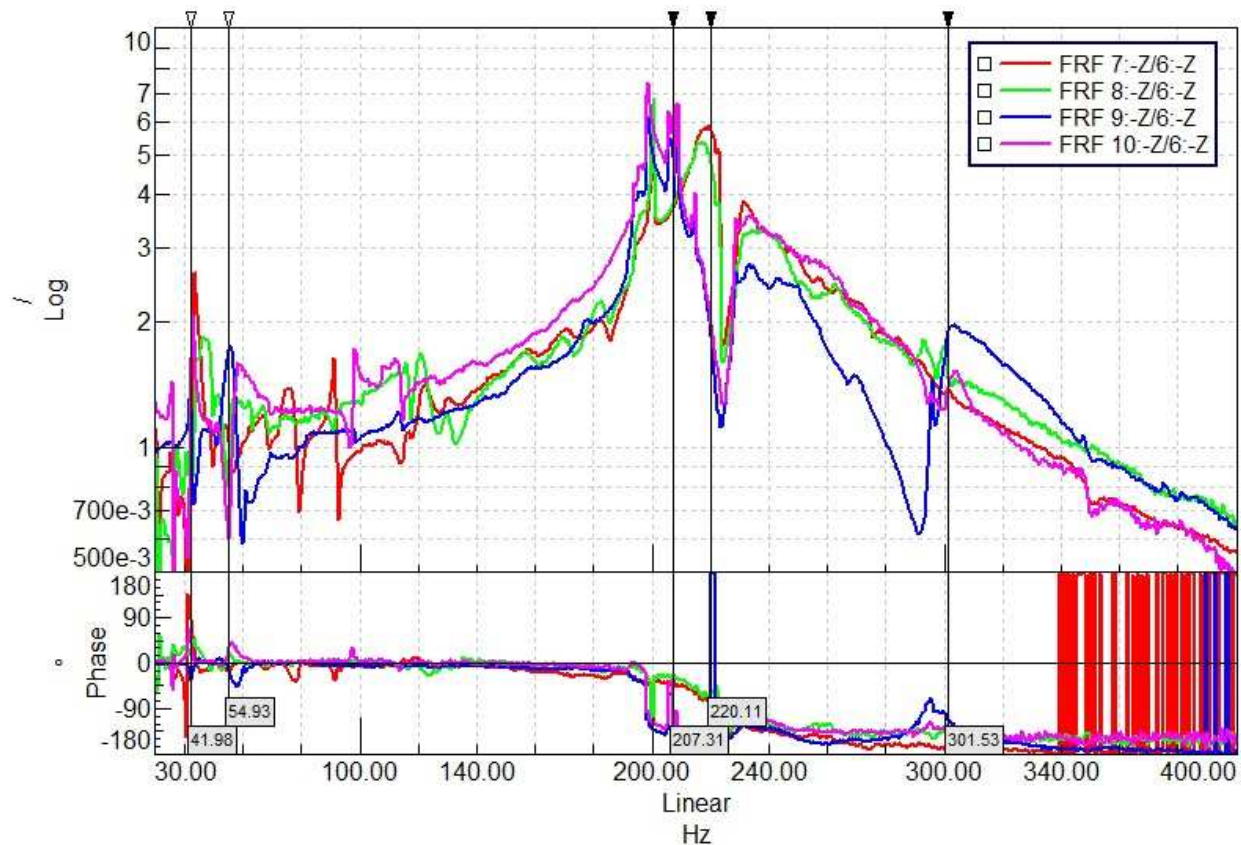


Figure 5.14 – Bode plot.

The modal parameters extraction is performed through the stabilization diagram. This procedure is required in order to define which are the "structural modes" and which are the "computational ones", numerically computed and based on errors.

Considering the FRFs, the structural modes are the ones which, at resonance peaks, are the most stable among the FRF.

In this case, the stable modes and the corresponding natural frequencies are presented in Table 5.3

Table 5.3 – Results for 0.01 mm input amplitude.

Mode	Frequency [Hz]	Damping [%]	Mode description
1	41.98	1.23	Pitch about Y axis
2	54.93	0.99	Roll about X axis
3	207.31	5.22	Not defined
4	220.10	9.16	Rigid translation in Z axis
5	301.53	2.37	Roll about X axis coupled with translation in Z axis

It is important to remark that during the analysis it is detected a contact between omega pad and metallic body around 250 Hz, which introduces a non linearity. This produced an error in the computed results so that it is required to lower the input amplitude.

5.3.2 Input vibration amplitude: 0.005 mm

During this second analysis, the device is tested according to the parameters presented in Table 5.2, with an input amplitude equal to 0.005 mm. That's because we're trying to eliminate the non linearity caused by the contact between omega pad and metallic body which was present in the previous analysis.

The same procedure is applied as before.

The resulting FRFs and synthesized FRFs are presented in the following Figures.

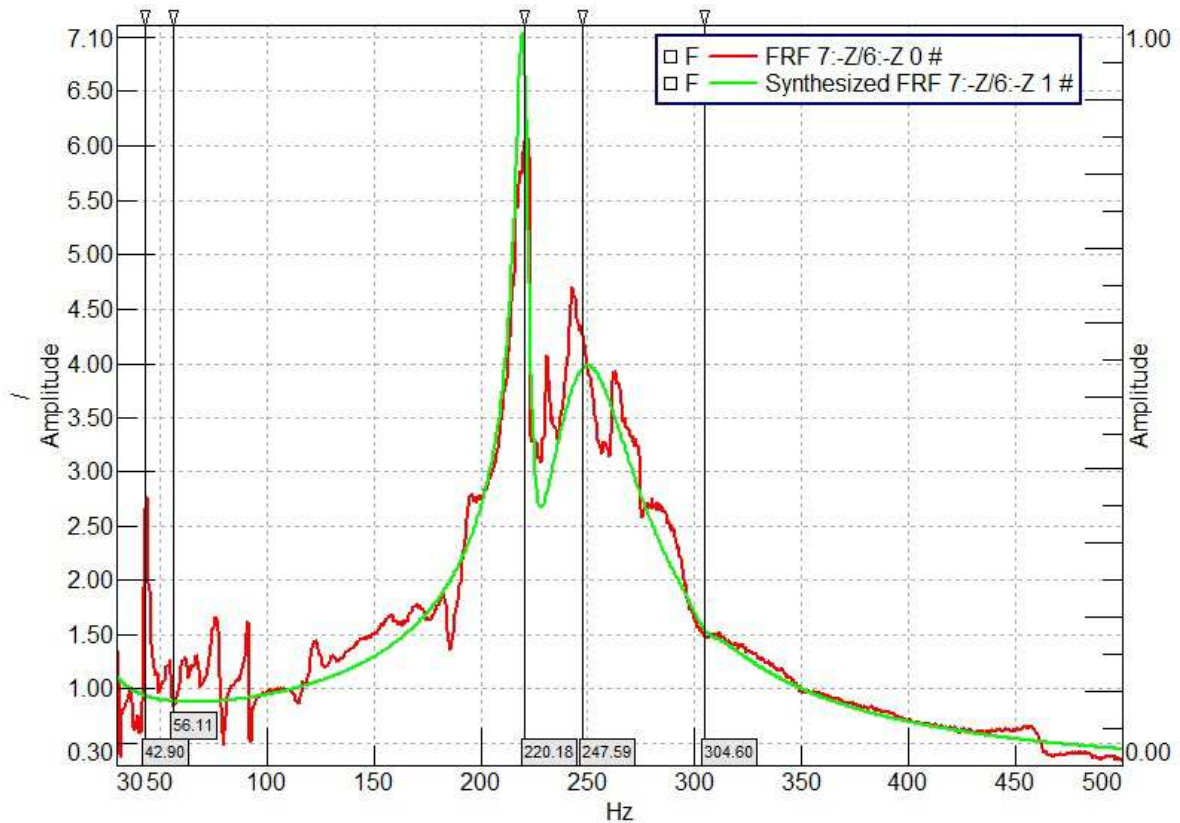


Figure 5.15 – FRF and synthesis of point 7.

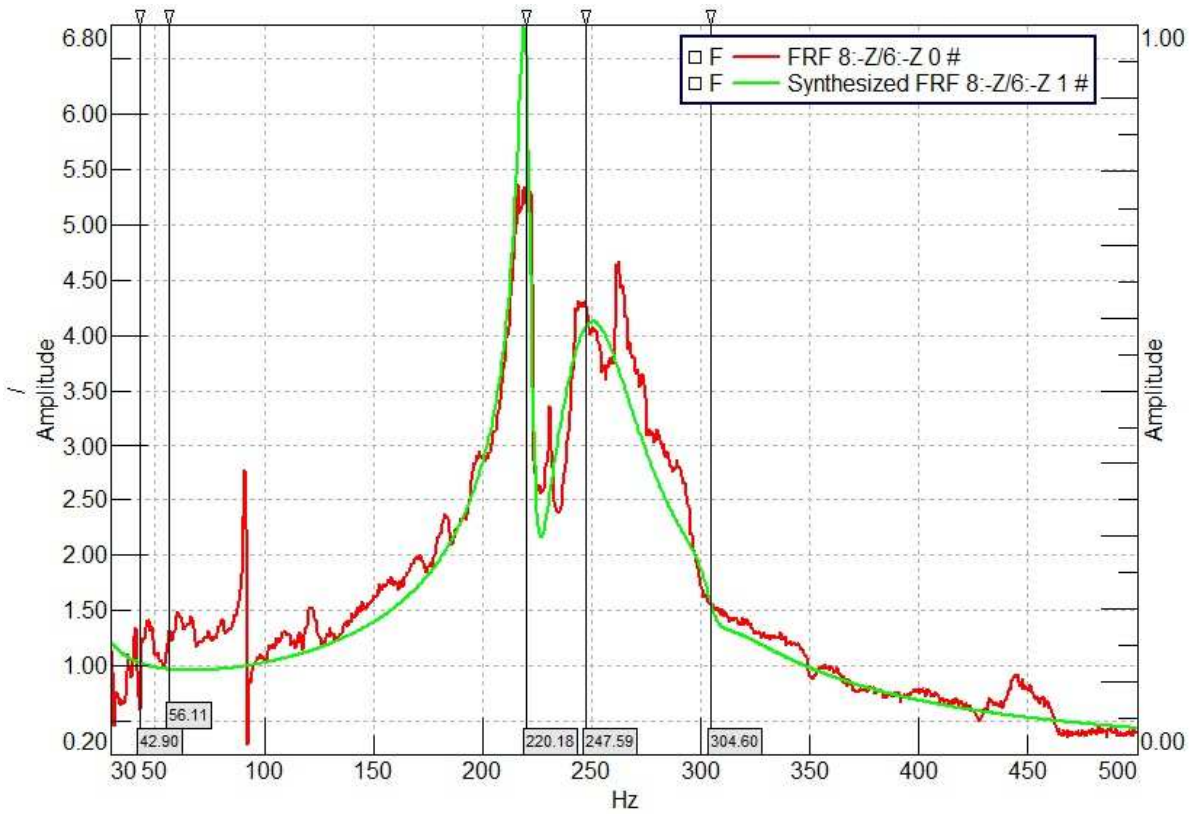


Figure 5.16 – FRF and synthesis of point 8.

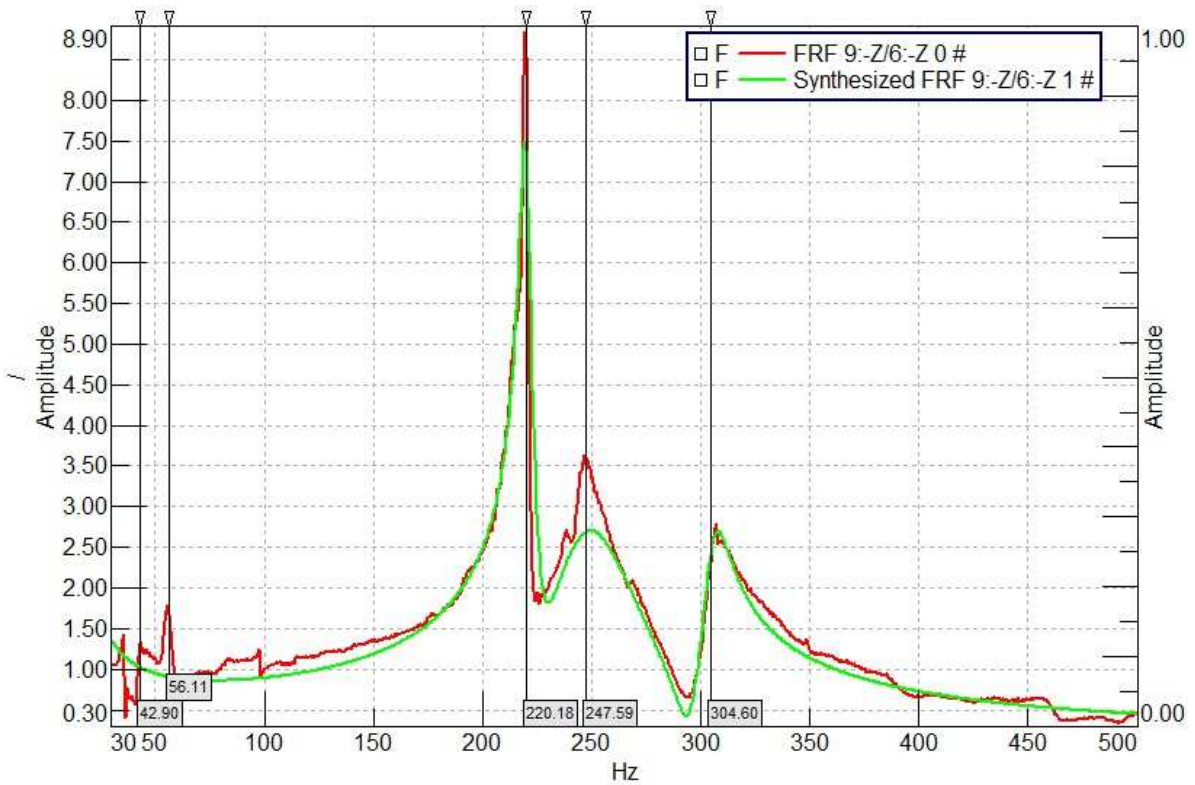


Figure 5.17 – FRF and synthesis of point 9.

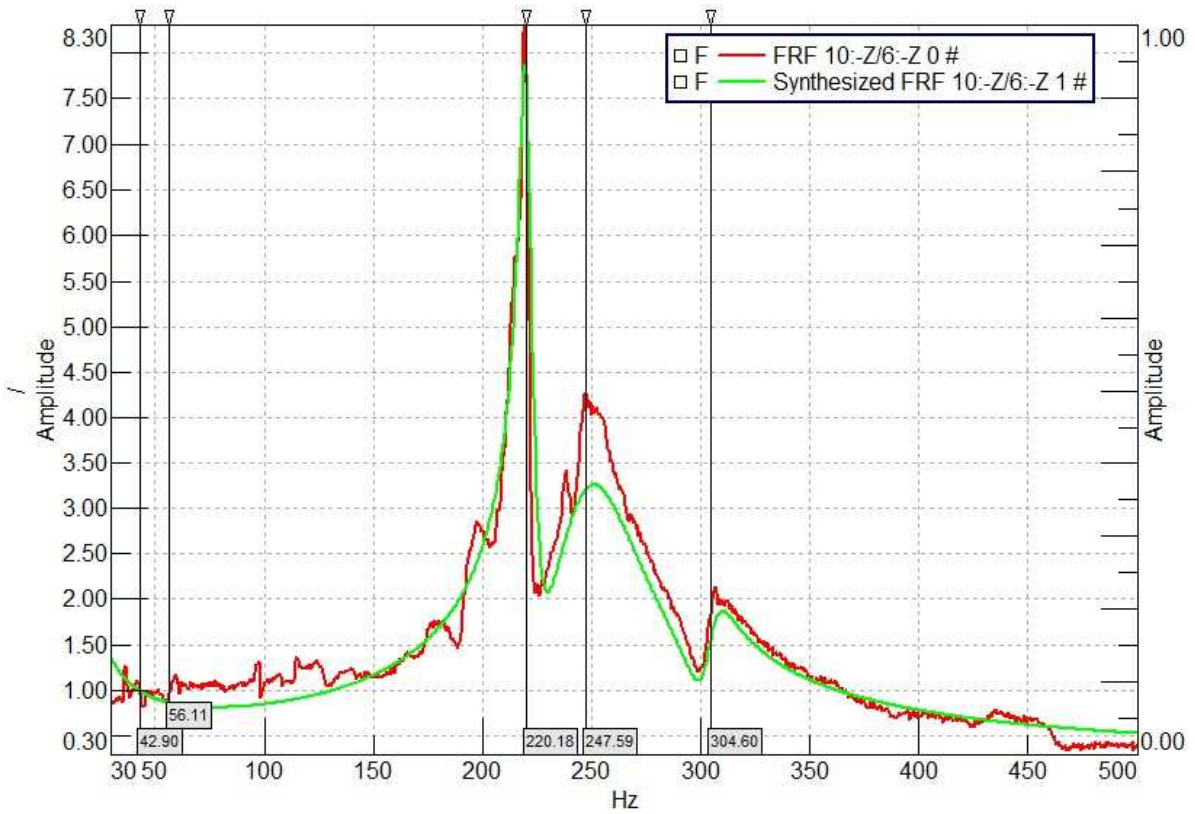


Figure 5.18 – FRF and synthesis of point 10.

The Bode plot is presented in Figure 5.19.

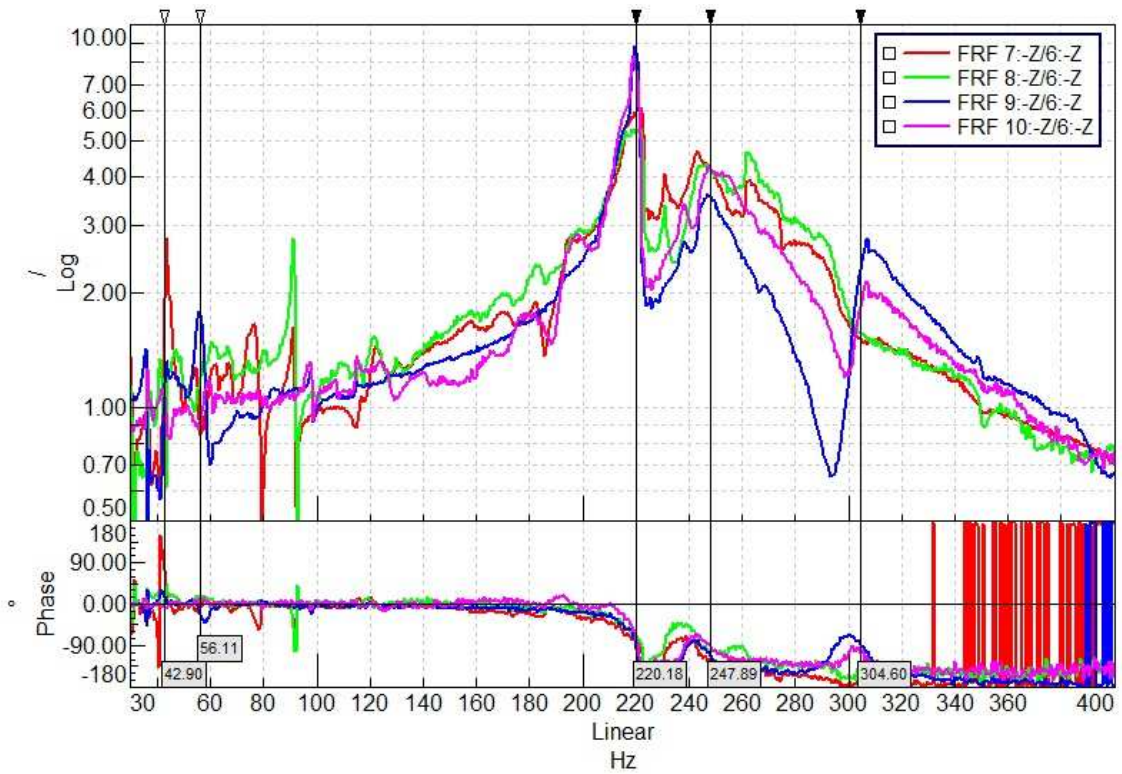


Figure 5.19 – Bode plot.

The modal parameter extraction procedure produces the following results, presented in Table 5.4.

Table 5.4 – Results for 0.005 mm input amplitude.

Mode	Frequency [Hz]	Damping [%]	Mode description
1	42.90	1.72	Pitch about Y axis
2	56.11	0.37	Roll about X axis
3	220.18	1.43	Rigid translation in Z axis
4	247.59	9.61	Pitch about Y axis coupled with translation in Z axis
5	304.6	2.32	Roll about X axis coupled with translation in Z axis

All mode shapes, shaking, roll and pitch are present, with a coupling between axial and rotational motion in modes 4 and 5.

In the following figures are presented a stylized omega pad and its main 5 mode shapes.

The edge of the plane element represent the measured point and their displacement according the principal mode shapes.

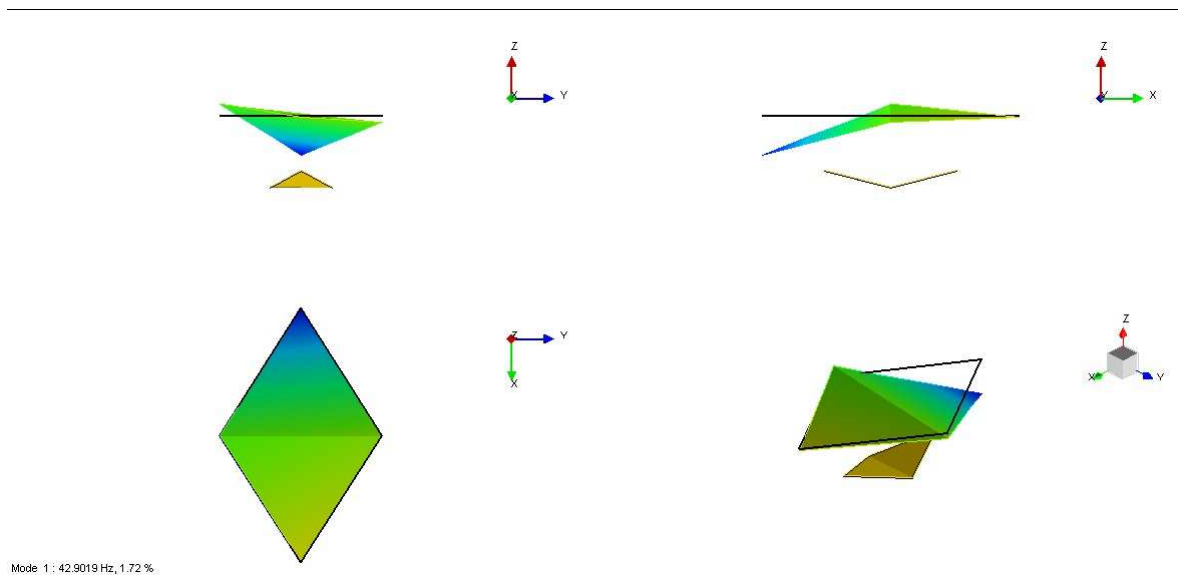


Figure 5.20 – Mode 1, 42.902 Hz, pitch motion.

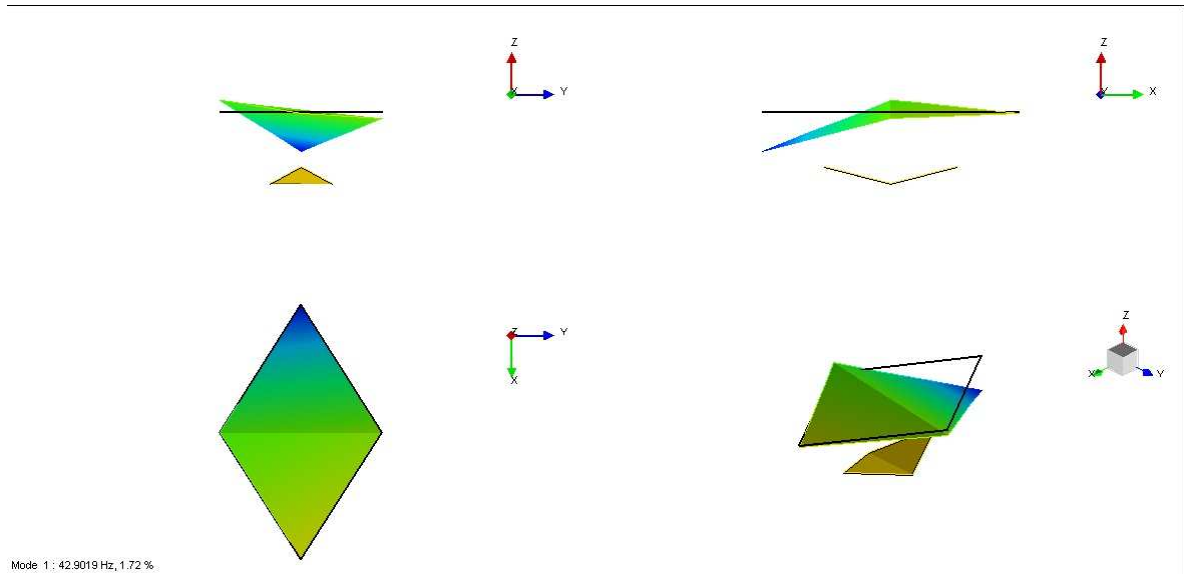


Figure 5.21 – Mode 2, 56.113 Hz, roll motion.

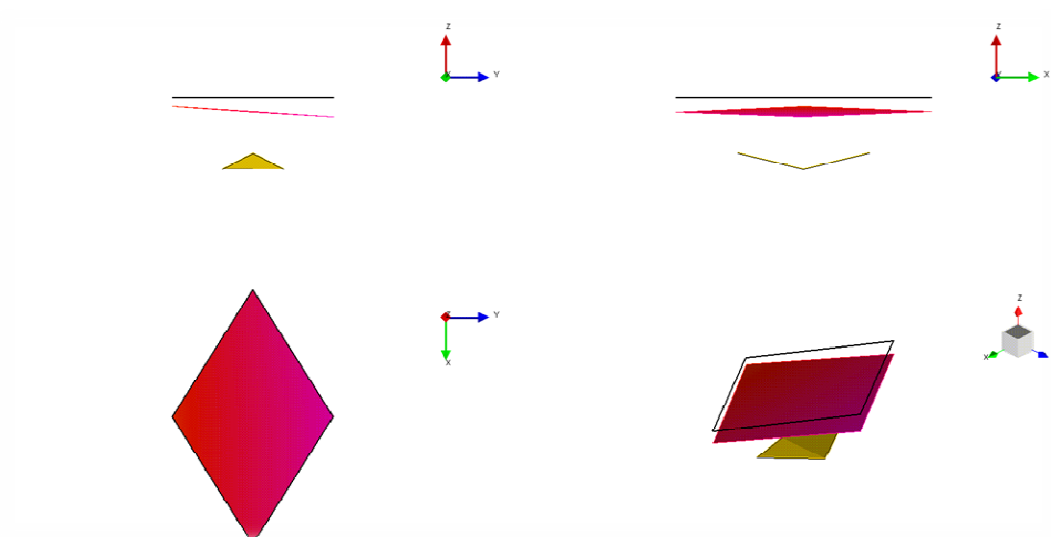


Figure 5.22 – Mode 3, 220.18 Hz, rigid translation.

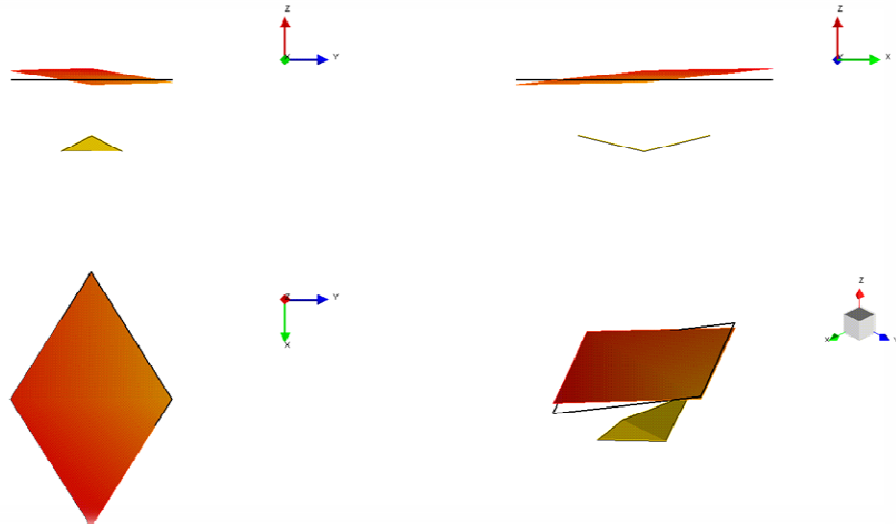


Figure 5.23 – Mode 4, 247.59 Hz, pitch and rigid translation coupling.

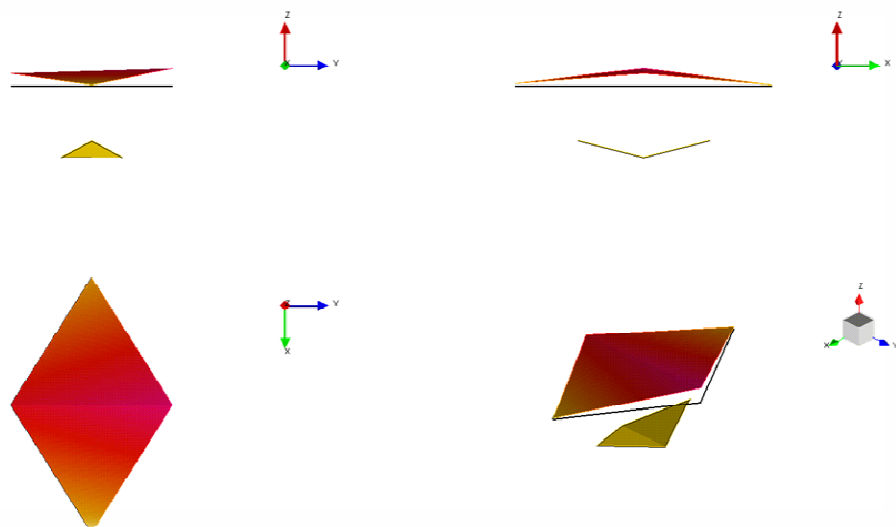


Figure 5.24 – Mode 5, 304.6 Hz, roll and rigid translation coupling.

5.4 Conclusions

The modal experimental analysis performed on the device allows a clear identification of the first global modes.

Considering the reduced dimensions and mass of the device, some modifications to the system are required, like the utilization of an additional mass applied to the omega pad.

The first set of data, relative to the input amplitude shows a non linearity due to a contact between the omega pad and the metallic body, which certainly introduces error during the computation of the mode shapes.

The second set of analysis, based on a lower input amplitude is able to produce satisfying results with a clear identification of the 5 global mode shapes: axial shaking, pitch and roll

6. Finite elements modal analysis

The FE modal analysis is conducted in order to analyze the natural frequencies and the mode shapes of the mathematical model, considering the inertial and elastic properties that were compute in previous chapters.

A comparison between the experimental results and the FE analysis results is the presented.

6.1 Mathematical model and boundary conditions

In order to reproduce the configuration used during the experimental modal analysis, the device is updated by adding 2 additional masses, fully representative of the physical one, of a total weight of 60.64 g.

The final model is presented in Figure 6.1.



Figure 6.1 – Updated mathematical model.

The model is considered to be constrained by the metallic body lower base through a fixed joint. No external load are applied.

6.2 Analyses and results

In the following tables are presented the setup parameters.

Table 6.1 – Mesh parameters.

Parameter	Units of measurements	Value
Type of mesh	-	Tetraedric elements
Mesher	-	Curvature based
Number of Jacobian points	-	4
Max dimension	[mm]	2.70
Min dimension	[mm]	0.54
Nodes	-	3020
Elements	-	17828
AR<3	-	91.1
AR>10	-	0.224
AR max	-	23.869
Jacobian (distorted elements)	%	0

The model and the relative mesh is presented in Figure 6.2

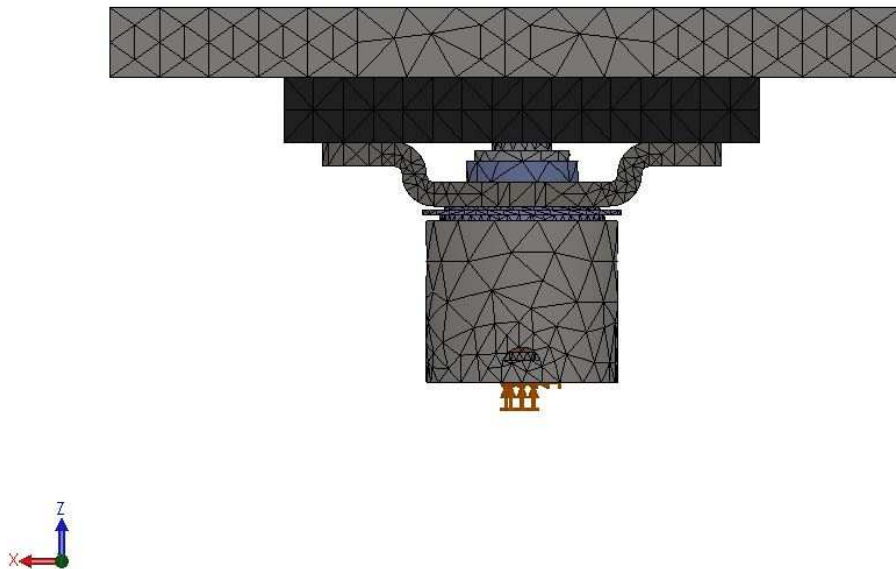


Figure 6.2 – Mathematical model, <X,Z> plane.

Results from the analysis are presented in Table 6.2

Table 6.2 – Results.

Mode	Frequency [Hz]	Mode description
1	32.84	Rigid rotation about Z axis*
2	38.71	Pitch about Y axis
3	47.5	Roll about X axis
4	122.85	Pitch coupled with longitudinal motion
5	154.24	Roll coupled with transversal motion
6	209.53	Axial displacement in Z

*This rigid motion is not detectable during the experimental analysis.

In the following Figures are presented the computed modes.

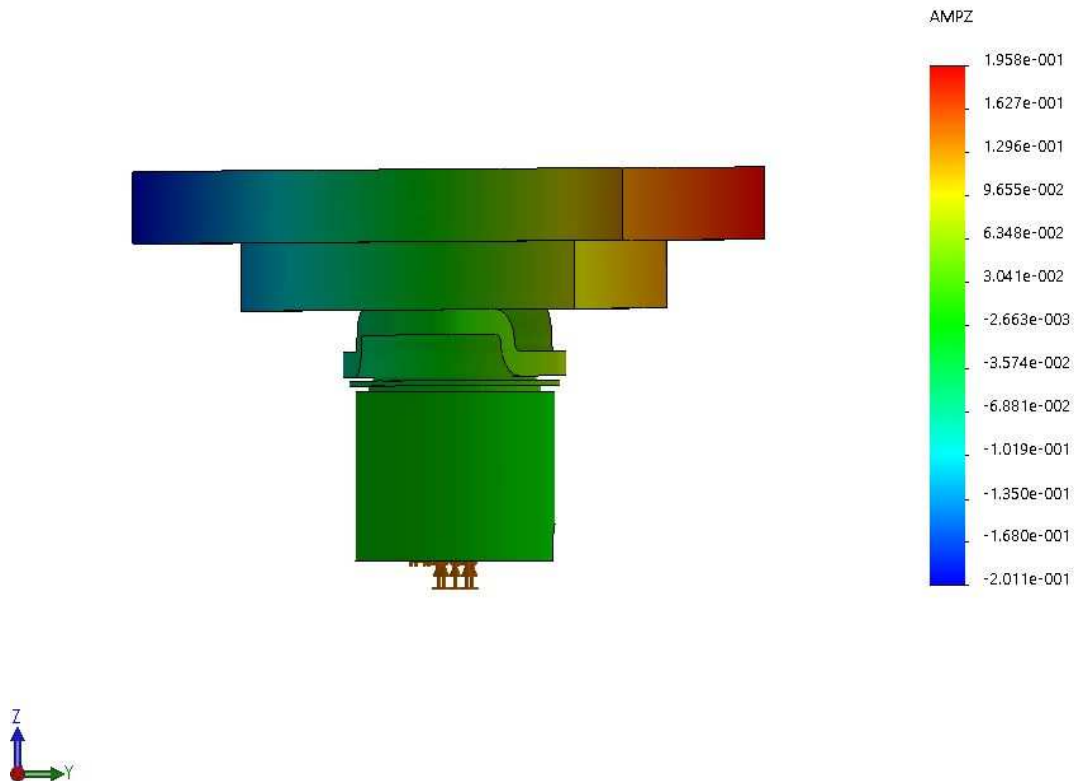


Figure 6.3 – Mode 1.

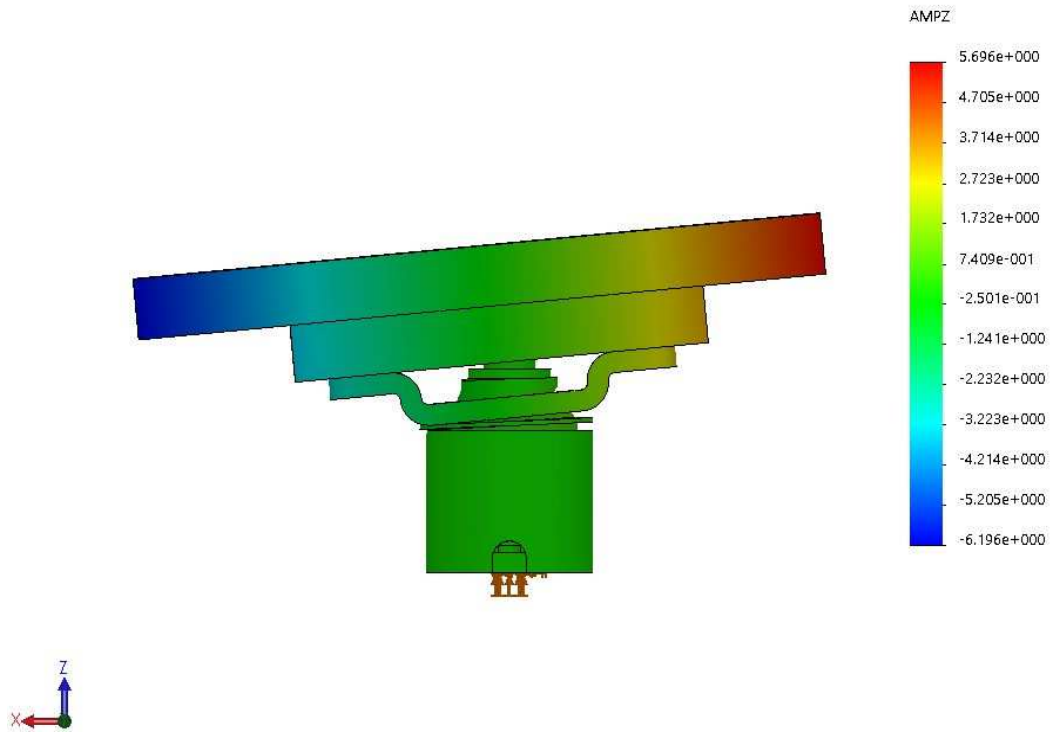


Figure 6.4 – Mode 2.

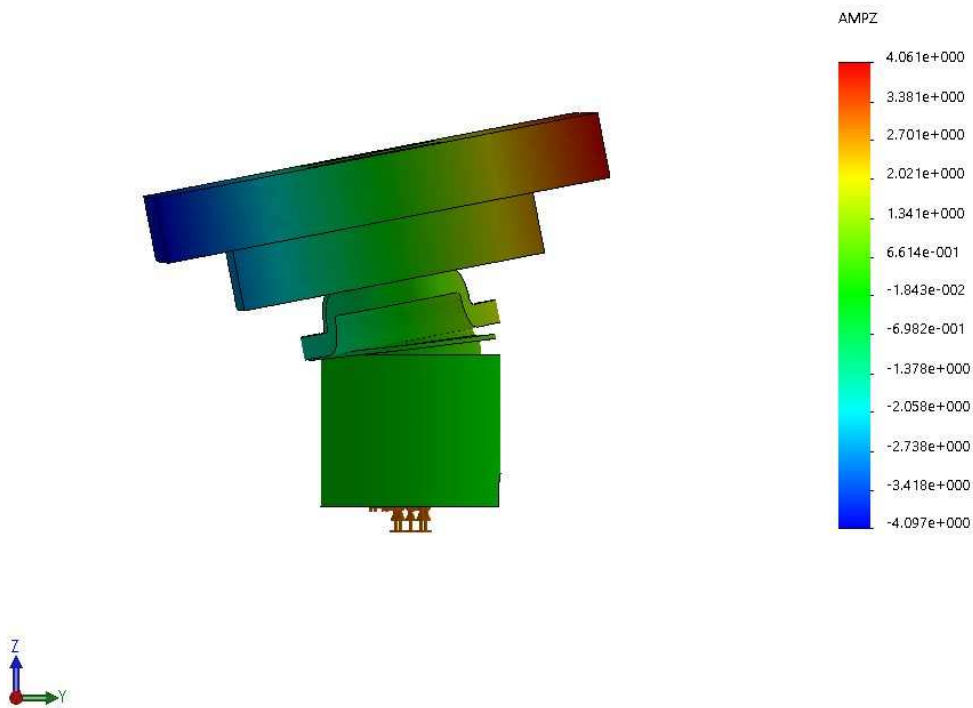


Figure 6.5 – Mode 3.

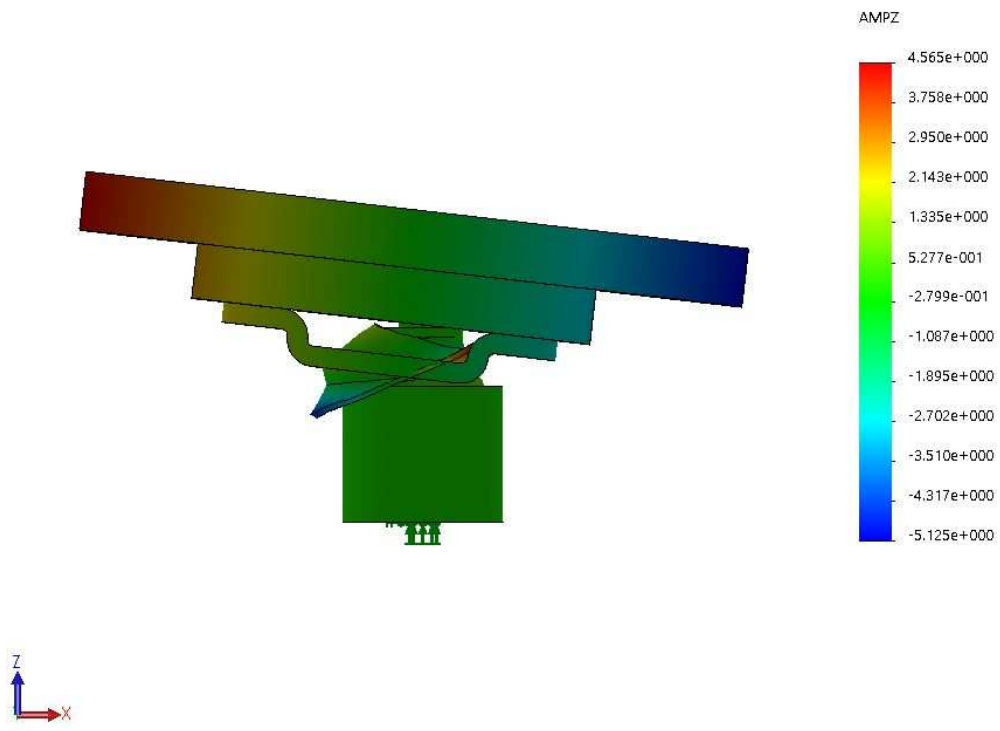


Figure 6.6 – Mode 4.

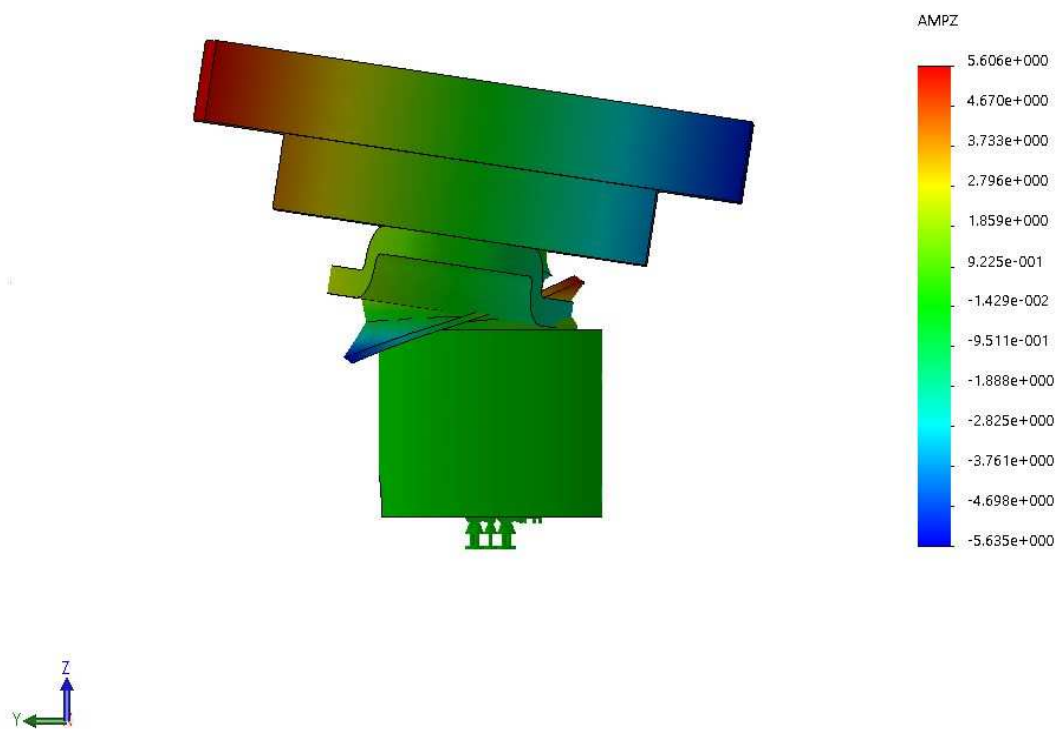


Figure 6.7 – Mode 5.

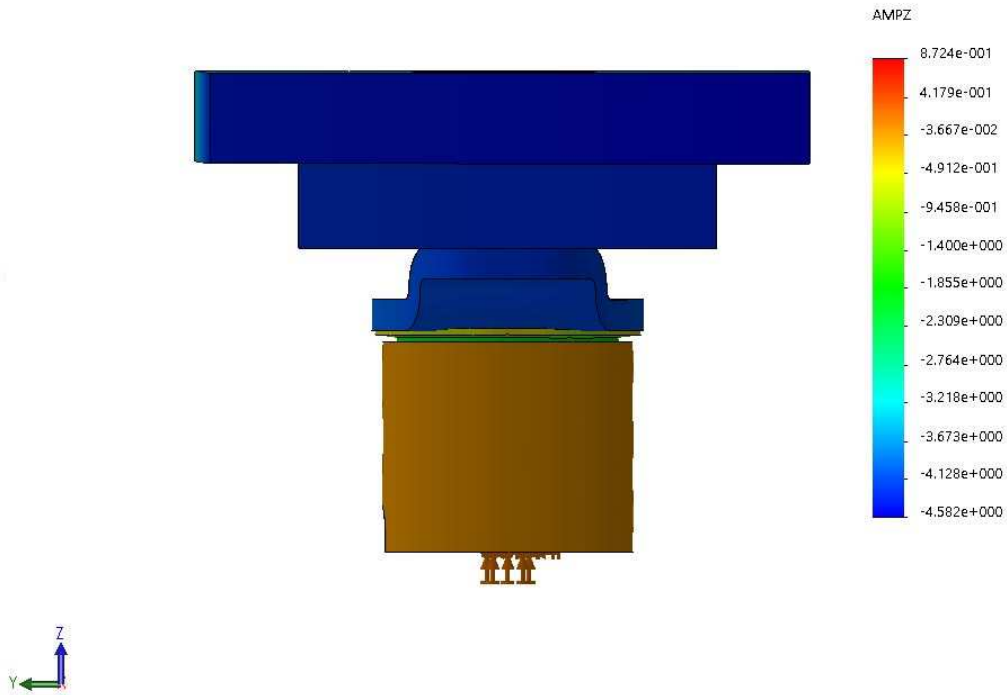


Figure 6.8 – Mode 6.

6.3 Conclusions

Results from modal analyses shows that the model reproduces with an acceptable error the data computed from the experimental analysis.

It is important to highlight that modes 4 and 5, which present a coupling between rotation and longitudinal/transversal motions is linked to the axial stiffness of the elastic elements, which has not been analyzed. In this sense, the model cannot be representative of these behaviours.

7. Conclusions

In this thesis work the aim was to characterize an electromechanical actuator, investigating its characteristic in a non-operating mode, so that to be able to produce a representative simplified model.

The work was mainly focused in the procedure and shows the steps taken to reach the objective.

It is important to remark that, due to the complexity of the system, different simplifications and approximations were considered, and the study was mainly focused on the analysis of the inertial and elastic properties of the components. In this sense, the final result can be considered as a first "raw model", which can be certainly developed and further improved.

The analyses were carried out partly at laboratories at Valeo Santena and partly at DIMEAS laboratory at Politecnico di Torino.

In chapter 1 and 2, an overall description of the actuator is made, and a simplified mathematical model is proposed.

The architecture and the mass properties were measured and a first model was produced.

In chapter 3 were investigated the stiffness properties of the elastic elements and in chapter 4 the model was updated in order to achieve an acceptable approximation of the experimental results.

The modal analysis, presented in chapter 5 gives the description of the dynamic behaviour of the actuator with its principal frequencies and mode shapes.

These results were partially reproduced during the finite elements modal analysis presented in the last chapter.

It could be concluded that, with respect to the objective of the thesis and the simplifications, the obtained model reproduces with an acceptable approximation the main features of the electromechanical actuator. However, further steps could be taken in order to reduce the error and further increase the accuracy of the model.

Reference

- [1] <http://www.matweb.com/>
- [2] https://www.shinetsusilicone-global.com/catalog/pdf/rubber_et.pdf
- [3] <https://www.primasil.com/info-hub/data-sheets/>
- [4] VALEO, VALEO internal drawings
- [5] TRAMA S.R.L., device and technical datasheets
- [6] Bonisoli E., "2018-03-08_StructuralSimul_NVO", Valeo, 2018, pp. 4.
- [7] COMET S.R.L., Silicon datasheet
- [8] Fasana A., Marchesiello S., "Meccanica delle vibrazioni" 2006 C.L.U.T. Editrice
- [9] D.J. Ewins, "Modal testing theory and practice", 2 edition, Research studies press ltd.
- [10] <https://www.youtube.com/watch?v=vWjizHma16Y&list=PLuDPxP5HI-qbsnvQ6q36vHqr3RRPcVvKP&index=2&t=822s>

